The Use of Magnetic Resonance Imaging to Evaluate *Chlamydia* as an Aetiological Agent in Alzheimer's Disease

By

Stephen Michael Szczerba

A Thesis submitted to the Faculty of Graduate Studies of The University of Manitoba

In Partial Fulfillment of the Requirements of the Degree of

MSc. In Medical Microbiology

Department of Medical Microbiology and Infectious Disease
University of Manitoba

List of Abbreviations and Symbols

Ab - Antibody
AD – Alzheimer's disease
ADC - Analog-to-digital converter
APP – Amyloid precursor protein
βA - β amyloid
B_0 – Magnetic field
BBB – Blood brain barrier
CCAC - The Canadian Council of Animal Care
CT – Computed tomography
dE9 – Delta E9
DPI – Days post infection
EB – Elementary body
ELISA - Enzyme linked immunosorbant assay
FID – Free induction decay
FOV – Field of view
FT - Fourier transformation
h - Planck's constant
IFN-γ – Interferon gamma
IFU – Inclusion forming units
LPS – Lipopolysaccharide
MRI – Magnetic resonance imaging
MSME - Multi-echo spin-echo
NMR – Nuclear Magnetic Resonance
PCR – Polymerase chain reaction
PET - Positron emission tomography
PrP – Prion protein
PS1 – Presenilin 1
PS2 – Presenilin 2
RB – Reticulate body
ROI – Region of interest
RF – Radio frequency
SEM – Standard error of the mean
SPG - Sucrose-phosphate-glutamic acid
T - Tesla
TE – Echo time
TNFα – Tumor necrosis factor alpha
TR – Repetition time
T/R switch – Transmit/receive switch
ω_0 – Angular frequency
Wt – Wild type

Acknowledgements

Over the course of my Master's studies at the University of Manitoba I received support and guidance from a number of individuals. Above all I would like to thank Marco Gruwel, my current supervisor, who has been a tremendous source of encouragement and support. Marco's expertise and guidance, especially in the field of MRI, was invaluable to success of this project.

I would also like to thank all the members of my graduate studies committee both past and present including Mike Jackson, Tim Booth, Michelle Alfa and Lin-P'ing Choo-Smith. A special thanks to Mike Jackson for providing me the opportunity to continue my studies in infectious disease and also for his contributions to the conceptualization of the study, which included obtaining ethics board approval for the research conducted in this work. I would also like to express gratitude to Xi Yang and Shuhe Wang for providing me with *C. muridarum* samples for the study as well as their advice and guidance in techniques performed in the study. Thank you to David Borchelt at the University of Florida for his positive support and advice regarding the transgenic animal model.

I would like to thank members of the Biosystems group at NRC-IBD, both past and present for their contributions to this work. In particular Richard Baydack, Eilean McKenzie, Darren Manley, Earle Edie, Crystal Fulton and Trish Yanke. I would also like to thank members of the animal care services group, including surgical services for their assistance in MR experiments and animal facility workers for day-to-day care of the mice. A special thanks to Randy Summers for his assistance and advice regarding the statistical analysis.

I would like to thank The University of Manitoba, specifically the Department of Medical Microbiology and Infectious Disease, for the opportunity to further my studies and providing financial support. I would also like to thank NRC-IBD for the use of equipment, resources and financial support that were necessary for this study. I would like to acknowledge The Alzheimer's Society of Manitoba for their financial contributions over the course of this project.

Lastly I would like to thank my family and friends, most importantly my wife Michelle; my parents, Connie and Roman; and my sister Tasha for their encouragement and support throughout my studies.

Abstract

It has been suggested that infection with *Chlamydia* may play a role in the initiation/progression of Alzheimer's disease (AD). To evaluate this hypothesis APP/PS transgenic mice (genetically manipulated to express AD pathology) and wild type (Wt) mice were infected with *C. muridarum*, and magnetic resonance imaging (MRI) and histopathology were used to assess pathological changes.

Congo red staining of tissue sections demonstrated no AD plaque pathology in Wt infected and non-infected mice, while clear pathology (neuritic plaques) was seen in transgenic mice, with a trend towards higher plaque counts in the brains in the infected transgenic mice.

When MRI was used to evaluate the effects of infection *in vivo*, hyperintensities in T_2 times were observed in APP/PS infected mice compared to APP/PS control mice both at month 5 and month 20. Together these results suggest that infection with *Chlamydia* may accelerate the development of AD.

Table of Contents

List of Figures

List of Copyright Material

Figure 1: Reprinted from Expert Reviews in Medicine, Volume 8, Issue 29, Swanborg, R. H. , D. L. Boros, J. A. Whittum-Hudson and A. P. Hudson. Pages 1-23, Copyright 2006, With Permission from Cambridge University Press.

Figure 2: Reprinted from Biomolecular Engineering, Volume 17, Jankowsky, J. L., H. H. Slunt, T. Ratovitski, N. A. Jenkins, N. G. Copeland, and D. R. Borchelt. Co-expression of multiple transgenes in mouse CNS: a comparison of strategies. Pages 157-165, Copyright 2001, With Permission from Elsevier.

1. Introduction

1.1 Hypothesis:

It has been hypothesized, somewhat controversially, that infection with *Chlamydia* may play a role in the development or progression of Alzheimer's disease (4, 48, 56). This study aims to establish whether infection with *Chlamydia* species can indeed trigger or alter plaque progression associated with AD in transgenic mice.

1.2 Infection and chronic disease:

It is becoming increasingly apparent that many chronic illnesses (for example heart disease and some forms of cancer) previously thought to be environmental, life style or stress related are in fact the result of a persistent microbial infection (3, 11, 34). While this novel approach to the underlying cause of chronic disease is relatively new (originating only in the late 1980's), in 2005 it led to the award of the Nobel Prize for Medicine to Barry J. Marshall and Robin Warren of Australia who proved a conclusive link between bacterial infection and gastrointestinal ulcers. The discovery that ulcers are caused by the bacterium *Helicobacter pylori* is highly significant given that more than half the world's population is infected with this bacterium, and its persistence can be life long. This persistent infection has also been linked to stomach cancer. Given this link between infection and chronic disease, it is not surprising that bacterial persistency, a long lasting balanced relationship with the host, is currently receiving a great deal of attention (6).

In some cases, disease linked to chronic infection is actually the result of this host-infection interaction. For example, disease may be the result of the body trying to

remove this persistent infection. In other words, disease may arise as a result of the activities of the body's immune system. For example, *Staphylococcus epidermidis* is a bacterium primarily found on the skin, and can lead to different chronic diseases such as arthritis, inflammation of the heart and kidney disease (43). *Streptococcus pyogenes* is the causative agent in both the autoimmune disease rheumatic fever and acute glomerulonephritis (a serious form of kidney disease). In both cases, disease is caused by an immune response triggered by some material present in the bacterium that closely resembles material present in human tissues. Unfortunately, this means that the immune response will not only be directed against the bacterium, but also against the human tissues. A process known as molecular mimicry can then lead to severe chronic disease, such as inflammation of the heart valves or arthritis (3). In other instances the disease may be the result of a direct interaction between the infectious agent and the body, for example certain viruses, such as Hepatitis B, Hepatitis C, Epstein-Barr virus, and human papillomaviruses, have been linked to some forms of cancer (11).

What is perhaps most worrying about the link between infection and chronic disease is that it is not exotic bacteria or viruses that are implicated: it is common bacteria and viruses. There is a proven link between hepatitis virus and cirrhosis in the liver resulting in liver cancer and species of the common bacterium C*hlamydia* has been implicated in a variety of chronic disease (82). Previous studies have shown a strong association between chronic *Chlamydia* infection and atherosclerosis (3). As coronary artery disease accounts for almost 50% of premature deaths in North America, the implications of this association are significant. *Chlamydia* has also recently been

implicated in inflammation of the heart, a condition called endocarditis.

1.2.1 *Chlamydia* and AD:

Chlamydia species have also been implicated in non-cardiovascular chronic diseases. Previous studies have shown *Chlamydia pneumonia* (a species of *Chlamydia* causing pneumonia) infection of the brains of AD patients upon autopsy (3). Both *C. pneumoniae* DNA as well as viable organisms present in post mortem brain tissue of AD patients (4, 48, 49, 56). PCR assays were used to examine 19 samples of post-mortem brain tissue from late-onset AD patients and 19 non-AD patients (4). Results of the study indicated 17 out of 19 AD patients were positive for *C. pneumoniae* DNA in the hippocampus and cortex, while 18 out of 19 non-AD patients were negative for *C. pneumoniae* in brain tissue. Electron microscopy and immunoelectron microscopy corroborate some of these results. *C. pneumoniae* was successfully cultured from the sites of infection in the AD brain in a monocyte cell line demonstrating the presence of the organism at the site of disease. Finally, viability of the organism was tested by targeting mRNA of the gene encoding for the 3-deoxy-D-Manno-2-octulosonic acid transferase enzyme, responsible for lipopolysaccharide (LPS) synthesis on *C. pneumoniae*. The results showed the presence of viable *C. pneumoniae* in regions of the brain known to be associated with AD.

Perhaps the most convincing evidence for a role of *C. pneumoniae* infection in AD comes from a recent study that demonstrated AD pathology in the hippocampus, amygdalae, cortex and thalamic region of the brain in mice infected intranasally with *C. pneumoniae* (44). The authors observed the organism in the nasal olfactory epithelia,

which lead to infection of the olfactory bulb. From this region it is plausible that infection may have spread to adjacent areas of the brain. In a follow up study, researchers were unable to repeat these findings but rather reported immunoreactive AD pathology in mice infected with *C. pneumonia* and also in mice given a sham infection (9). The authors state that there were a number of experimental variations between the studies, which may account for the different results. The purpose of this study is to provide further evidence that may shed some light on the possible relationship between *Chlamydia* and AD. For clarity the pathology of a *Chlamydia* infection is addressed first, followed by the hallmarks of AD and finally how MR imaging was used to detect changes in the tissue associated with these two effects.

1.2.2 Transmigration to the central nervous system:

C. *pneumonia* may enter the brain by a number of different mechanisms. *C. pneumonia* was isolated in the olfactory bulb of infected mice, so the olfactory pathway is suspected to be a mode of entry to the brain by the pathogen (31, 44). Previous studies have demonstrated an alternate mechanism where *C. pneumoniae* may infect immune cells, such as human monocytes (1), and cross the blood brain barrier (BBB) (47). The BBB impedes the influx of dangerous compounds from entering the brain (5). It is a selective barrier that excludes dangerous compounds from crossing while at the same time allowing necessary compounds to enter. *C. pneumoniae* infected monocytes and macrophages have been observed in and in close proximity to blood vessels in patients with AD (4). This evidence makes a strong case for immunopathology of *C. pneumonia* in humans facilitated by infection of monocytes and macrophage. Interestingly new

evidence suggests that the presence of LPS, an endotoxin located on the surface of *Chlamydia*, may impair function of the BBB, increasing its permeability (66). This increase in permeability of the BBB may allow dangerous compounds to enter the brain, suggesting that the central nervous system is at risk during a *Chlamydia* infection.

It is possible that *Chlamydia* is merely an opportunistic infection entering the brain when a breakdown in the BBB occurs. Organisms may penetrate the BBB after the onset of AD, which also has an effect on BBB permeability (5). AD patients may acquire a *C. pneumonia* infection from low activity or being bedridden and the pathogen enters the brain in later stages of the disease. Interestingly a link has been established between AD and pneumonia infections although the exact nature is not well understood (4, 68, 78).

1.2.3 *Chlamydia* lifecycle:

Chlamydia has a unique developmental cycle consisting of two different morphological states: the infectious form known as the elementary body (EB), and the reproductive form known as the reticulate body (RB) (6).

The EB attaches to the cell membrane and is then taken up by endocytosis (26) (Figure 1). *Chlamydia* species are intracellular bacteria that are dependent on host energy for protein synthesis. The EB then differentiates into a RB, reproduces by binary fission and collects in a micro-colony known as the inclusion body.

At this stage the organism may initialize a persistent state, usually induced by treatment with an antibiotic, a cytokine such as interferon-gamma released by the host to

Figure 1: The intracellular lifecycle of *Chlamydia* species (75).
Chlamydia exhibit two distinct states in the lifecycle, the infectious form known as the elementary body and reproductive form known as the reticulate body.

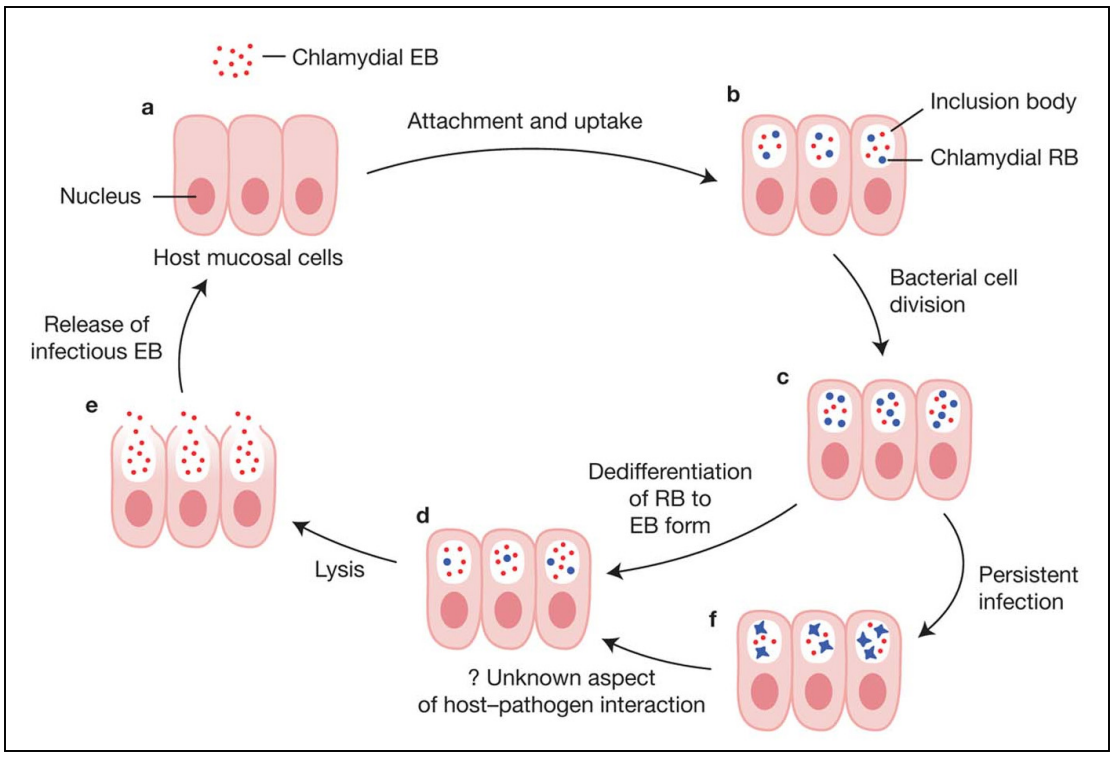

fight infection, or by a restricted state of nutrients in the cell. Persistence is characterized by the inability of the host immune response to clear the infection completely where bacteria are unable to be cultivated but remain viable (26, 30). Persistence is a means of avoiding threatening external factors and aids in immune response evasion (6). If persistence is not established, differentiation occurs back into EBs. Despite having a large infectious load, the host cell is minimally disrupted by the infection. Bacteria are either released by lysis of the cell or extrusion of the entire inclusion through the cell membrane, leaving the cell viable.

The persistent state allows *Chlamydia* to establish a balance with the host, allowing for chronic infections that have been implicated in a number of chronic disease states. This unique stage of lifecycle may result in multiorgan dissemination to different tissues in the body including privileged areas, such as the brain. A previous study showed *C. pneumonia* established a persistent infection in neuronal cells *in vitro* by interfering with apoptotic pathways (2). This evidence suggests that if *Chlamydia* was able to establish a persistence infection in the brain it could induce neuroinflammation and have an impact on AD.

1.2.4 *Chlamydia muridarum*:

Chlamydia muridarum, which has specific mouse host tropism and naturally causes respiratory tract infections in mice, was chosen to assess the impact of a *Chlamydia* infection on chronic AD (52). The main advantages of using the *C. muridarum* over the human pathogen *C. pneumoniae* include: both strains exhibit a similar pathology including the ability to undergo a persistent infection, it is safer to work

with *C. muridarum* from a biosafety perspective as it is not a human pathogen and *C. muridarum* is a natural cause of infection in the mouse. The lack of tryptophan biosynthesis genes in *C. muridarum* may contribute to murine species tropism because proinflammatory interferon gamma (IFN-γ) cytokine contributes to tryptophan depletion in humans (59).

Chlamydia species, including *C. muridarum* and *C. pneumonia*, have a highly conserved genome with respect to gene order and content (59). There are several important similarities in pathology between *C. pneumoniae* and *C. muridarum*. The route of infection for both organisms is by aerosol to the respiratory tract and lungs. Both a cell mediated and humoral immune response is elicited by the host during an acute *Chlamydia* infection. Humoral immunity includes the activation of plasma cells and production of antibodies (Ab), such as IgG and IgA. Plasma B cells play an important role in activating the T cell response during infection (25, 39, 85).

Both organisms carry genes associated with nucleotide scavenging and biosynthesis not found in the *C. trachomatis* serovar D genome (59). The organisms also have a broad range of host tissue tropism exclusive to human and murine hosts in *C. pneumoniae* and *C. muridarum*, respectively. In both cases the organism has been isolated from lung epithelial cells as well has heart tissue (17). Significant growth was observed in the heart and aortic valves following intranasal infection with *C. muridarum* indicating dissemination to cardiac tissues.

C. muridarum infection in the mouse was the model chosen for this study because *C. muridarum* can persist in the body and readily infect different cells. For example, recent evidence shows *C. muridarum* was not only able to survive in dendritic cells in

excess of 9 days but the number of bacteria cultivated from these cells was less than originally estimated (60). Organisms recovered from infected dendritic cells were able to infect other mice, indicating *C. muridarum* was viable. The fact that fewer bacteria were isolated than expected coupled with the viability of the organism strongly suggests *C. muridarum* was in a state of persistence (60). This evidence supports previous findings that following an acute lung infection with *C. muridarum*, active bacteria were readily detectable in multiple organs including cardiac tissue and the kidneys (17). The infection may have spread systemically from the lungs to other organs in the body, resulting in immunopathology (17). The authors suggest that *C. muridarum* may induce cardiovascular disease in mice. Interestingly cardiovascular disease has been linked to AD and may have an effect on plaque progression associated with AD (64). Vascular pathology has a high incidence rate in patients with AD. Both AD and cardiovascular disease have common risk factors, including inflammation which may be induced by a pathogen such as *Chlamydia*.

If *Chlamydia* is able to enter the brain it is possible it may be involved in orchestrating plaque pathology events in AD. In fact, *C. muridarum* have demonstrated the ability to enter the brain after an acute infection in the lungs (Unpublished results, Dr. Yang). More specifically, mRNA of *C. muridarum*'s major outer membrane protein was detected in a PCR assay in C3H mice after inoculation. The presence of *C. muridarum* mRNA indicates viable *C. muridarum* was present at some point as mRNA is only transcribed from DNA in instances where bacteria are viable and replicating. Although the inoculum size differed as well as the mouse strain (C57/B6 and C3 cross in the present study) the evidence supports the hypothesis that *C. muridarum* has the ability

to enter the brain either systemically through the BBB or perhaps via the olfactory pathway. Regardless of the mode of entry the obvious question is since *C. muridarum* is able to enter the brain what affect would the infection have on AD pathology?

1.3 Alzheimer's disease:

1.3.1 Hallmarks of AD:

AD is the most significant cause of senile dementia and this threat increases with age (4, 31). Currently over 20 million people suffer from AD worldwide and that number is expected to increase in the future due to an aging population (4, 34, 61). Symptoms of the disease include progressive memory loss, decreased cognition, problems with spatial and perceptual recognition and impairment of daily living (4). As the disease worsens it interferes with the patient's ability to function independently and causes a strain on the individual, health care workers and family members. The result is an incredible cost burden to the health care system.

AD pathology is characterized by extracellular neuritic senile plaque deposits composed of amyloid peptides termed β amyloid (βA) and intraneuronal neurofibrillary tangles composed of tau protein (8, 27, 40, 50). These biomarkers are linked to neuronal loss and progressive dementia (Figure 2). AD occurs in two forms: familial and sporadic, with the major clinical difference being the age of onset (42). The onset of the familial form precedes the sporadic form, thus familial AD is usually referred to as early-onset and sporadic AD as late-onset. The underlying cause of early onset is genetic, however, the cause of late onset AD has yet to be elucidated, and it is likely that more than one causal factor exists. It is possible that a *Chlamydia* infection may play an important role

Figure 2: The amyloid hypothesis (27).
A hypothesis of events for amyloid protein accumulation resulting in Alzheimer's disease. The arrow on the perimeter indicates that accumulation of βA may be responsible for neuritic injury or neuronal cell death.

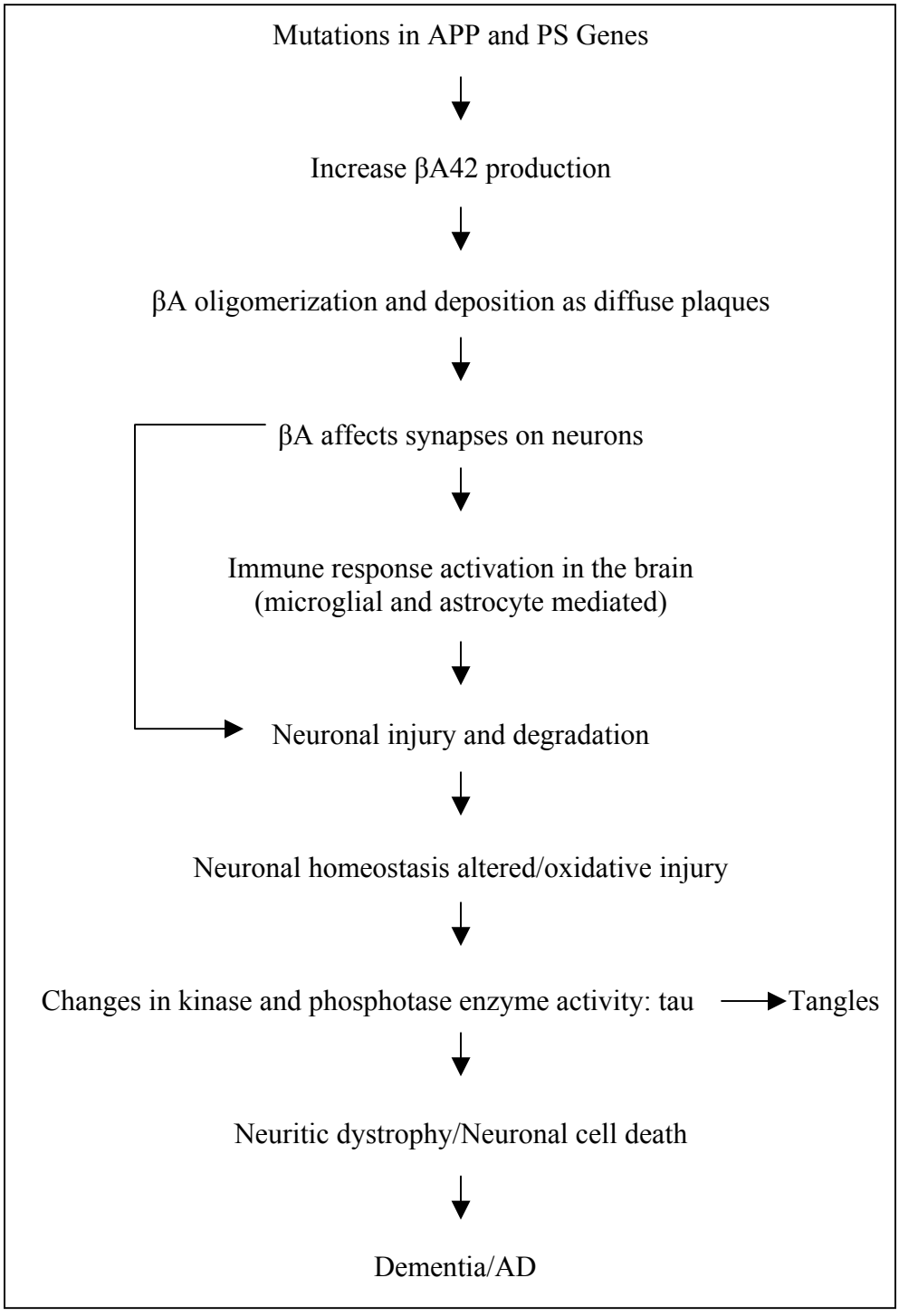

in late onset AD. Extracellular neuritic plaques, aggregates of the 4 kDa 39-42 amino acid βA peptide derived from the C-terminus region of the amyloid precursor protein (APP), are a defining pathological feature of AD (21, 44, 50). βA peptide aggregates in a β sheet conformation, which can be observed in the presence of Congo red stain (68). Congo red is the gold standard used to diagnose AD post mortem by binding to βA in tissue sections (46).

βA may induce membrane lipid peroxidation and impair function of ion-motive ATPases, glucose transporters and ion channels in the cell resulting in degeneration of synapses and neurons (24, 51). Inflammatory events resulting from βA accumulation are critical to disease progression. Reactive microglia and monocytes are responsible for activating a tyrosine kinase-based signal response to plaque progression, which result in neurotoxic products, cytokines and reactive oxygen species (14). Microglia make up 5-10% of glial cells in the brain and surround neurons of every type so plaques are in constant contact with microglia cells (33).

APP is expressed throughout the central nervous system and is highly conserved among different species including mice, indicating its importance in neuronal biology. It is unclear whether the association between βA and AD is causative or if βA is the end result of the disease stimulated by other factors (27). Mutations in the APP gene on chromosome 21 play an important role in the familial form of AD, which may indicate a causal role in the disease (22).

The pathologically important mutations are located at sites within the APP gene. APP is cleaved by enzyme complexes known as secretases, with γ-secretase being the most important for AD pathology (27, 69). The identity of γ-secretase has proven

elusive, but evidence points to it being a membrane-associated complex of multiple proteins. There is increasing evidence that the presenilin proteins are important components of this complex, and the active site of the complex may reside in a dimeric form of presenilin (69, 73). Mutations in the APP genes and genes for presenilin-1 (PS-1) and presenilin-2 (PS-2) can therefore lead to over-expression of βA and hence to formation of neuritic plaques.

1.3.2 Transgenic animal model:

Modeling AD in laboratory animals is challenging, as rodents do not develop AD naturally. Fortunately transgenic mice have been genetically engineered to develop the plaques associated with AD. Transgenic mice have human genes associated with AD inserted into their genome. In this study B6C3-TG(APPswe, PSEN1dE9)85Dbo/J (Line 85) mice were used because they display human AD proteins including chimeric mouse/human amyloid precursor protein (APPswe) and human presenilin 1 protein (PS1) in the brain, resulting from the inserted transgene expression.

Line 85 mice have several modifications to the transgenes that act to accelerate βA production. The first alteration was replacing three amino acids in the full length APP coding sequence for βA expression as well as encoding the Swedish mutations at amino acids 595/596 to elevate the quantity of βA produced (36).

βA is derived from APP through cleavage steps by a number of enzymes including γ-secretase, which is derived from, or related to, PS1 (36). The delta E9 (dE9) mutation is a deletion of exon 9 in the PS1 gene. The deletion in PS1 favors Aβ42 processing over Aβ40, which is more prone to aggregation *in-vivo*. The modified

transgenes were cloned into two separate expression plasmids (MoPrP.Xho) and coinjected into pronuclei of B6C3 mice. The pronuclei were then surgically transferred to surrogate mothers. The plasmids contained cDNAs encoding APPswe and PS1 genes. cDNA of each transgene was cloned into the Xho I site of the vector between PrP (prion protein) exons 2 and 3 (Figure 3). Transgenes were co-integrated and co-segregated at the same chromosomal loci.

APPswe and PS1 gene expression are controlled from the mouse PrP promoter (Figure 3). The PrP promoter was chosen so transgene expression was directed to central nervous system neurons and astrocytes (36). This ensures a greater amount of βA pathology in the brain rather than other organs in the body.

Co-injection is an efficient strategy for co-expressing transgenes because APPswe and PS1 are inserted into a single locus. Characteristics of the B6C3-TG(APPswe, PSEN1dE9)85Dbo/J cell line include high transgene copy numbers (estimated by PCR), which correlate to high APPswe and PS1 expression levels (37). Mice exhibit plaque pathology as early as 6 months largely due to the dE9 mutation in PS1 (36). Significant plaque deposition is observed in the hippocampus and cortex by 9 months (36). Changes in these regions will thus be the primary focus of this study.

1.4 MRI as a tool to study AD:

A number of options are available to assess progression of AD in animal models. The simplest option would be to infect experimental animals with *Chlamydia*, euthanize animals at discrete time points after infection and analyze the brains for signs of disease using immunohistochemical or histological techniques. This approach has three main

Figure 3: Construction of APP/PS using the coinjection strategy (37).
The coinjection strategy for constructing double transgenic mice expressing mutant APP and PS1 proteins. Co-segregation in offspring suggests the constructs are inserted in the same location and genes are translated from a single mouse PrP promoter.

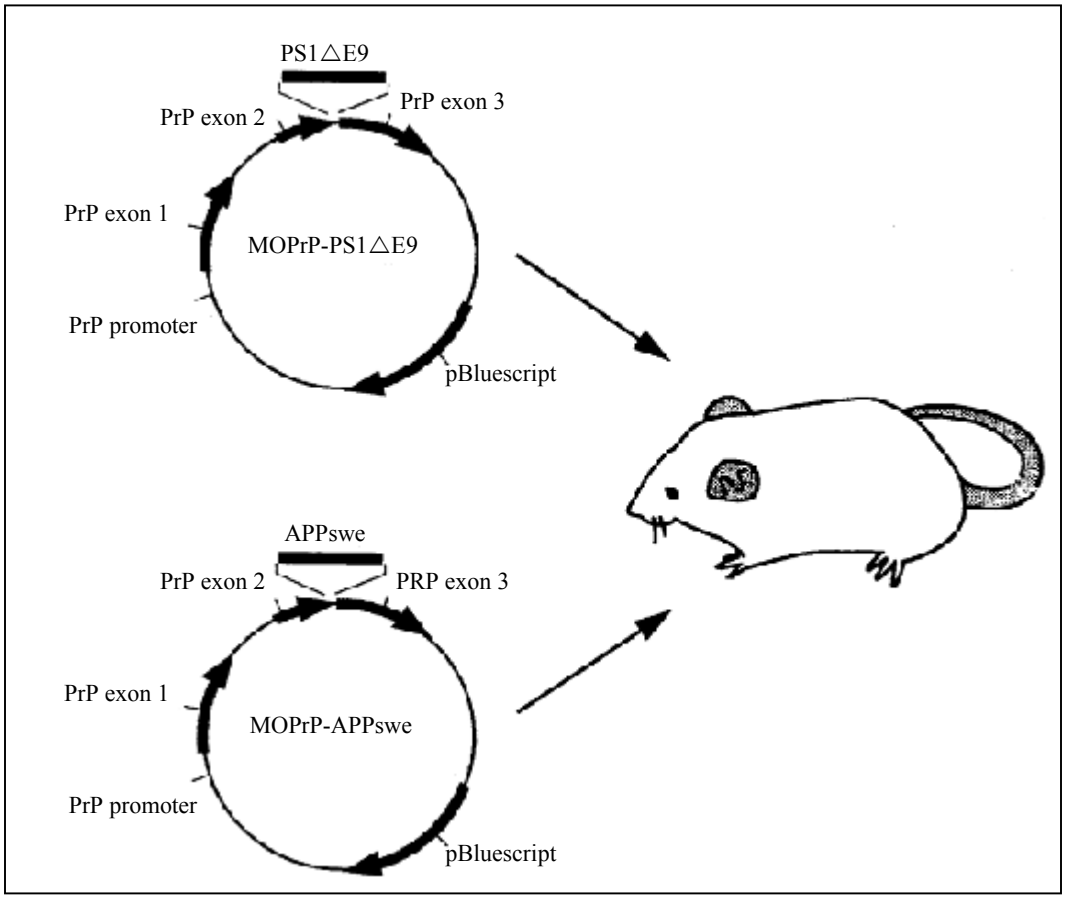

drawbacks: 1) It requires large numbers of animals. 2) It requires the assumption that the disease progresses in the same fashion in all animals euthanized at different time points. 3) It is expensive, due to the large number of animals required. These drawbacks are minimized by the use of magnetic resonance imaging (MRI) in combination with a chronic study.

1.4.1 MRI Background:

The first successful attempt to observe nuclear magnetic resonance (NMR) was made by Bloch and Purcell in 1945 using a magnetic field and a radio frequency (RF) source (12). NMR as a spectroscopic tool is an established technique with widespread applications in the fields of physics, chemistry, biochemistry and molecular biology. Since the 1970's NMR has also been developed as a 2 and 3 dimensional imaging technique, often referred to as magnetic resonance imaging (MRI).

At the present time MRI is the pre-eminent clinical non-invasive imaging modality for the human body. In contrast to computed tomography (CT) it does not require ionizing radiation and provides excellent soft tissue contrast for diagnostic purposes. Clinical MRI uses the NMR signal generated by the proton nuclei (^{1}H) of water and lipid molecules (70). Although NMR, as an analytical technique, is rather insensitive, the large amount of water in the human body, together with the high specific sensitivity of the proton nucleus, makes proton MRI a useful diagnostic tool. Over the years specific RF pulse sequences have been developed to study anatomy and biochemical processes (*in vivo*) in detail (12). Functional information (brain, neuronal activity) can also be studied by MRI using so-called fMRI sequences.

1.4.2 Spin physics:

Protons possess a characteristic called spin (for ^1H its value is ½), which provides the hydrogen nucleus with a magnetic moment (15, 70). This makes the nuclei behave much like a classical bar-magnet when placed in an external magnetic field. Due to its angular momentum the proton spin will precess about the direction of this magnetic field once exposed to it (Figure 4). This precession is call the Larmor precession and is field dependent:

$$\omega_0 = \gamma B_0$$

This angular frequency (ω_0) depends on the strength of the magnetic field (B_0) given in Tesla or Gauss (15, 70). The gyromagnetic ratio (γ) is a constant and is specific for each element in the periodic table with non-zero nuclear spin. For protons the gyromagnetic ratio has a value of 42 MHz/Tesla. Proton spins can only occupy one out of two possible orientations when placed in a magnetic field due to the value of the spin (1/2). Both orientations are then characterized by an energy difference. The lower energy state corresponds to the orientation of the spins in the direction of the external field (Figure 4). In the absence of a magnetic field, the sum of all nuclear spins add to zero, however, once placed in a magnetic field a net magnetization develops. Transitions between these orientations can be made using RF energy.

$$E = (h/2\pi)\,\omega_0 = (h/2\pi)\,\gamma B_0.$$

Figure 4: The orientation of protons in nature and in the presence of a magnetic field.
Protons orientate themselves randomly in nature (A), but behave differently in the presence of a magnetic field. Protons align in either a high or low energy state where the lower energy state is preferred (A). Protons precess in the presence of a magnetic field at a specific frequency (B).

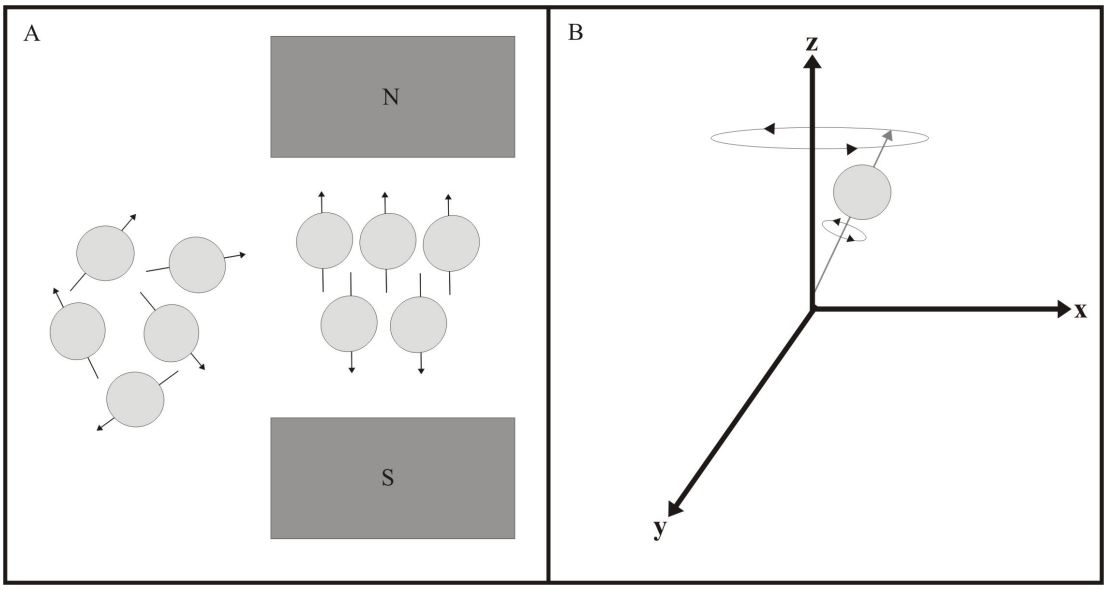

As indicated by the equation above, where *h*= Planck's constant, the most efficient transfer of energy occurs at the Larmor frequency (ω_0). This is known as the resonance condition.

1.4.3 The MR signal:

Detection of the NMR signal is achieved through the use of a receiver coil. Often the receiver coil is also the RF-transmit coil and the switching between transmit and receive mode is directed by the pulse programmer (software) which controls the transmit/receive switch (T/R switch). Once the spins have been flipped into a plane perpendicular to the main magnetic field, the precessing magnetization induces a current in the RF coil, which is recorded as the free induction decay (FID) and digitally sampled using an analog-to-digital converter (ADC) (15). The RF pulse used to tip the net magnetization of a phantom (a large collection of spins) is classified by the tilt of the magnetization; for example, a 90^o pulse tilts magnetization 90^o (Figure 5). The resulting FID is the basis of both spectroscopy and imaging. Using a Fourier transformation (FT) the acquired signal can be transformed from the time into the frequency domain to form a spectrum or a line in an image.

The shape, or decay, of the FID is very important for spectroscopic or image reconstruction and is controlled by a process called transverse relaxation, also known as T_2 relaxation (70). Transverse relaxation arises from interactions of the nuclear spin with other neighboring nuclear spins and inhomogeneous magnetic fields. This property can be extremely useful in imaging to create contrast. Next to transverse relaxation, the

Figure 5: The effect of a radio frequency pulse on net magnetization.
Protons precess in an external magnetic field (A) and produce a net magnetization vector in the direction of the magnetic field along the longitudinal z-axis (B). If an RF pulse is administered, protons switch from the lower energy state to a higher energy state and precess in synch with one another; the effect of a 90^0 flip is demonstrated here (C) causing a net transverse vector along the xy plane. As energy is released from the system protons begin re-aligning to the original state in the magnetic field (D).

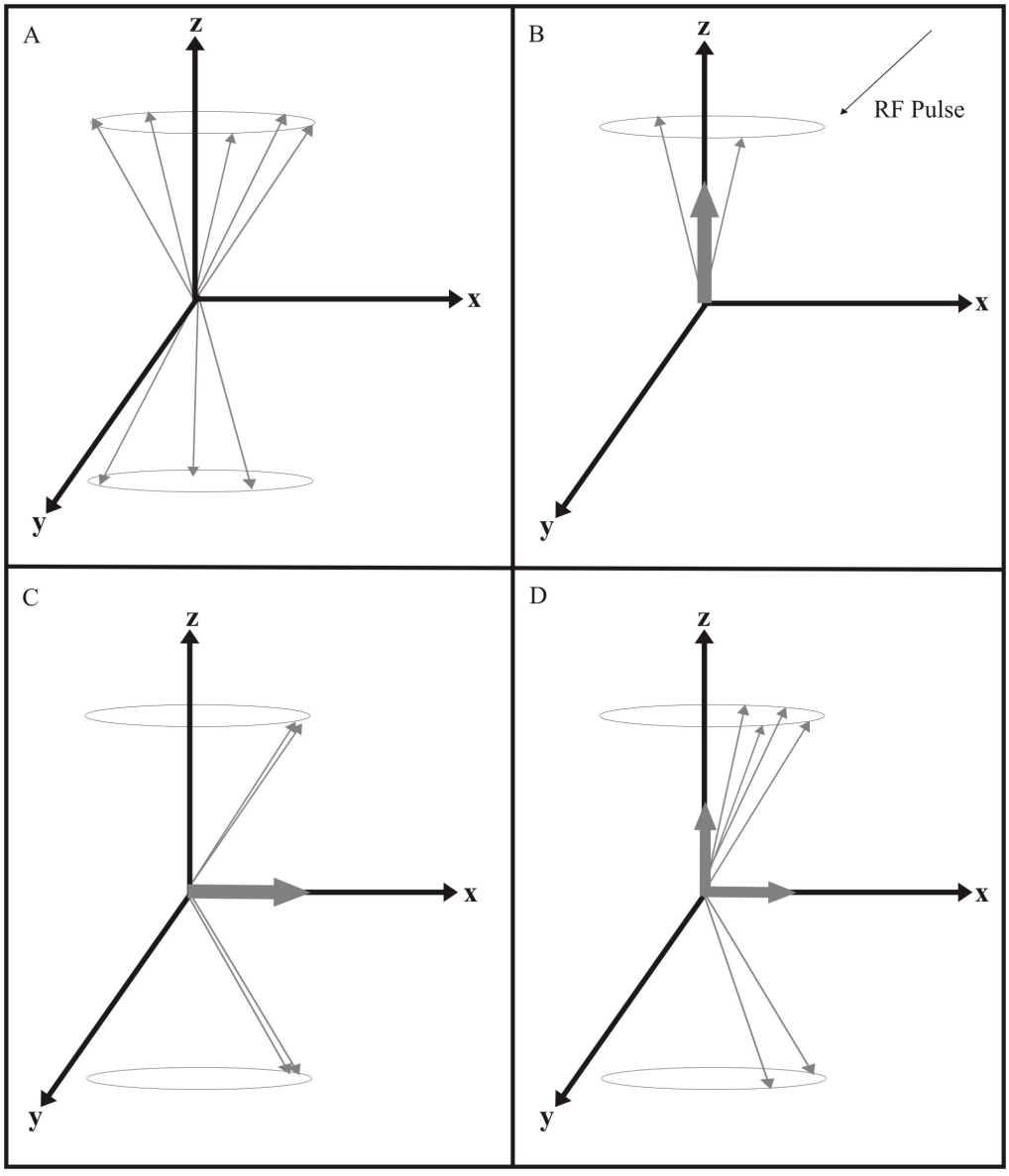

dynamics of nuclear spins in a field is also influenced by longitudinal relaxation, or T_1. Longitudinal relaxation describes the process needed for the spins to return to their equilibrium position. If experiments are repeated much faster than T_1 the total magnetization available for imaging or spectroscopy will slowly vanish due to saturation of the signal. In short, too much energy is given to the system in the form of RF pulses while it is not given enough time (T_1 sets the scale for this) for this energy to dissipate. Longitudinal relaxation, also referred to as spin-lattice relaxation, describes the process where the excited nuclear spins dissipate their energy by means of molecular motion.

1.4.4 T_2 weighted images:

Transversal magnetization, the vectors oriented in the xy plane of net magnetization, dephase with time through a process known as transversal relaxation time or T_2 (70). T_2 is influenced by a non-homogeneous magnetic field and the differences in small magnetic fields of neighboring nuclei as indicated above (12, 70). This property of magnetic relaxation can be exploited to generate image contrast.

1.4.5 MRI experiments:

In this study two imaging techniques were used: gradient- and spin-echo imaging (Figure 6). Gradient echo imaging has a much shorter acquisition time than spin echo imaging as it uses gradients rather than an additional RF pulse to produce an echo for data acquisition. A typical gradient echo pulse program is shown in Figure 6, showing the RF and gradient switches. To speed up data acquisition even more, small flip angles can be used for the RF-pulse. Using small flip angles allows for a faster acquisition as

Figure 6: A) Gradient- and B) spin-echo sequences for MR experiments.
Gradient- echo experiments A) were performed to obtain scout images for a positional guide to line up slices in the brain for spin- echo experiments B).

A)

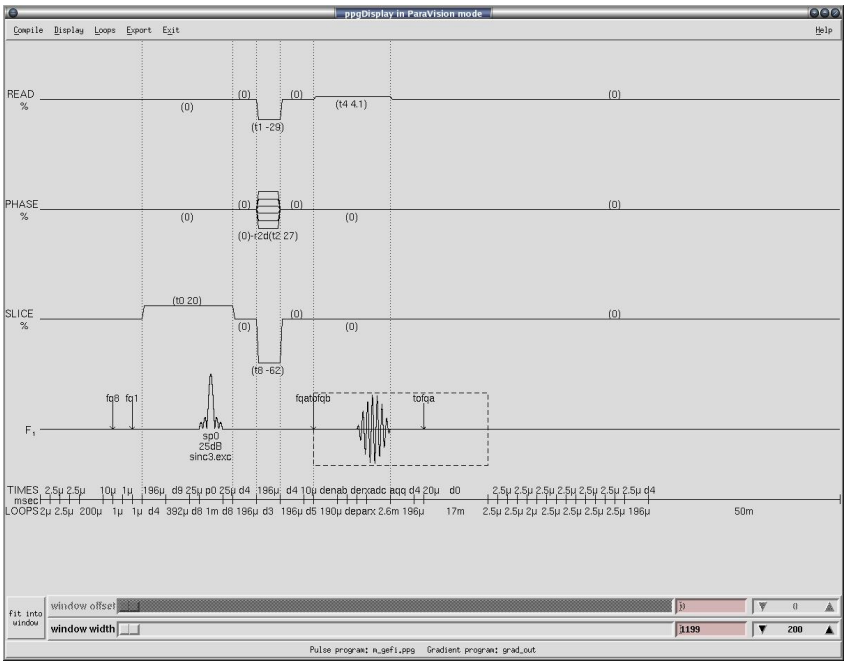

B)

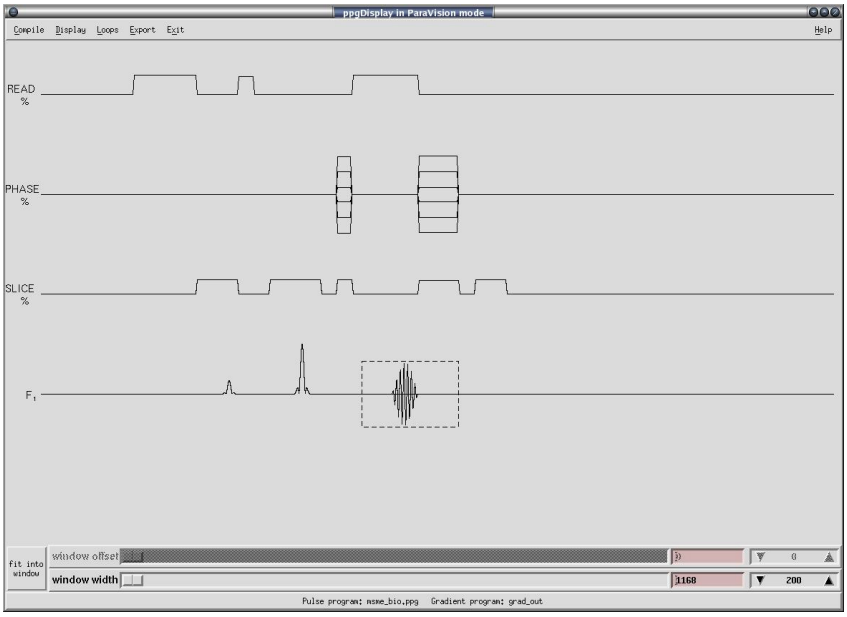

the issue of signal saturation is avoided (see above, T_1). In this study gradient echo acquisitions were used to obtain scout images. Scout images are used as a guide to position the slices for the acquisition of the multi-slice multi-echo brain images in a series of T_2 weighted image experiments.

Spin echo imaging is a technique using a 90^0 RF pulse that flips the net longitudinal magnetization into the transverse plane (xy) or perpendicular to the external magnetic field (Figure 5). Slice selection gradients are applied during the RF-pulses and the proton spins were re-phased using a 180^o pulse. At the top of the echo, effects from field inhomogeneities will have vanished. A phase encoding gradient, it's strength based on the field of view (FOV) and matrix size, is applied to the system followed by a slice selective 180^0 RF pulse after a time period of half the echo time (TE), creating an echo. The echo is detected and a frequency-encoding gradient is applied during acquisition. Each acquisition acquires one line for the raw image data set. The experiment needs to be repeated as many times as there are phase encoding gradients, stepping through values from maximum to minimum value. In the experiments described in this work a data matrix of 350x350 points was employed, meaning that the phase encoding gradients were stepped 350 times. For each value of the phase encoding gradient, 350 data points of frequency-encoded data were collected. The sequence is repeated after a repetition time (TR) period to allow for relaxation of the signal.

1.5 Pre-clinical imaging assessments of plaque progression in transgenic mice:

Several approaches have been used to study AD in transgenic mice involving imaging techniques. One method involves direct imaging of plaques using a probe such

as ^{125}I-radiolabelled βA in transgenic mice (80). Positron emission tomography (PET) has been shown to be effective for early detection of AD plaque pathology *in vivo* (77). There are many imaging tools available for observing subtle changes in the brain associated with AD; in this study MRI was used to measure disease pathology as it has several advantages over the alternative strategies. For example, MRI produces images with better resolution than other techniques without the use of x-rays, radioactive materials or other potentially damaging materials. AD is characterized by the degeneration of tissue as well as accumulation of toxic proteins in the brain over time. The non-invasive nature of MRI allows for repeated measurements of regions of interest (ROI) over a long period of time, therefore MRI can be used to detect the appearance of disease markers as well as ongoing disease pathology. MR images may be acquired in such a way as to reflect the fluid content of tissues resulting from changes in the brain associated with early and late stages of disease.

It has proven extremely difficult to use MRI to detect plaque formation and track plaque progression associated with AD using standard imaging techniques. Researchers have used a number of different strategies to study βA plaque progression in transgenic mice. The most successful studies use MR microimaging on perfusion fixed animals or isolated fixed brain (7, 29, 87). These studies required up to 24 hrs to acquire images of sufficient quality for plaque detection. Other groups have used a contrast agent, such as gadolinium or monocrystalline iron oxide nanoparticles, to enhance the MR signal in *ex vivo* studies (57, 79). Once the mouse brain is fixed and perfused there are no time constraints and images can be acquired for long periods eliminating the time factor constraints of *in vivo* studies. The images produced can resolve plaques because of a

high signal to noise ratio. The disadvantage of the fixed brain approach is mice are euthanized to retrieve the brains and observing plaque progression at a later time in the same animal is not an option. This technique is also limited in that there are no options to develop it further in human studies. These limitations prompted us, as well as other investigators, to investigate plaque progression in an *in-vivo* animal model without the use of a potentially harmful contrast agent (10, 16, 35, 76, 81). These studies have demonstrated that MRI can be used to track the onset and progression of plaques related to AD in transgenic mice. These models may be used to study factors, like infection, that may have an impact on AD plaque progression. In this work, MRI was chosen to study the relationship between *Chlamydia* infection and the pathology of AD in APP/PS transgenic mice. The purpose of this study was to identify any MRI markers of disease progression; markers are gross indicators of disease. The results may be construed as a bioassay for plaque progression associated with AD, not the disease itself.

Wengenack 2008 *et. al.* and Braakman 2006 have shown that T_2-weighted imaging can be used with realistic time frames (under 2 hours) for localization of plaques in APP transgenic mice (10, 81). Hypointensities in T_2 were apparent in the hippocampus, cingulate and retrosplenial cortex. While the reason of the shorter T_2 is not completely clear a number of suggestions have been made to explain this phenomenon. Plaques are hydrophobic and result from an accumulation of βA protein in the brain. The nature of the plaque composition is contributed to by various factors. One factor is aggregation of APP in β sheet conformation, that would have a T_2 shortening effect (35, 76). Another possibility is the accumulation of iron in plaque deposits observed in both humans and transgenic AD mice (35). The co-localization of iron with plaques may act

as a natural contrast agent and contribute to shorter T_2 times observed in these studies. Plaque deposition itself may not be completely responsible for hypointensities in T_2; a change in cell physiology due to neurodegeneration resulting from surrounding plaques may contribute to less fluidity in the tissue (29). Another physiological change associated with AD is a reduction in cerebral blood flow to the brain, which is associated with hypointensities in T_2 (23, 41).

Regardless of the reason for the change in T_2 relaxation time, the differences observed were significant between transgenic and non-transgenic mice. These changes are related to the effects of the APP/PS transgenes, which are either directly or indirectly related to plaque progression. Changes in T_2 can be used as markers in a bioassay for βA plaque progression in transgenic mice.

Previous studies have shown a mechanism by which metabolically active (i.e. living) *Chlamydia* have entered the brain in AD (4). This suggests a relationship between AD and *Chlamydia pneumonia* infection. It is worth noting that pneumonia is a major cause of death in Alzheimer's patients (78). However it is unclear whether *Chlamydia* triggers the disease, influences the progression of the disease or if it is merely an opportunistic infection. This is an important distinction: in the United States more than half of adults have evidence of past infections (often asymptomatic) with *Chlamydia* by age 20 and re-infection throughout life is a common occurrence (4). It is estimated that 4 million people in North America have AD and that number is expected to triple in the next 40 years (4, 34). AD is the leading cause of dementia accounting for as high as 70% of the cases in the elderly (61). AD is the third most costly disease to treat and the cost to the US health care system exceeds more 100 billion dollars a year. If broken down the

cost average is $27,672 per person annually for formal care and between $10,400-$34,517 in lost wages and productivity (61). If *Chlamydia* species are implicated in the triggering or progression of AD, then *Chlamydia* infection is a major public health concern. It is therefore vital to determine what role, if any, *Chlamydia* plays in AD onset and progression.

Here I evaluate the impact of a *Chlamydia* infection on AD with the use of T_2-weighted MR images to study the AD plaque onset and pathology in transgenic mice. While this technique is one of the more simple MRI techniques in use, it has the following advantages: 1) Based upon studies by Wengenack 2008 *et. al.* and Braakman 2006, we know that it can provide the necessary information on plaque pathology, 2) it is technically simple to perform, 3) it is rapid, T_2-weighted imaging will require a maximum of 1 hour for implementation including the 20 minutes of imaging times needed for the actual T_2 study.

2. Materials and Methods

2.1 Mice:

The NRC-IBD Animal Care Committee approved animal-use protocols for the study. Experiments were followed in accordance with The Canadian Council of Animal Care (CCAC) rules and regulations. Ten B6C3-TG(APPswe, PSEN1dE9)85Dbo/J mice and ten Wt controls from the colony were purchased from The Jackson Laboratory (Bar Harbor, Maine, USA). Mice were quarantined upon arrival in the animal facility for one week for recovery from transportation stress and for an adjustment period.

2.2 *C. muridarum*

2.2.1 Culture:

C. muridarum was cultured in HeLa 229 cells containing 10% bovine serum and 2mM glutamine in Dr. Xi Yang's laboratory at the University of Manitoba. Organisms were purified by discontinuous density gradient centrifugation including 15 min at 500 X g and 30-min at 30, 000 X g as previously described (84). Cells were harvested using sterile glass beads and lysed using an ultrasonic device. Cells were resuspended in SPG (sucrose-phosphate-glutamic acid) buffer in aliquots of 1×10^5 inclusion forming units (IFU) and frozen at -70°C. The same stock of *C. muridarum* was used throughout the study.

2.2.2 Intranasal inoculations:

Intranasal inoculations were preformed in a biosafety cabinet. Mice were moved into a chamber and anesthetized using 4% isofluorane with 100% oxygen as a carrier gas.

After induction mice were placed on a pad surface with head positioned in a nose cone mask to maintain anesthesia at 1.5% isofluorane until a breathing rate of one breath per second was established. Using a 10-100 μL pipette, 50 μL of SPG buffer containing 1000 (10^3) infection forming units (IFU) of *C. muridarum* were suctioned from a stock solution. For non-infected mice 50 μL of SPG buffer without *C. muridarum* was administered at the same time point in the experiment. Buffer mix was slowly expelled, drop-by-drop, on to the nose of the anesthetized mouse. As the mouse inhales, the buffer was taken up through the nose. After administration of inoculum the mouse recovered in isolation and was provided soft food and water.

The IFU concentration for intranasal inoculations was chosen based on a previous study where similar C57BL/6 mice were infected with 1000 IFU *C. muridarum* (84). In the study mice were euthanized at different time points during acute infection. Lung tissue was homogenized and *C. muridarum* was recovered from the lungs and measured. The results showed significant IFU in the lungs of mice following a 1000 IFU inoculum of *C. muridarum*. Based on this evidence it was determined that infecting mice with 1000 IFU of *C. muridarum* would establish an acute infection in animals.

In this study ten APP/PS mice and ten Wt mice were divided into infected or non-infected groups, based on the type of intranasal inoculation administered: five APP/PS mice were intranasally infected with 1000 IFU *C. muridarum* and five APP/PS mice were administered a sham SPG buffer inoculation. The ten mice in the Wt group were also divided into infected and non-infected groups. The total mouse population of this study was thus divided into four groups with five animals per group:

1. Five Wt non-infected mice
2. Five Wt *Chlamydia* infected mice
3. Five APP/PS non-infected mice
4. Five APP/PS *Chlamydia* infected mice

2.3 Serology:

Serum samples were collected from mice during euthanasia at 20 months for serological studies. Serum samples were transported to the University of Manitoba, Medical Microbiology Department for testing using an enzyme linked immunosorbant assay (ELISA). For the ELISA, each well in two flat bottom 96 well ELISA plates (Corning Science Products, Corning, NY, USA) was coated with C. *muridarum* antigen by aliquoting 50 μL coating buffer (bicarbonate buffer 0.05 M at pH 9.6) containing $1x10^5$ IFU/mL *C. muridarum* EBs. Plates were covered with parafilm and placed at 4°C overnight. The following day coating buffer was discarded and 200 μL of blocking buffer (2% BSA and 0.05% Tween 20 solution) was added to each well, covered with parafilm and incubated at room temperature for two hours. Blocking buffer was discarded and plates were washed with washing buffer (phosphate buffered saline containing 0.1% v/v Tween 20) four times.

Serum samples were diluted to a 10% solution for the primary Ab binding step by adding 10 μL of sample to 90 μL dilution buffer (1x blocking buffer). A Sequential 1:2 serial dilution was conducted to a maximum dilution factor of 128x. Plates were covered with parafilm and incubated at 37°C for 3 hours. Plates were washed four times with washing buffer following the primary Ab-binding step. For the secondary Ab binding

step 50 µL aliquots of the antibody solution, included a 1 µg/mL dilution of biotinylated goat anti-mouse IgG2a or a 1 µg/mL biotinylated goat anti-mouse IgA (Southern Biotechnology Associates, Inc., Birmingham, AL) in dilution buffer, were added to each well. Plates were covered with parafilm and placed overnight at 4°C. The following day the secondary antibody solution was discarded from the plates, followed by four washes in washing buffer. A stock solution of alkaline phosphatase-conjugated streptavidin (Jackson ImmunoResearch Laboratories, Mississauga, Canada) was diluted 1:6000 in aliquots of 100 µL per well. Plates were covered with parafilm and incubated at 37°C for approximately 50 minutes followed by six washes in washing buffer. After the final wash step 100 µL of substrate buffer (*p*-nitrophenyl phosphate in 0.5 mM $MgCl_2$, 10% diethanolamine, pH 9.8) was added to the wells. The substrate buffer interacts with the streptavidin-biotin complex, which caused an enzymatic reaction resulting in a color change from clear to yellow in the sample. Optical density (OD) values were calculated at 405 nm at 15 minutes on a microplate reader (Versamax; Molecular Devices). Light at 405 nm is passed through the sample, the resulting absorbance associated with the color change from the enzymatic reaction between the streptavidin-biotin complex and substrate buffer is read as an OD value. OD values were recorded and transferred to Microsoft Excel for statistical analysis (See appendix 1). Results were obtained after 15 minutes using the endpoint $OD_{0.5}$ value at 405 nm.

2.4 MR experiments:

2.4.1 Anesthetic preparation and induction:

The induction chamber was placed in the biosafety cabinet and the anesthetic and scavenger lines were connected to a rubber stopper. Mice were obtained from the animal facility; for infected mice the cages were placed in a large plastic bag before exiting the infected mouse room to prevent spread of infection through the facility. Experiments on control and infected mice were performed on different days to prevent accidental spread of *Chlamydia* infection to non-infected mice. The mouse was placed in the induction chamber and the end was covered with the rubber stopper connected to gas and scavenging lines. Isofluorane anesthetic was delivered at 3.5% in 1 liter of oxygen per minute until the mouse no longer displayed a righting reflex. After an absence of this reflex, animals were removed from the induction chamber.

2.4.2 MR experiments preparation:

After initial induction, the anesthetic line was removed from the induction chamber and attached to the MR imaging probe while working inside the biosafety cabinet (Figure 7). Two sets of imaging probes were used for MR experiments: one for non-infected mice and one for infected mice. The anesthetic line to the probe was flooded prior to removing the mouse from the induction chamber. The mouse was then moved from the induction chamber to the imaging probe, and its muzzle was positioned in the probe's nose cone (Figure 7). Anesthetic levels were adjusted to achieve a respiration rate of 1 breath per second. Eye drops were placed in each eye to prevent

Figure 7: The MR probe.
The components of the in house built MR probe (appendix 3), including mouse bed, surface coil and cover A). The surface coil is inserted into the mouse bed B) and the mouse is positioned with the head adjacent to the coil C). A nose cone was secured to the bed and connected to an anesthetic line D). Holes were drilled in the base of the probe for the respirometer wire attached to a Grass instrument and rubber tubing lines connected to the water bath E). When positioned correctly the cover is placed over the probe F).

A)

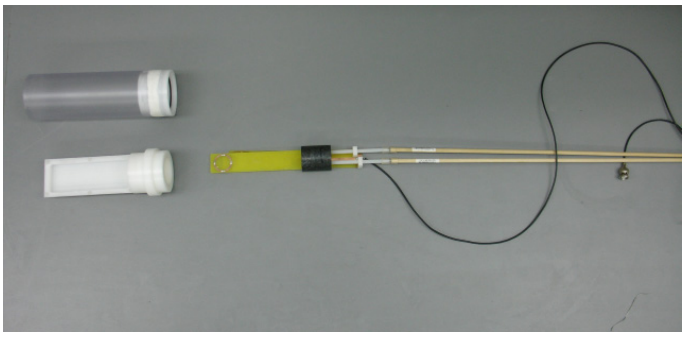

B)

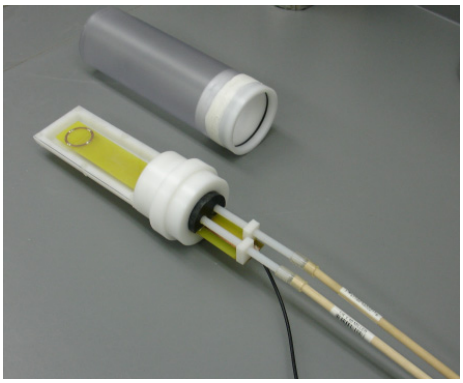

C)

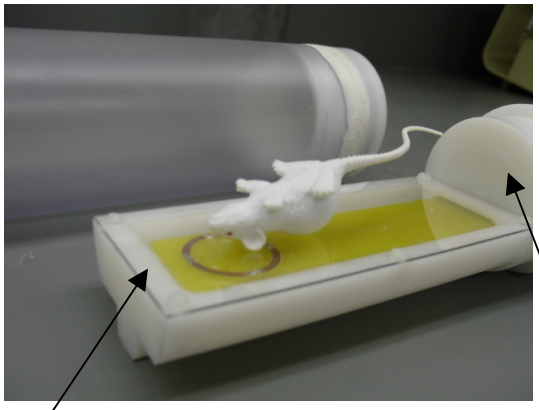

D

E

F)

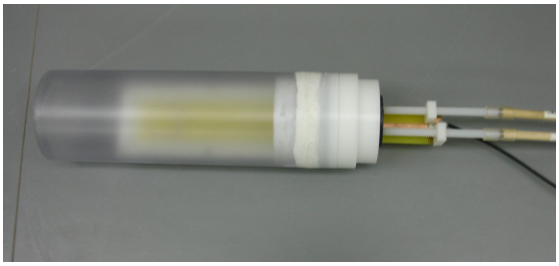

drying of the corneas during the duration of the experiment by gently spreading the eyelids and applying drops to the surface.

The mouse was positioned by securing the animal with a loose fitting abdominal strap to prevent movement in a vertical position used for MR experiments (Figure 8). The eyes were aligned with the top of the surface coil and a small foam wedge was inserted between the top of the mask and the jaw. The wedge ensured CO_2 was allowed to escape the anesthetic mask during imaging and immobilized the animal's head against the chamber adjacent to the surface coil to reduce possible motion artifacts in the MR images. The wedge was lightly taped into position to ensure the throat was not constricted and to extend the neck to provide a straight airway. Gauze was layered under the tail to provide further support when the mouse would be placed in the vertical position within the magnet. The mouse was also strapped across the hips of the hind legs for support. A respirometer probe was taped to the chest to monitor respiration during the experiment, care was taken to ensure that there was no constriction of chest or extremities that could affect respiration or blood flow. Lastly, the tail was taped to the respirometer to prevent an injury to the tail when the cover was slipped over the probe.

The holder and probe were held in a vertical position to check for any significant changes in position or respiration. If a major shift in position was observed or if respiration was affected the animal was repositioned before continuing. The probe was slid into the holder and inserted into the vertical magnet bore of the 11.7 T magnet (Figure 8). Anaesthesia and scavenging lines and water bath tubes were connected. The respirometer cable was connected to a Grass instrument (EEG and Polygraph data recording system, Model 7P4K and 7DAH, Grass Instruments Co. Quincy Mass, USA) to

Figure 8: The 11. 7 T magnet.
The 11.7 T vertical bore magnet used to acquire images in MR experiments.

monitor respiration during MR experiments. The chamber temperature was heated by running hot water from a water bath through the chamber with rubber tubing. A thermocouple was used to measure the temperature inside the probe during MR experiments. Initial respiration rate was recorded and anesthetic flow was adjusted to achieve a rate of one breath per second. Respiration rate was continuously checked and recorded on paper at 15-minute intervals.

2.4.3 T_2 MR imaging:

Mice were imaged at timed intervals on the 11.7 T magnet. The average experimental time was 30 minutes. The surface coil was tuned and matched at 500 MHz for each mouse using a Morris Instruments Inc (Gloucester, ON) frequency sweeper. The coil was connected to the pre-amplifier and the experiment was started.

The position of the mouse's head was checked using the MR position protocol. The position of the probe was adjusted to optimize of the signal. After positioning the magnetic field was shimmed with an offset of 2500 Hz using the linear shims. The one pulse experiment was used to create a uniform magnetic field and set the frequency prior to MR experiments. Scout images were acquired using a gradient echo sequence (sagittal and axial) to determine the position of the brain. After scout images were acquired, a spin-echo T_2 weighted experiment was conducted to acquire ten adjacent slices with 6 echoes per slice. The orientation of slices was checked using a geometry editor by loading the last sagittal gradient echo as a reference (Figure 9). Slices were adjusted to make sure all 10 slices covered the brain. The basic measurement parameters included: a multi-slice, multi-echo spin-echo pulse sequence (MSME), echo times (20, 40, 60, 80,

Figure 9: The geometry editor.
The geometry editor function was used to determine the orientation of slices in MR experiments. Orientation was established by first finding the centre of the brain in a gradient echo coronal scout A) and then arranging slices throughout the entire brain by adjusting the slices in a gradient echo sagittal scout B).

A)

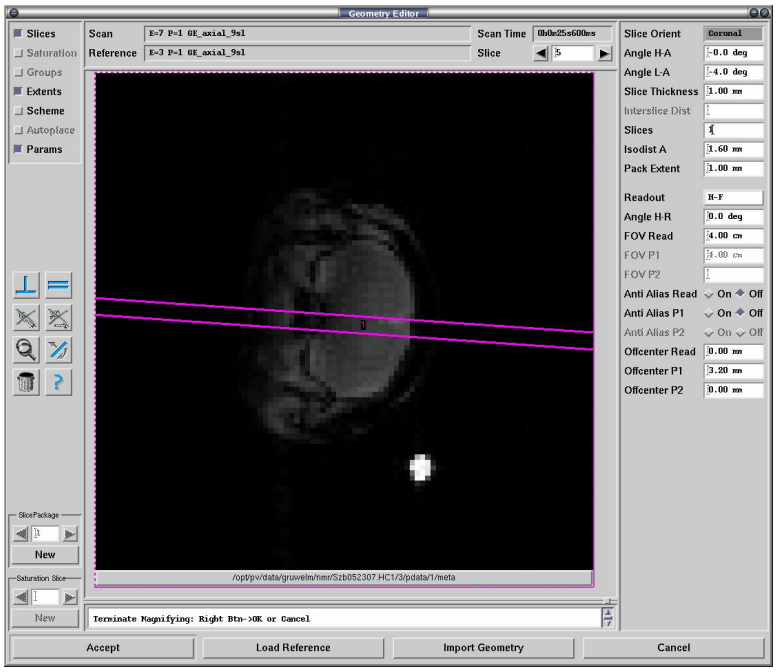

B)

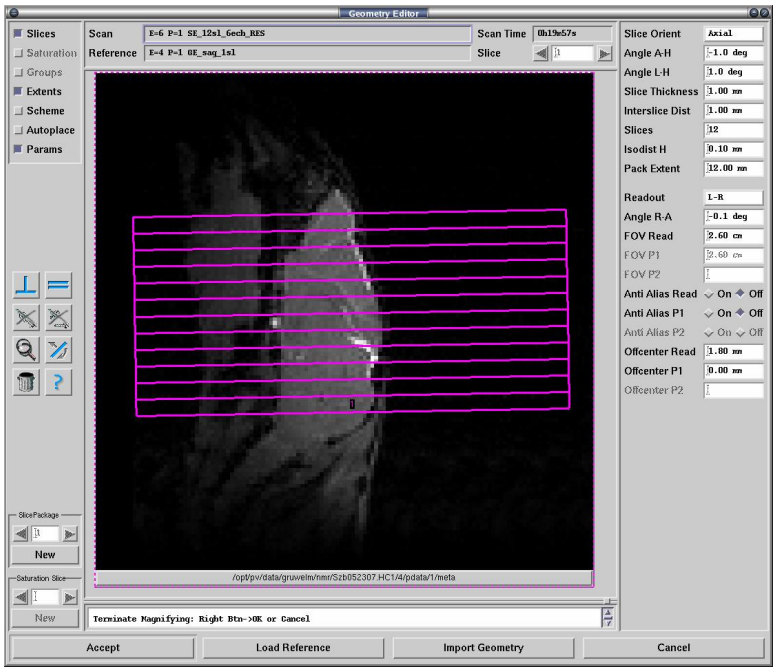

100 and 120 ms), repetition time = 1700ms, averages = 2, field of view = 26 x 26 mm and image matrix = 350 x 350. This provided an effective in-plane resolution of approximately 74 x 74 μm^2. In order to model plaque progression in non-infected transgenic mice as well as to observe effects of infection on plaque progression in infected transgenic mice, all APP/PS mice were imaged at two week time intervals. Wt mice were imaged at two-month intervals to observe T_2 changes in a healthy mouse and to establish a baseline measurement to compare the findings in the APP/PS plaque progression model. Secondly it was important to determine if a *C. muridarum* infection had an impact on T_2 in the Wt mice. Thus ten APP/PS mice were imaged in two-week intervals while ten Wt mice were imaged at 2-month intervals.

2.5 Euthanasia, blood collection and tissue harvesting:

Mice were anaesthetized in accordance with section 2.4.1. A breathing rate of 1 beat per second was established before conducting the cardiac blood draw. It was confirmed that palpebral (blink) and toe pinch/hind limb reflexes were absent to ensure the animal was fully anesthetized before proceeding.

Blood samples were acquired via cardiac puncture with indirect visualization of the heart ventrally below the xyphoid process. Contact with other tissues was minimized during the cardiac puncture procedure. A 23-gauge 3/4" needle attached to a 1 cc syringe was inserted into the left ventricle and blood was withdrawn gradually, allowing the heart to refill. A 0.5 -1.0 mL volume of blood was sufficient for serology tests and was easily withdrawn from mice weighing 25-30 grams. Blood was transferred into a pre-labeled serum tubes and stored in the refrigerator temporarily at 4°C. Usually 1.0 mL of blood

collection results in death, however prior to harvesting the brain tissue verification of death was confirmed. Steps included palpitation for heart pulse and observation of possible chest movement for respiration. If heart rate and respiration was verified then 0.2 mL of euthanyl (pentobaribital) was administered by intraperitoneal injection or intracardiac injection.

Blood samples were spun in the serum tube in a microcentrifuge at 13 000 X g for 7-10 minutes. Serum was separated from other components of blood in the supernatant, drawn off using a 100-1000 μL pipette and deposited into its corresponding 1.5 mL labeled tube. After processing, samples were placed at -80 °C for long-term storage. The brain was harvested and sliced into left and right hemispheres using a razor blade. The left side was fixed in 10% formalin for histological staining and the right side was frozen in cryotubes and store at -80 °C for further analysis.

2.6 Histology:

2.6.1 Congo red stain:

Tissue from the left side of the brain was sent to the Government of Manitoba Veterinary lab (545 University Crescent, Winnipeg, MB, Canada) for analysis. Anterior and posterior slices were selected for Congo red staining (Figure 10). A detailed procedure outlining the steps for Congo red staining has been included in Appendix 2. Anterior and posterior slices were selected by normalizing from the bregma landmark on the skull for consistency. Bregma is a standard reference point used to define sections in rodent brain libraries (18). The distance, either anterior or posterior, from bregma (in mm's) defines each coronal section in the library. The ROI in each section was observed

Figure 10: Histological slide demonstrating anterior and posterior slices.
A sample slide containing mounted Wt non-infected mouse left brain tissue slices stained with Congo red. A) Forebrain slice at 0.26 bregma and B) posterior slice at –1.70 bregma. The hippocampus and cortex can be distinguished in section B.

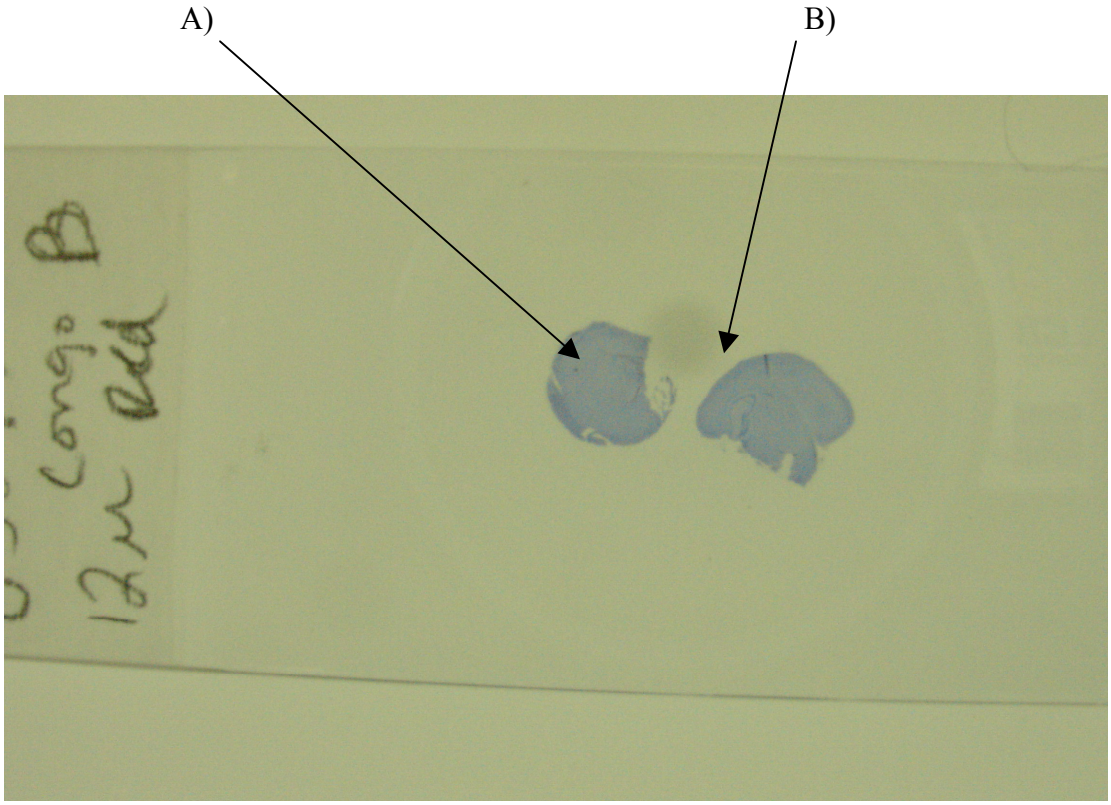

with the Olympus CX41 microscope using 100x optical zoom. The ROI image was captured using the Infinity 1 Digital Camera Kit with Infinity Analyze Software (Media Cybernetics Inc. Bethesda, MD, USA).

2.6.2 Selecting ROIs for histology:

The size of the ROI was determined using a special ruler where each line was 10 μM in length (Figure 11). Each ROI had a height of 420 μm and a length of 560 μm for a total area of 0.2352 mm^2. Two slices were sectioned and stained with Congo red for each mouse in the study, one slice was in the anterior part of the brain at approximately 0.38 bregma and the other in the more posterior area at approximately –1.70 bregma (Figure 12). Three regions were chosen from the anterior slice including the cingulated/motor cortex (motor cortex), somatosensory/audiosensory cortex (somatosensory cortex) and striatum (Figure 12). Three regions were chosen from the posterior slice including the retrosplenial cortex, somatosenosry cortex and hippocampus (Figure 12). For the motor cortex and retrosplenial cortex regions, the ROI was positioned above the corpus callosum. Somatosensory regions were identified by lining up the ROI with either the external capsule in the anterior slice or hippocampus in the posterior slice (Figure 12). The hippocampus region was determined by fitting the ROI into the entire hippocampus region on the slice.

Plaques were counted using the counting tool in the Infinity Analyze software and then counted a second time in an enlarged image to confirm original findings (Figure 13). Plaques counts were evaluated using the plaque core as a marker to avoid overestimating counts in cases where components of a plaque had been separated from the core.

Figure 11: The stage micrometer observed at 100x optical zoom.
Ruler measurement at 100x optical zoom was used to calculate plaques per mm^2 for histology and to determine ROI size in MR analysis.

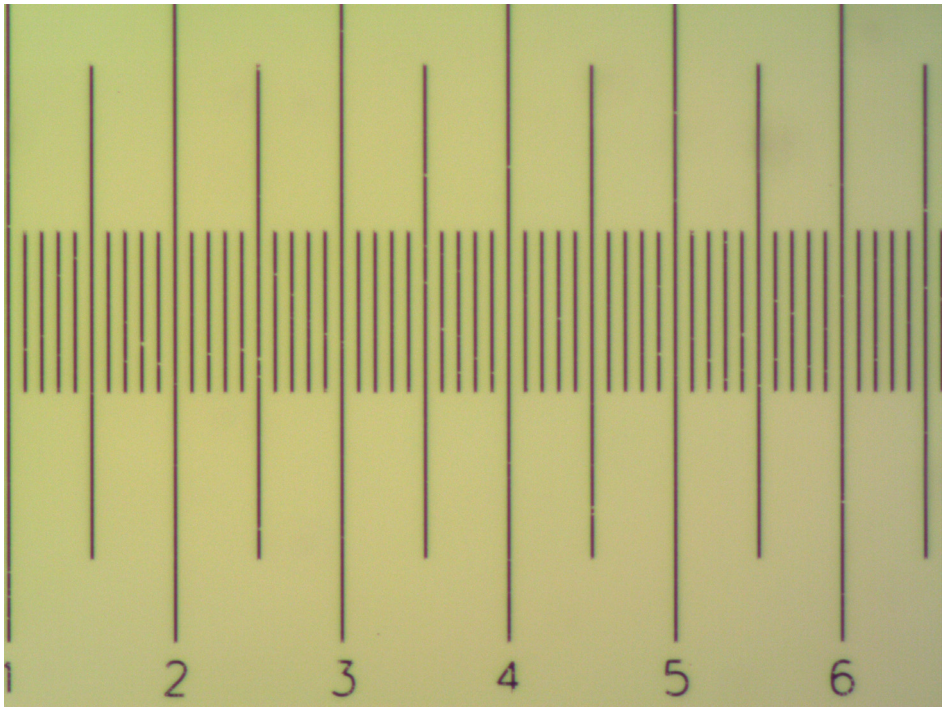

Figure 12: Mouse brain library images at –1.64 bregma and 0.38 bregma (65). Images of brain sections from a C57BL/6 mouse obtained from the Mouse Brain Library (65). A) Anterior slice observed at 0.38 bregma and B) posterior slice positioned at –1.61 bregma. Notable structures include i) cortex regions, ii) striatum and iii) hippocampus.

A)

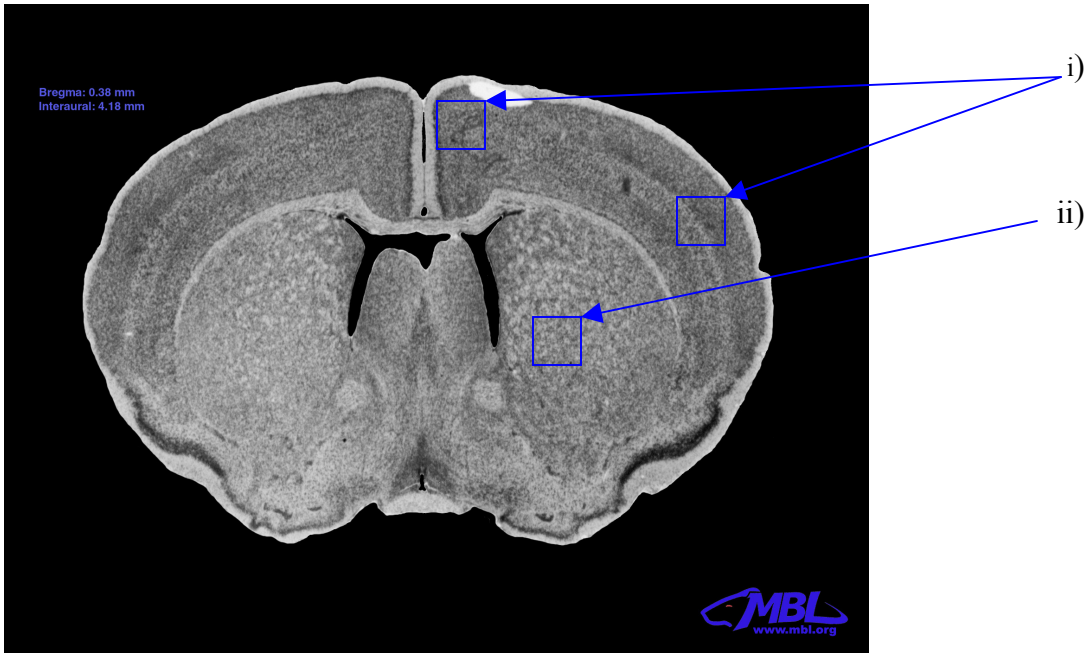

B)

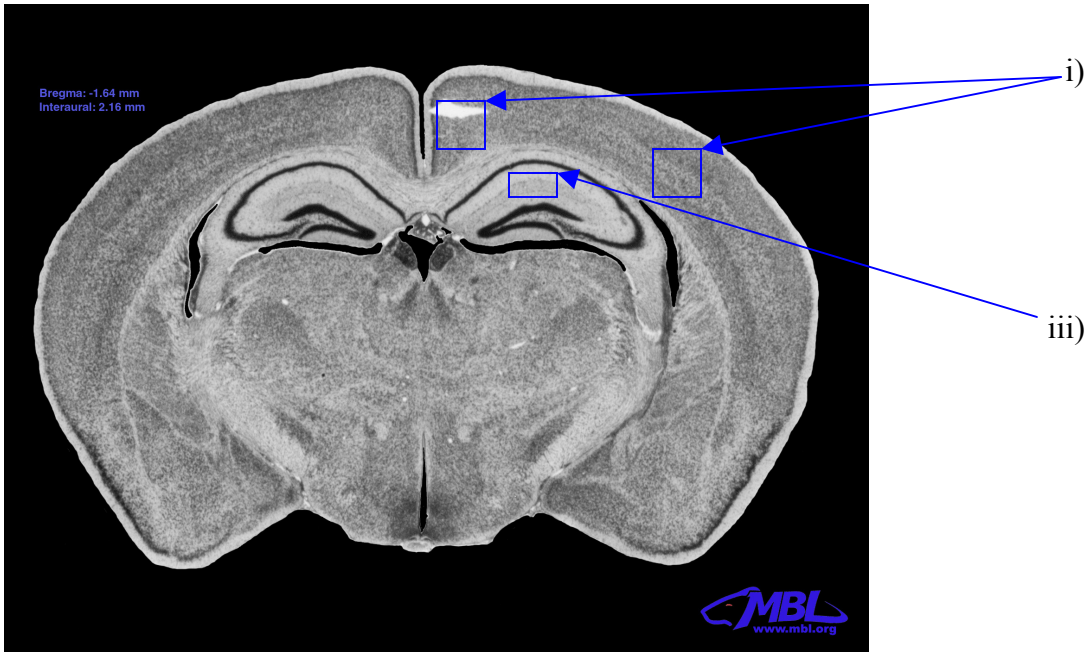

Figure 13: Plaques counts at 100x optical magnification.
An example of plaque counts in the hippocampus of infected APP/PS mouse. Plaque burden was determined by using the counting tool using Infinity Analyze software.

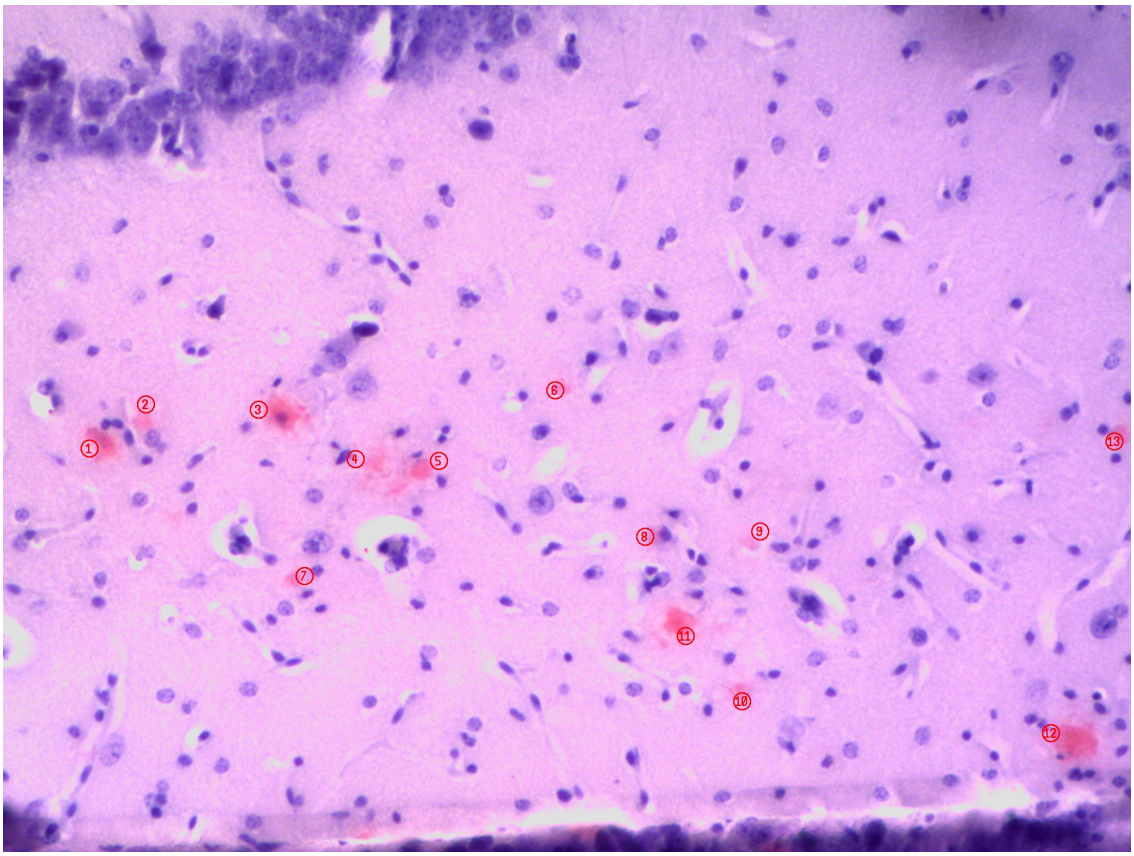

2.7 Determining ROIs for MR images:

ROIs in the MR images were selected based on previous findings of plaque pathology in areas of the hippocampus and cortex regions. ROI sizes were determined by correlating histology data ROIs so the measured areas were of the same size. The individual pixel size in the MR images was derived from the resolution of the image (74 μm x 74 μm).

$$74\ \mu m\ \text{x}\ 74\ \mu m = 5476\ \mu m^2 = .0055\ mm^2$$

To determine ROI size for MR analysis, the total ROI area used in the histology assay was divided by the individual pixel size to provide the number of pixels for the MR ROI.

$$0.2352/0.0055 = 43 \text{ pixels}$$

A standard shaped ROI is easier to analyze then an irregular shaped ROI. In histological analysis a rectangle was chosen for the ROI shape. For consistency a rectangle of the same area (43 pixels) was selected for MR studies. MR was analyzed using Marevisi 7.2 software (NRC-IBD, Winnipeg, MB). A total of six ROIs were examined, two on the anterior slice and four on the posterior slice at specific time points ending at 20 months of age (Figure 14).

Figure 14: An example of ROIs measured using Marevisi software.
An example illustrating the selected ROIs in anterior and posterior slices of an APP/PS transgenic mouse at 10 weeks. Three symmetrically placed ROIs are shown, including the motor cortex in A), and the retrosplenial {1, 2} and hippocampus {3, 4}in B).

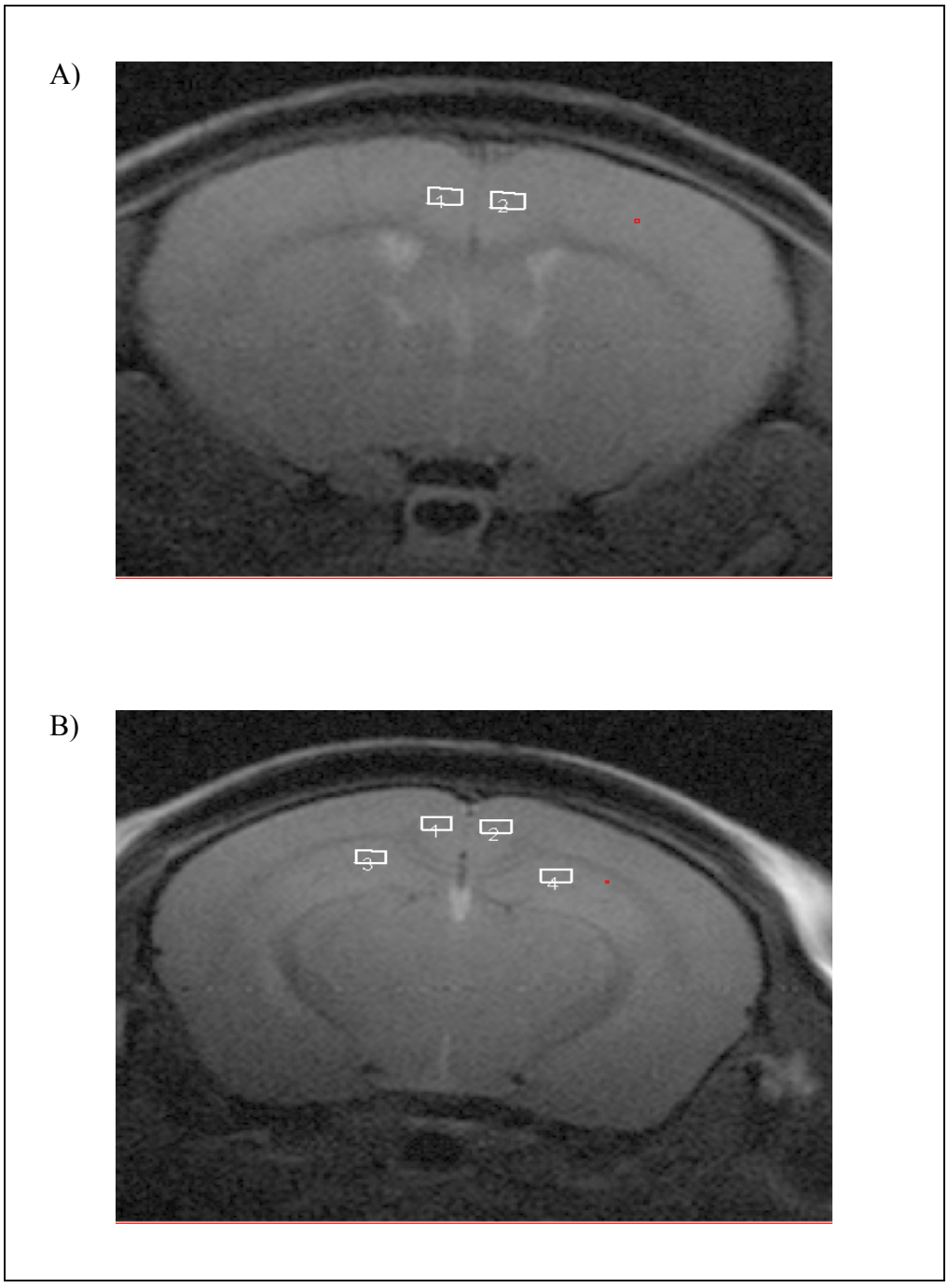

2.8 Statistical analysis:

2.8.1 Histology data:

For histology studies plaque burden was calculated in six ROIs (the anterior and posterior somatosensory cortex, striatum, hippocampus, motor cortex and retrosplenial cortex). Plaques were counted in APP/PS non-infected and APP/PS infected mice. The mean plaque count was calculated for each area and APP/PS non-infected mice were compared to APP/PS infected mice using a Student's t-test. The overall plaque burden was determined by counting plaques in ROIs and pooling the data for both the APP/PS non-infected group and APP/PS infected mouse groups. p-Values were calculated using a Student t-test and the error bars represent standard error of the mean (SEM) (86).

2.8.2 MR imaging data:

For MR studies, hippocampus and cortex regions were compared in the initial (month 2), month 5, month 10 and final (month 20) time points. Measurements were collected from both the right and left side for each ROI. T_2 values for each ROI were compared at each of the four time points using a parametric paired Student t-test (86). In cases where variances differed significantly, a non-parametric Mann-Whitney U-test was used to compare differences in T_2 times (86).

A Duncan's multiple range test was conducted to determine changes in T_2 within each group (86). p-Values were attained from repeated measurements within each group and results were considered statistically significant for $p<0.05$ compared using 95% confidence intervals. Within group tests across times have more statistical power than

between group tests because for within group tests animals are treated as their own controls.

3. Results

3.1 *Chlamydia muridarum* infection:

3.1.1 Body weight change:

Weight loss is an indictor of the overall heath of the mice. A decrease in body weight of approximately 20% was observed in 9 to 11 week old WT mice infected with 1000 IFU *C. muridarum* at 9 days post infection (DPI) (Figure 15). APP/PS infected mice displayed body weight loss ranging from 8%-15% that was not synchronous; therefore weight loss is displayed in a table rather then in the figure (Appendix 3). Non-infected mice intranasally inoculated with 50 μL SPG buffer showed a steady increase in body weight (Figure 15). By approximately 15 DPI in Wt mice and 28 DPI in APP/PS mice, the pattern of weight gain exhibited in *C. muridarum* infected mice mirrored weight gain in non-infected mice (Figure 15).

3.1.2 Visual observations/Animal monitoring:

In the early stages of infection (7 DPI) some mice had piloerection and appeared hunched when walking around the cage. Infected mice were more lethargic than control mice. At 14 DPI observations included piloerection and abnormal posture. By 21 DPI mice were observed exhibiting good grooming habits indicating recovery from acute infection. Mice were observed building nests during the period of infectivity. No unusual activity was observed subsequent to the acute infection.

Figure 15: Changes in body weight.
Changes in body weight observed in APP/PS and Wt mice inoculated with either 1000 IFU of *C. muridarum* biovar in SPG buffer or sham inoculum (SPG buffer only). Error bars represent SEM (n=5 APP/PS infected, n=5 APP/PS non-infected, n=3 WT infected, n=5 WT non-infected).

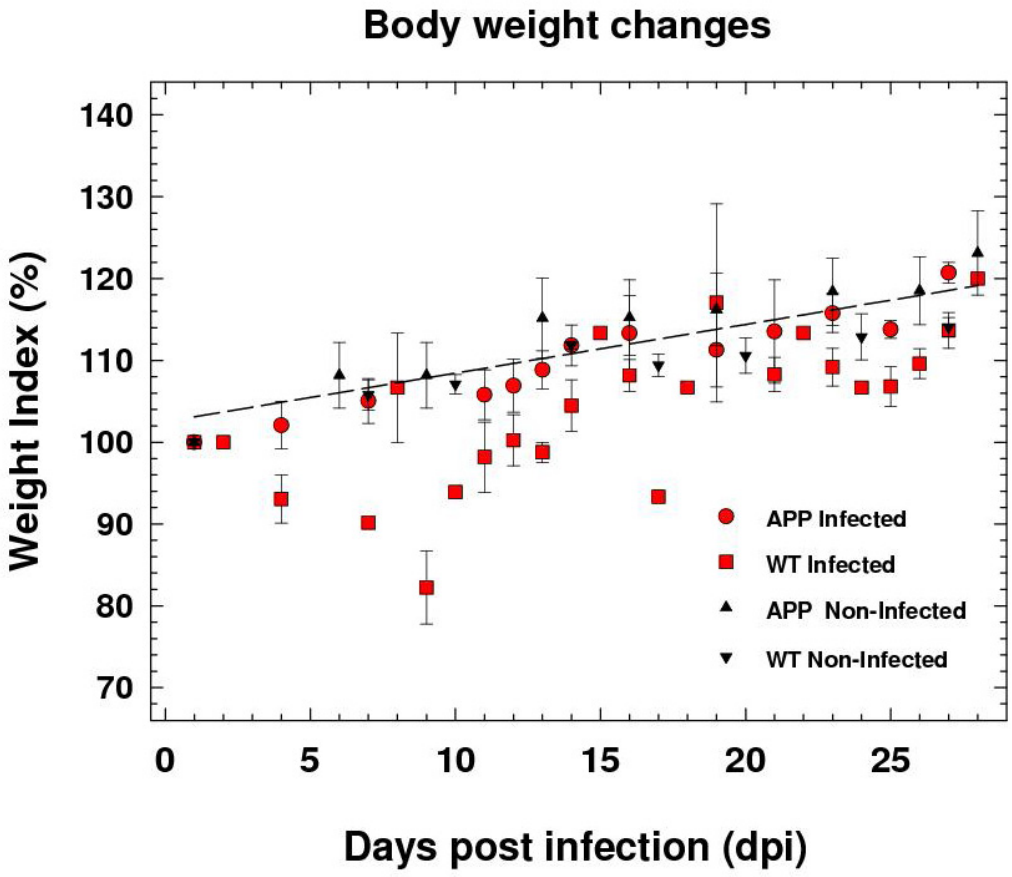

3.1.3 Serology:

Infected mice showed elevated levels of IgA and IgG2a Ab's specific to *C. muridarum* in serum samples collected at 18 months post infection (Appendix 4). Infected mice exhibited an average IgA titre of 2.86 ±0.46 and an average IgG2a titre of 3.09 ±0.28. Titres were calculated from the dilution factor where $OD_{.50}$ values were read from a microplate reader ($OD_{0.5}$ readings were compared as this ensures all readings are on a linear part of the instrument response curve). Ab titres are presented in Log_{10} values. A representative ELISA curve profile is displayed in Figure 16. Non-infected mice displayed very low $OD_{0.5}$ readings for IgG2a and IgA in serum samples collected at 18 months post infection (Figure 16). This translates into an insignificant or the complete absence of an Ab titre in non-infected mice (Appendix 4).

In some cases sera from infected mice were unable to be accurately read in the microplate reader due to a saturation of signal to the detector. This observation is due to a presence of high Ab concentration. In these cases Ab titres were estimated by predicting values from a least squares regression line derived from experimental values in the corresponding serial dilution (2x to 128x) (Appendix 1).

3.2 Histology plaque progression measurements:

3.2.1 Location of AD plaques in mouse groups:

There was no observed plaque pathology in Wt infected and non-infected mice in tissue sections stained with Congo red dye. Tissue sections from the retrosplenial cortex are depicted in a Wt non-infected mouse and Wt infected mouse (Figure 17). Plaque pathology was not observed in any regions examined in the Wt groups at 100x

Figure 16: IgA Ab response in *C. muridarum* infected and non-infected mice.
A typical ELISA curve profile comparing Wt infected Mouse 10 and APP/PS infected Mouse 13 with a non-infected APP/PS mouse (Mouse 5). Curves depicted illustrate differences in IgA level in serum of mice by optical density readings at 405 nm with respect to dilution factor. Results were acquired using a 1:2 serial dilution. Raw data can be viewed in Appendix 1.

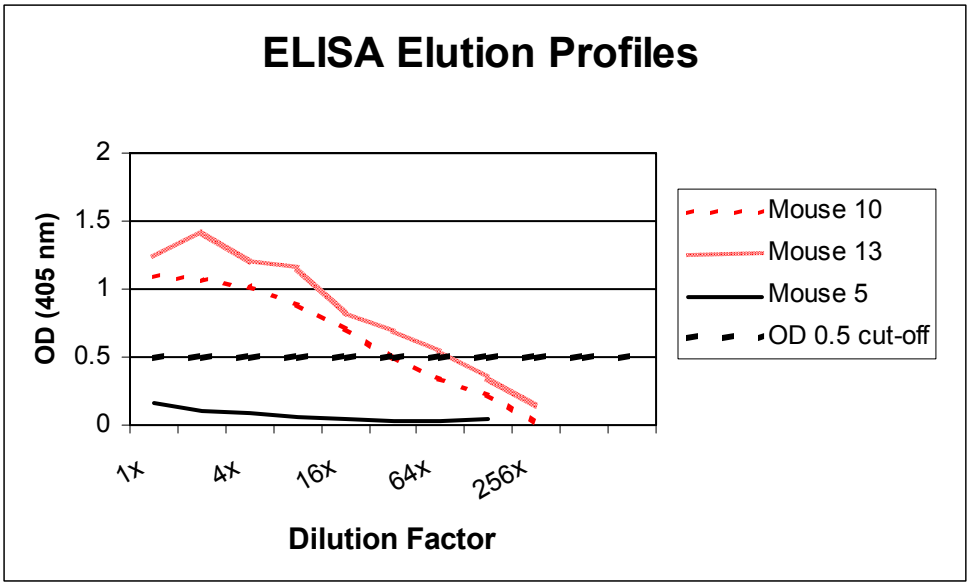

Figure 17: Sections from Wt mice stained with Congo red dye (enlarged 100x). Plaque pathology was not observed in A) Wt non-infected and B) Wt infected mouse brains. Representative Congo red stains are from the retrosplenial cortex region in the posterior slice.

A)

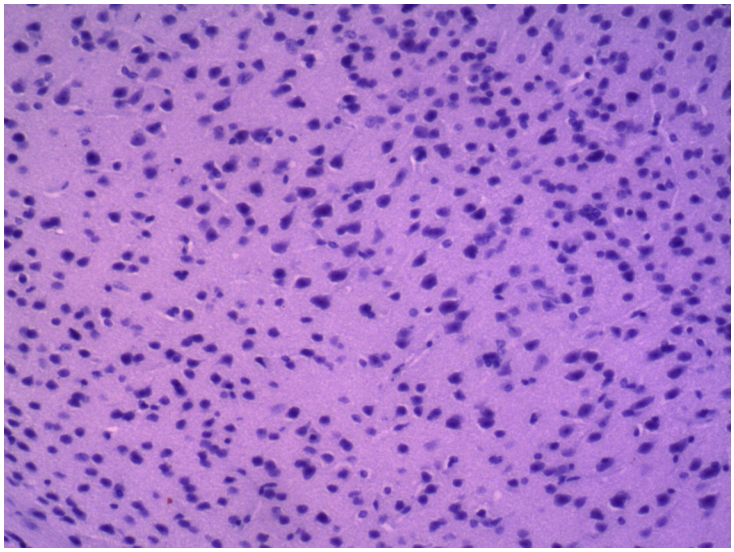

B)

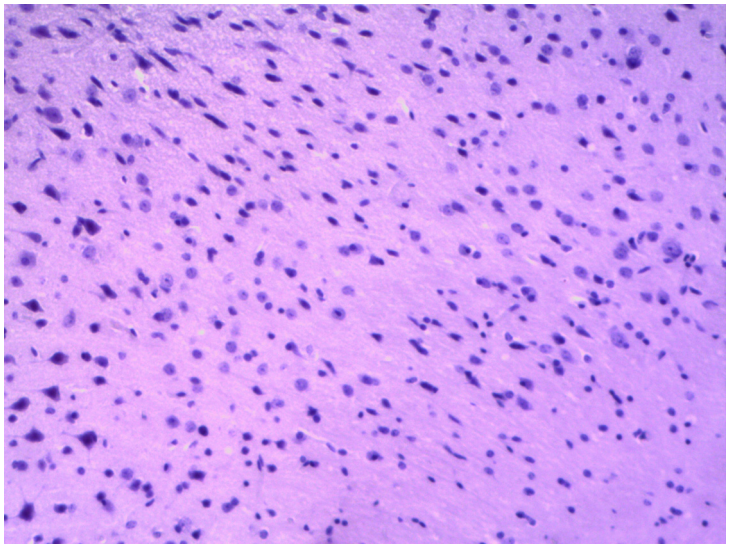

magnification, as shown in representative posterior tissue sections stained with Congo red in figure 17. A sample APP/PS mouse is included to show a positive result in the Congo red stain (Figure 18). In this figure, the motor cortex region in the anterior slice for Wt non-infected mouse and APP/PS non-infected mouse are shown at 40x total magnification for orientation purposes. The area is then viewed at a total magnification of 100x to observe AD plaque pathology in an APP/PS mouse and an absence of plaque pathology in a Wt mouse (Figure 18).

3.2.2 Overall plaque burden:

Plaque pathology was observed in both the non-infected APP/PS group and the APP/PS infected group (Figure 19). A comparison of a Congo red stained tissue section of the hippocampus from a Wt non-infected, an APP/PS non-infected and an APP/PS infected mouse is shown in figure 19. The total plaque burden was calculated by counting plaques in each of the 6 previously described ROIs. The total plaques for each mouse were added together and the mean was calculated from 4 APP/PS in the non-infected group and compared to the mean of 4 mice in the APP/PS infected group. The mean value calculated for each of the two groups is an indicator of the overall plaque burden and will be referred to as such. The mean plaque counts were 46.75±8.59 in the non-infected APP/PS group and 68.25±10.16 in the infected APP/PS group (Figure 20). Error bars represent standard error of the mean (SEM), see Figure 20. A Student t-test was conducted to determine if overall plaque burden differences between the APP/PS non-infected group and APP/PS infected group were significant. A p-value of 0.157 was found, indicating the change was not significant.

Figure 18: A comparison of tissue sections stained with Congo red dye.
Motor cortex anterior regions in a Wt mouse (A, C) and APP/PS mouse (B, D) enlarged to 40x (C, D) and 100x (A, B).

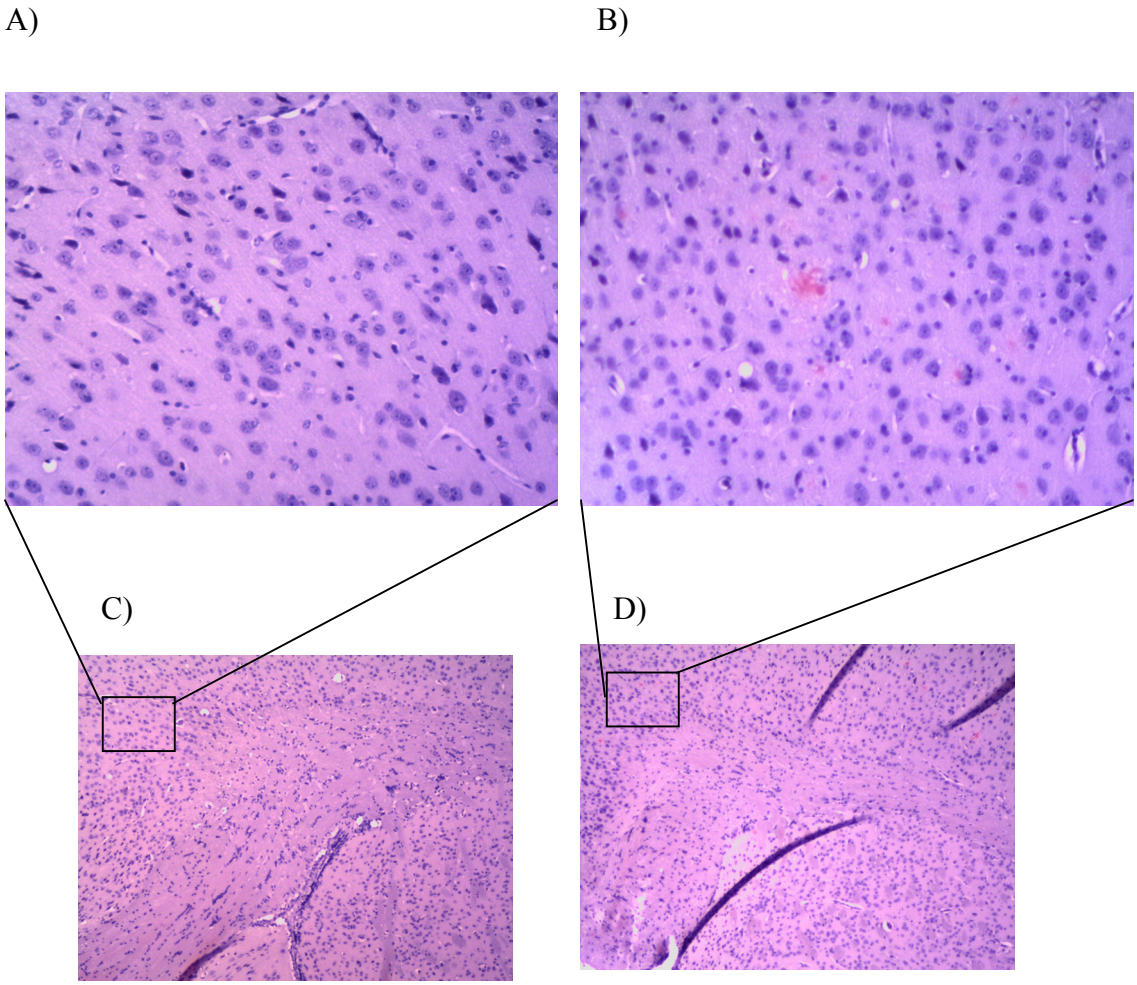

Figure 19: Examples of brain tissue sections stained with Congo red.
Representative histology at 100x magnification from the hippocampus region of a Wt non-infected (A), APP/PS non-infected (B), and APP/PS infected mouse.

A)

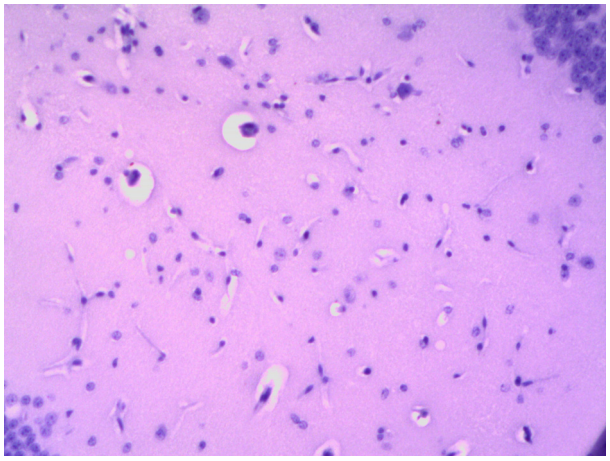

B)

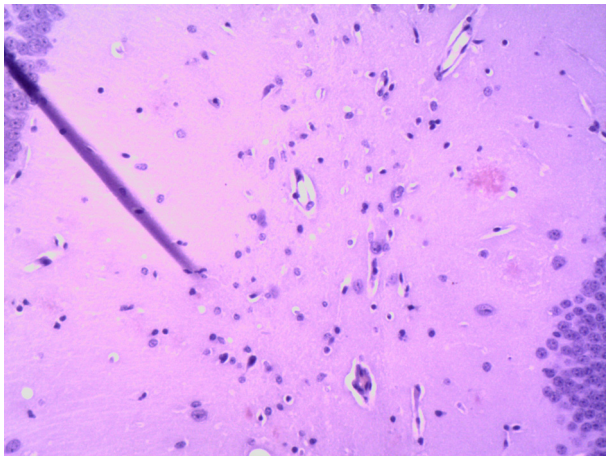

C)

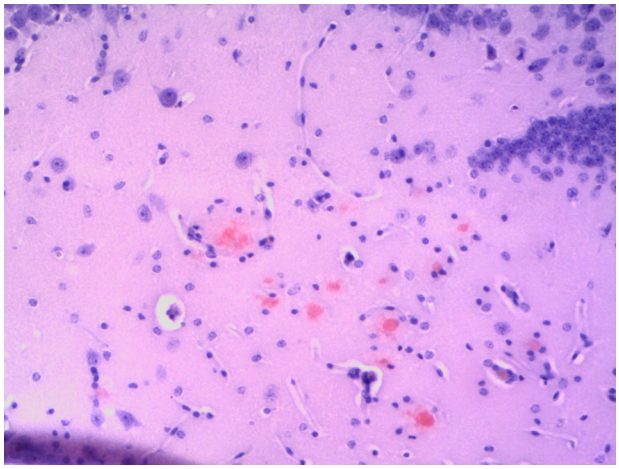

Figure 20: Overall plaque burden in APP/PS mice.
Overall plaque burden calculated in APP/PS control mice and APP/PS mice infected with 1000 IFU *C. muridarum*. The total mean plaque burden was calculated at month 20 by averaging the total number of plaques for all ROIs per mouse and then determining the overall average number of plaques per group. Error bars represent SEM and a Student t test determined p= 0.157.

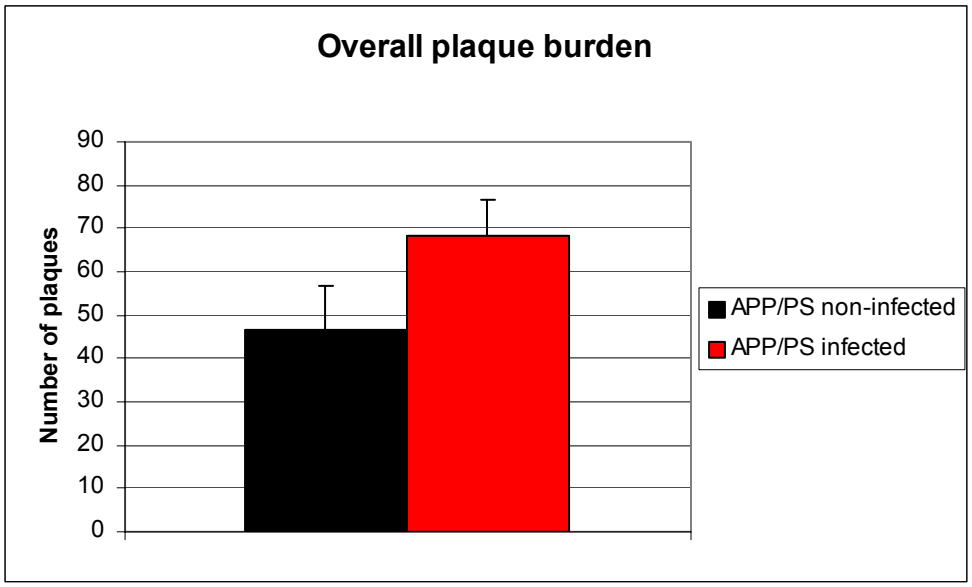

3.2.3 Plaque distribution:

An assessment of plaque distribution was conducted by comparing a single ROI in the APP/PS non-infected group to the same ROI in the APP/PS infected group. Higher plaque counts were found in the infected group in 5 out of the 6 ROIs selected (Figure 21). Higher plaque counts were observed in hippocampus (p=0.121) and striatum (p=0.131) in the APP/PS infected group when compared to the APP/PS non-infected group (Figure 21). Higher plaque counts were also observed in regions of the motor (p=0.332), retrosplenial (p=0.254), and anterior somatosensory (p=0.729) cortex regions (Figure 21). There was very little variation in plaque burden when comparing areas of the somatosensory cortex in both anterior and posterior slices (p=0.729 and p=0.746). The only region where plaque counts were higher in the APP/PS non-infected group compared to APP/PS infected group, however, without statistical significance, was in the posterior somatosensory region (p=0.746). p-Values for comparing plaque distributions were calculated using Student t-tests.

3.3 Longitudinal study:

3.3.1 MR results overview:

A total of 15 mice were assessed for changes in MR T_2 relaxation times. A summary of MR findings is displayed in Figures 22-24. Each group was evaluated at time points of 2 months, 5 months, 10 months and 20 months. Originally 20 mice were allocated for MR testing at the beginning of the experiment. In order to include individual mouse data sets for MR evaluation, it was required that the mouse survived to the endpoint of the experiment (20 months). As a result, data sets consisted of 4 mice in

Figure 21: A comparison of average plaque burdens in different ROIs.
A comparison of plaque deposition in different ROIs including 1) retrosplenial cortex, 2) hippocampus, 3) posterior somatosensory cortex, 4) motor cortex, 5) anterior somatosensory cortex, and 6) striatum at month 20. Plaque burden is determined based on plaque count and error bars represent SEM.

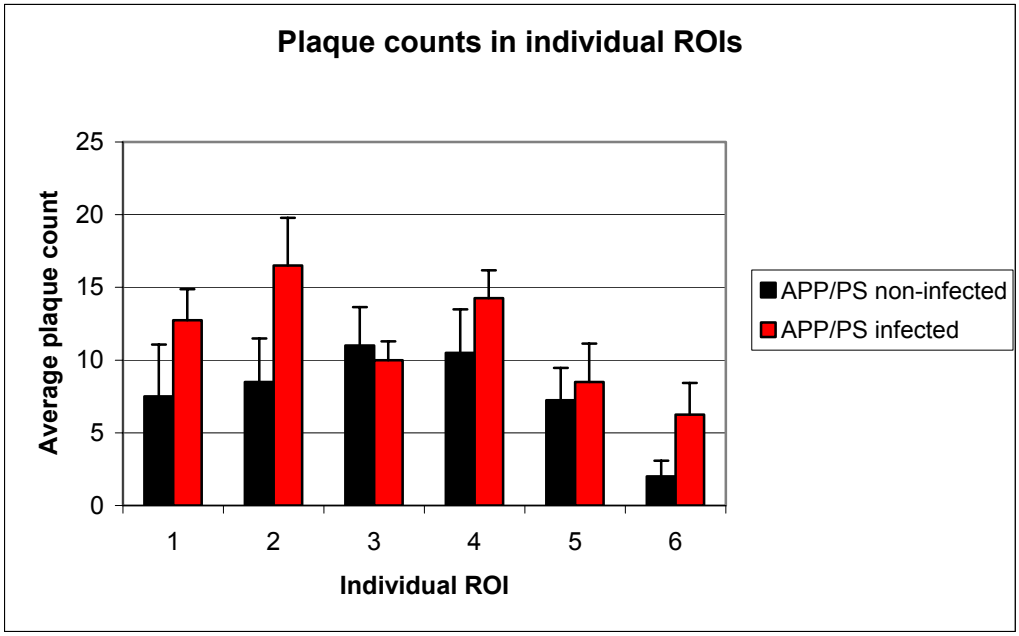

Figure 22: A T_2 comparison summary of right (A) and left (B) motor cortex regions.

A)

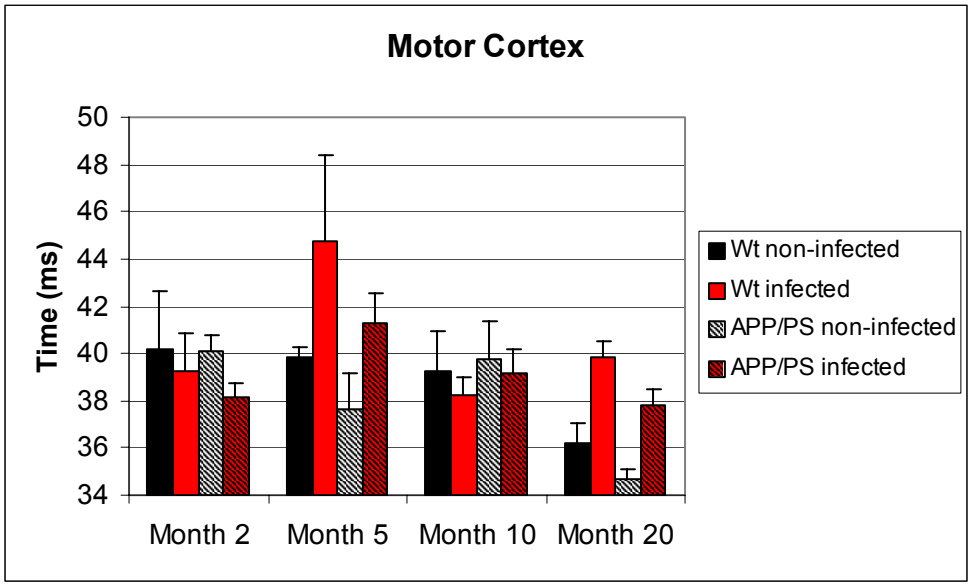

B)

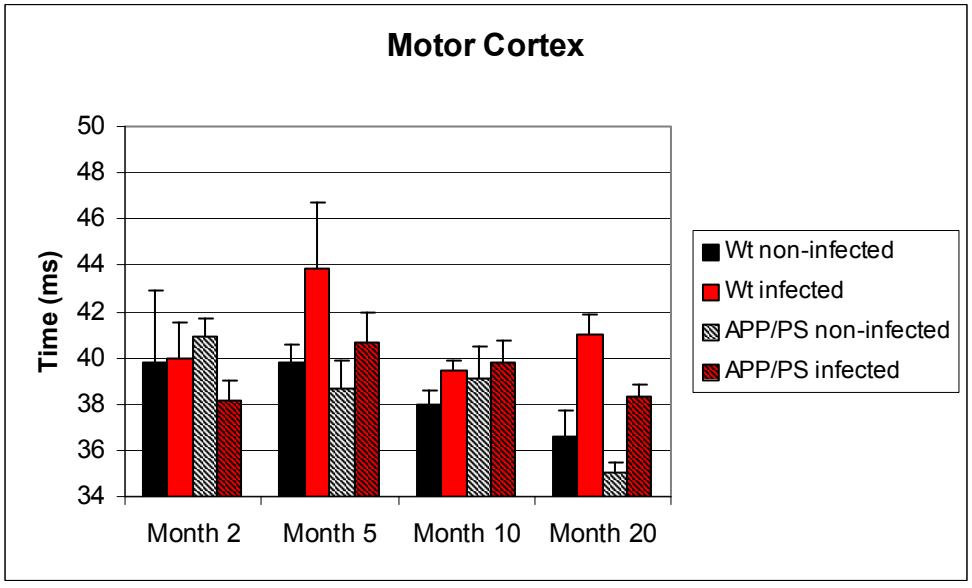

Figure 23: A T_2 comparison summary of right (A) and left (B) retrosplenial cortex regions.

A)

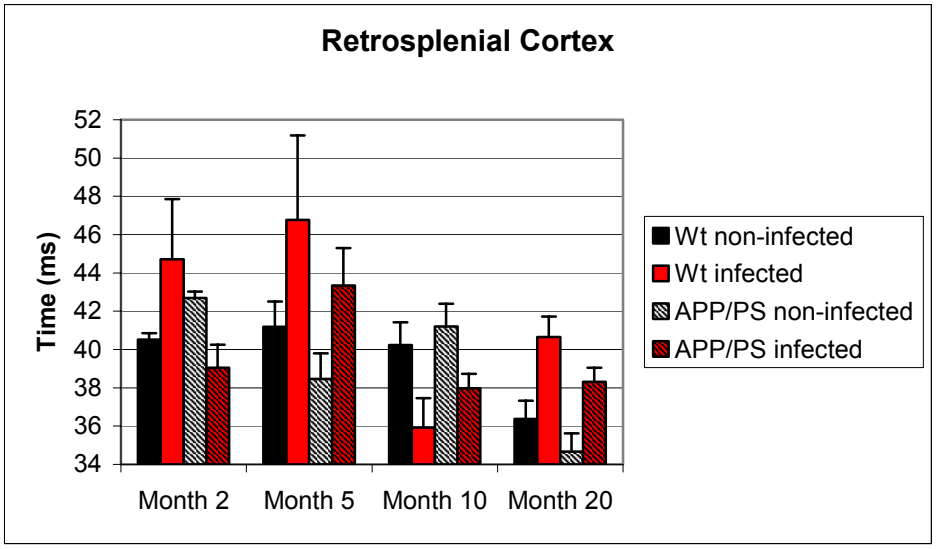

B)

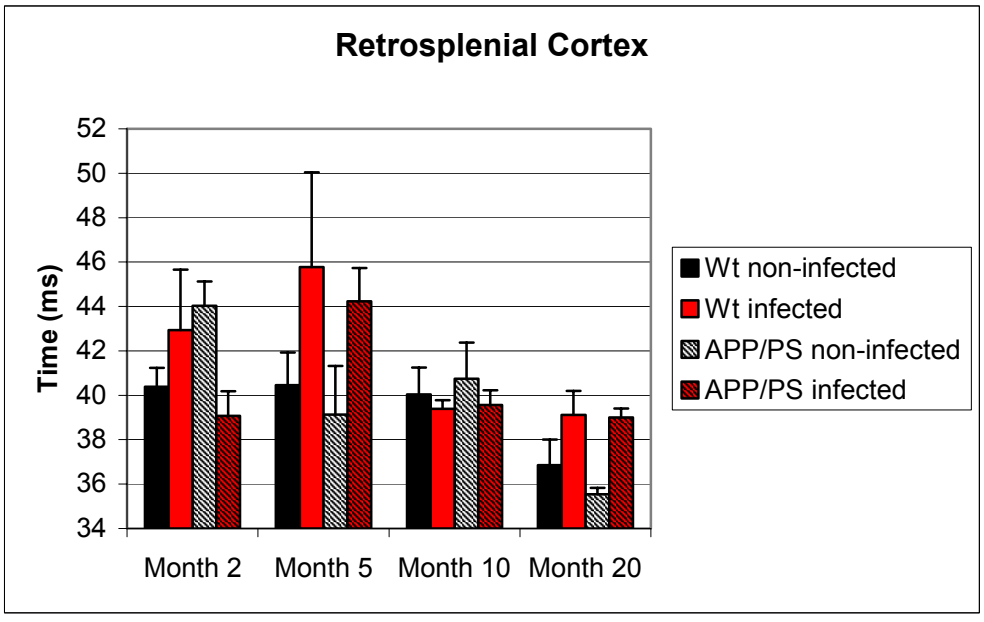

Figure 24: A T_2 comparison summary of right (A) and left (B) hippocampus regions.

A)

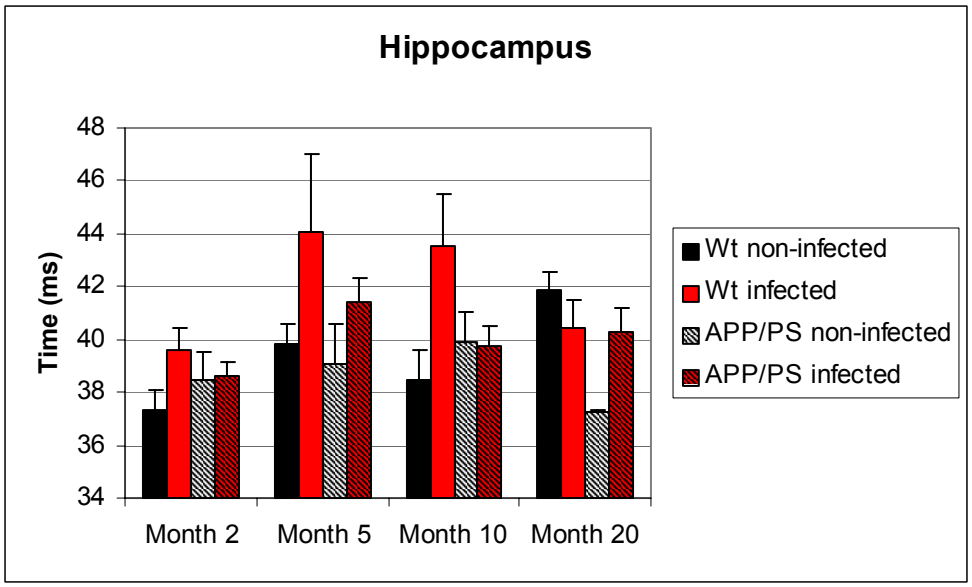

B)

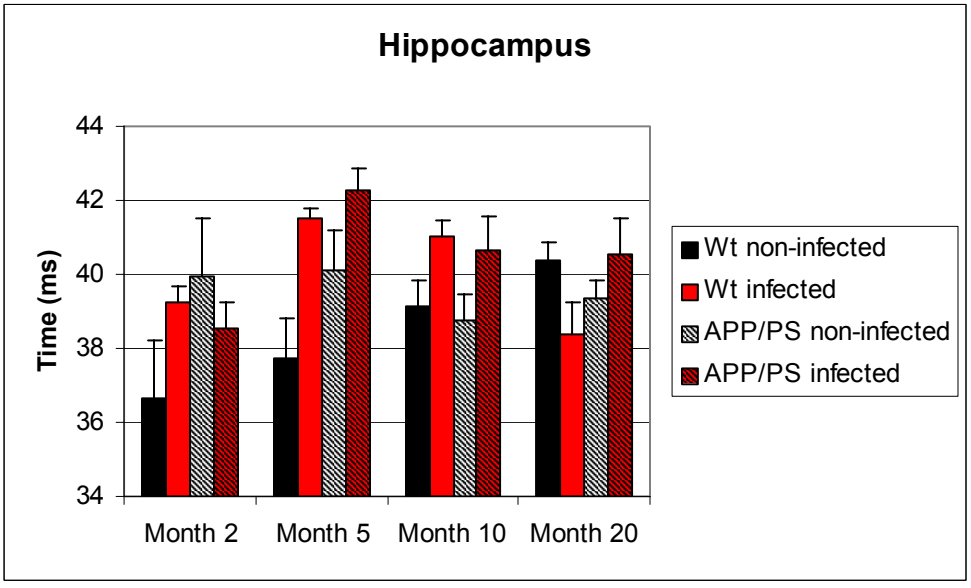

the APP/PS non-infected group, 5 mice in APP/PS infected group, 3 mice in the Wt non-infected group and 3 mice in the Wt infected group. The mean values were calculated for each ROI (see materials and methods) by pooling the T_2 value from each mouse in the group at each individual time point. For clarity, the left and right side of the ROIs are distinguished in the graphs. Error bars in the graphs represent the SEM. Hyperintensities in mean T_2 times were observed in every ROI tested at month 5 in both infected mouse groups (APP/PS and Wt) (Figures 22-24). A hyperinteinsity in T_2 is observed at month 20 in the APP/PS infected group compared to the APP/PS non-infected group.

3.3.2 Non-infected APP/PS and Wt groups:

An overall trend of shorter T_2 time was observed within the APP/PS non-infected group when comparing the final time point at 20 months to the initial time point at 2 months (Figures 22-24). The Wt non-infected group displayed a marked decrease in T_2 times in the motor cortex and retrosplenial cortex (Figures 22 and 23) and an increase in T_2 in the same time frame in the hippocampus (Figure 24). Shorter T_2 times were observed in all ROIs tested in the APP/PS non-infected group compared to the Wt non-infected group at month 20 (Figures 22-24).

Results were analyzed using statistical tests to determine if any significant changes in T_2 were apparent between APP/PS non-infected and Wt non-infected groups at month 20. Differences in mean T_2 times at month 20 were compared in the motor cortex, retrosplenial cortex and hippocampus using Student t-tests (Figures 22-24 and in a detailed comparison in Figures 25-27). The right side of the hippocampus in the APP/PS

Figure 25: A T_2 comparison of right (A) and left (B) motor cortex regions in Wt non-infected and APP/PS non-infected mouse groups.

A)

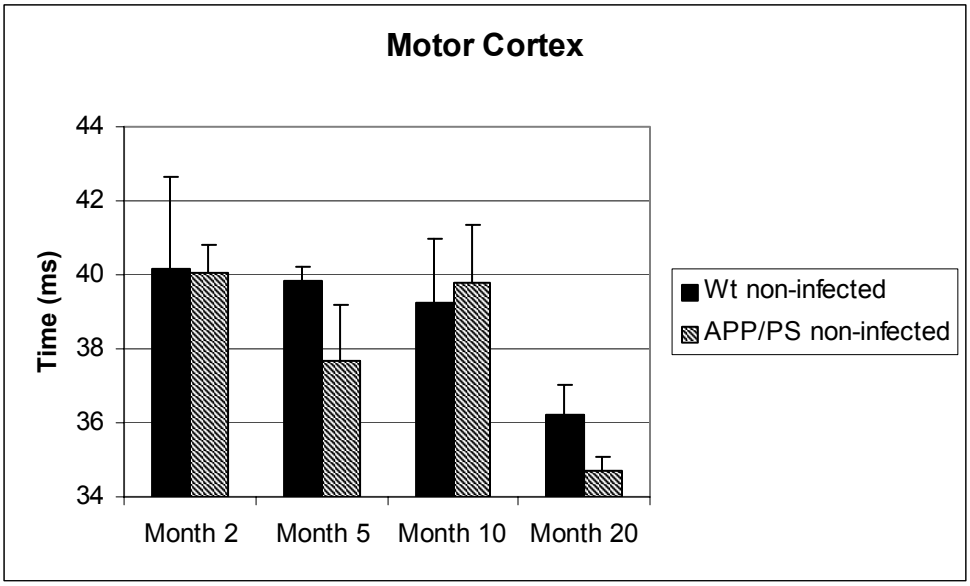

B)

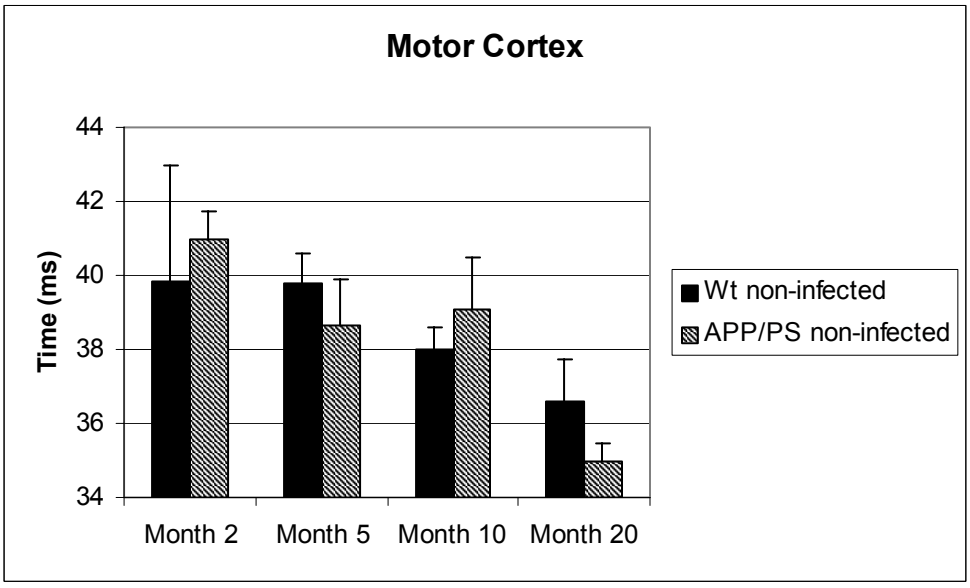

Figure 26: A T_2 comparison of right (A) and left (B) retrosplenial cortex regions in Wt non-infected and APP/PS non-infected mouse groups.

A)

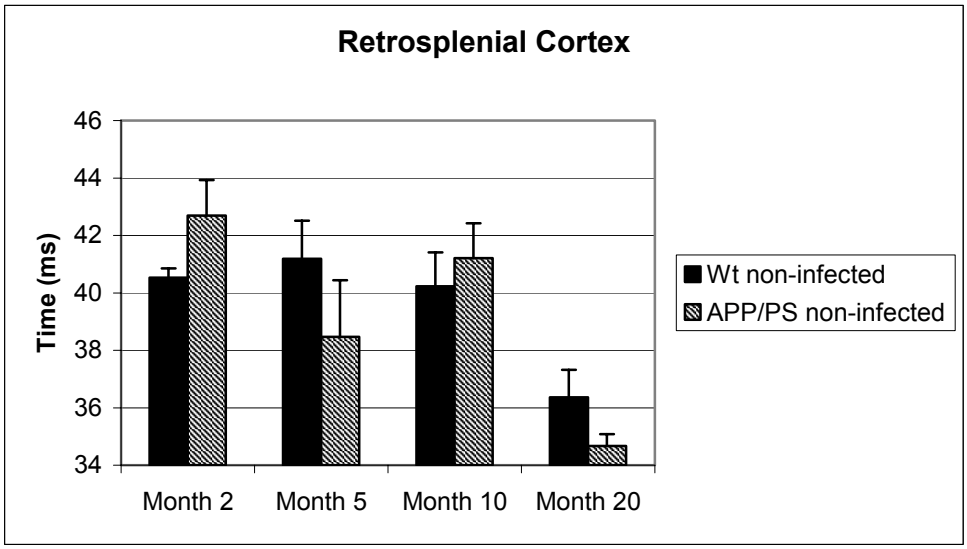

B)

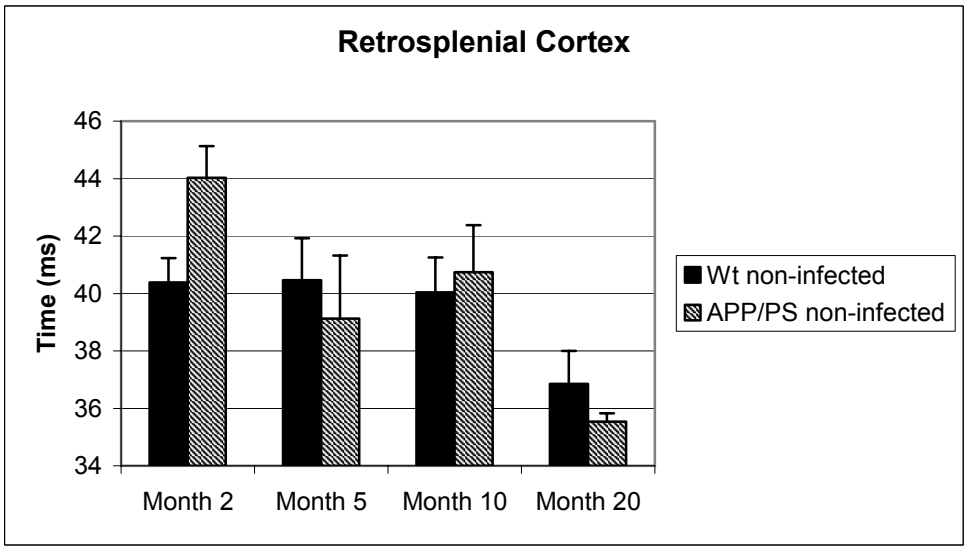

Figure 27: A T_2 comparison of right (A) and left (B) hippocampus regions in Wt non-infected and APP/PS non-infected mouse groups.

A)

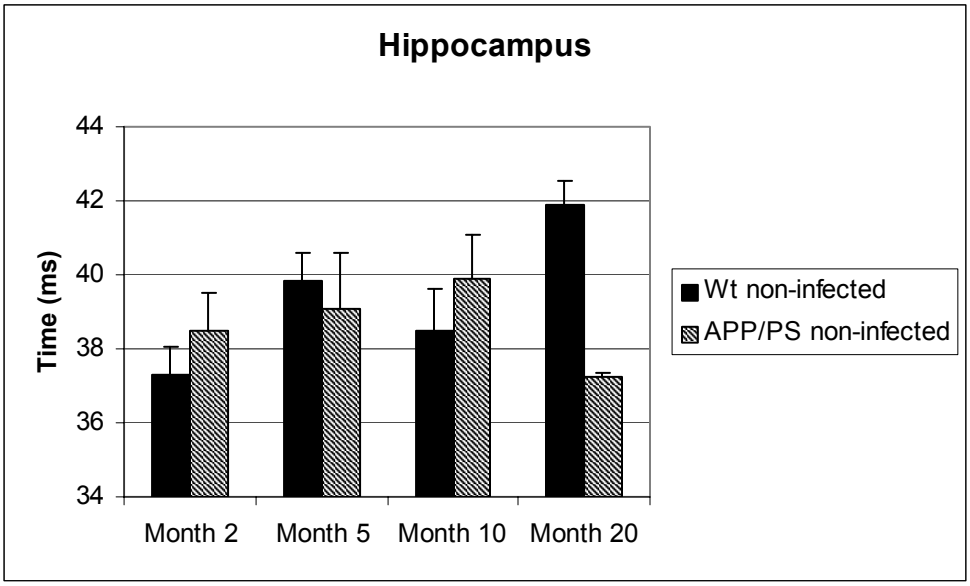

B)

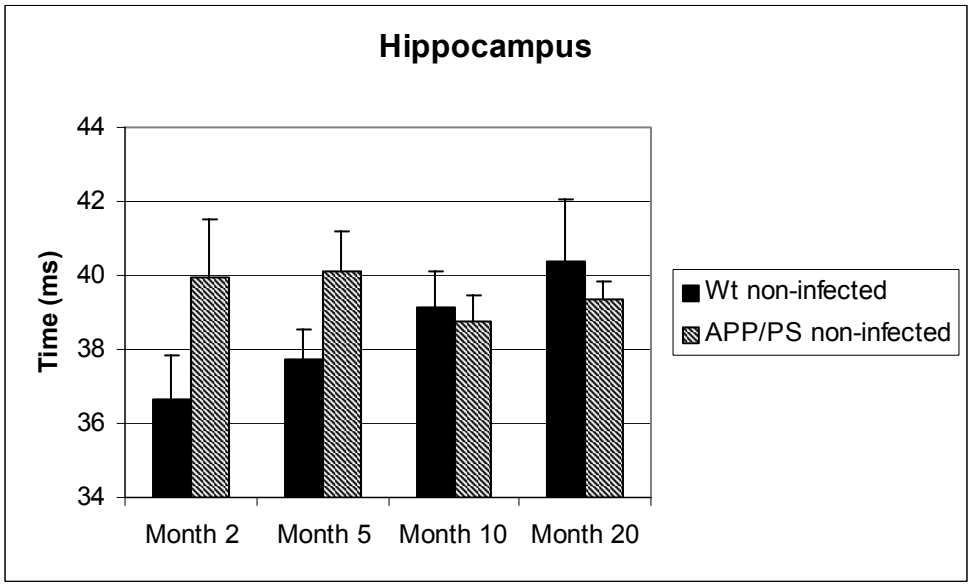

non-infected group displayed shorter T_2 values compared to the Wt non-infected group at the final time point (p=0.0003) (Figure 27).

An increase in mean T_2 time over the course of the experiment was apparent in both sides of the hippocampus in the Wt non-infected group. A Duncan's multiple comparison test was used to compare month 2 to month 20 in the right (p= 0.015) and left hippocampus (p= 0.055) in the Wt non-infected group. A comparison of cortex regions in the Wt non-infected group showed a decrease in T_2 when comparing month 2 to month 20 time points (Figures 25 and 26). A Duncan's test revealed the decrease in T_2 was only significant in the right retrosplenial region (p= 0.044) (Figure 26).

As reported above there was an observed marked decrease in T_2 in the APP/PS non-infected group from month 2 to month 20. A Duncan's multiple range test was used to compare T_2 values at various time points within the APP/PS non-infected group. A significant decrease in T_2 was apparent when comparing initial to final T_2 values in all regions of the cortex tested, including the right (p =0.0046) and left (p= 0.0007) motor cortex, and right (p=0.002) and left (p=0.002) retrosplenial cortex (Figure 25 and 26). A significant decrease in T_2 was found between the month 10 and month 20 time points in the right hippocampus (p=0.047) but not in the left hippocampus (Figure 27).

3.3.3 Wt non-infected and infected groups:

Hyperintensities in T_2 times were found in the cortex regions of the Wt infected group compared to the Wt non-infected group at month 20 (Figures 22 and 23). The opposite was true in the hippocampus where T_2 values were higher in the Wt non-infected group at month 20 compared with the Wt infected group (Figure 24).

Hyperintensities in T_2 values were observed in month 5 for all ROIs tested in the Wt infected group (Figure 22-24).

An independent Student t-test was conducted to determine whether differences in T_2 at month 20 were significant. The statistical analysis determined that the Wt infected group displayed higher T_2 values at month 20 than the Wt non-infected group in the right ($p=0.030$) and left ($p=0.037$) motor cortex (Figure 28). An increase in T_2 was apparent in month 20 in the retrosplenial cortex as well, with a significant increase in T_2 in the Wt infected group in the right retrosplenial cortex ($p=0.041$) (Figure 29). Shorter T_2 values were observed in the hippocampus of the Wt infected group when compared to the Wt non-infected group at month 20, although values were not significant (Figure 30).

A Duncan's multiple range test was conducted to identify areas exhibiting a significant hyperintensity in T_2 in months 5 compared to values at month 2 in the Wt infected and non-infected groups. Although all areas in the Wt infected group show a trend of an increased T_2 at month 5 (Figures 22-24), a significant increase between month 2 and month 5 was only found in the left hippocampus region ($p=0.013$) (Figure 30).

Changes in T_2 values between the month 5 and month 10 time points were investigated using a Duncan's multiple comparison test. A significant decrease in T_2 was found between month 5 and month 10 in the right motor cortex ($p= 0.042$) and right retrosplenial cortex ($p=0.013$) in the Wt infected group. A significant decrease in T_2 was not observed in any ROIs tested between month 5 and month 10 in the Wt non-infected group.

Figure 28: A T_2 comparison of right (A) and left (B) motor cortex regions in Wt non-infected and Wt infected mouse groups.

A)

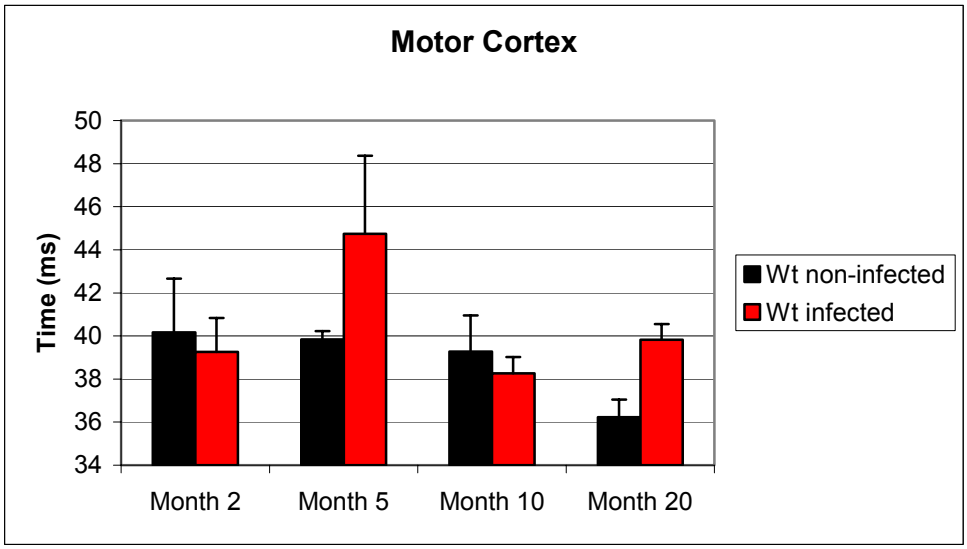

B)

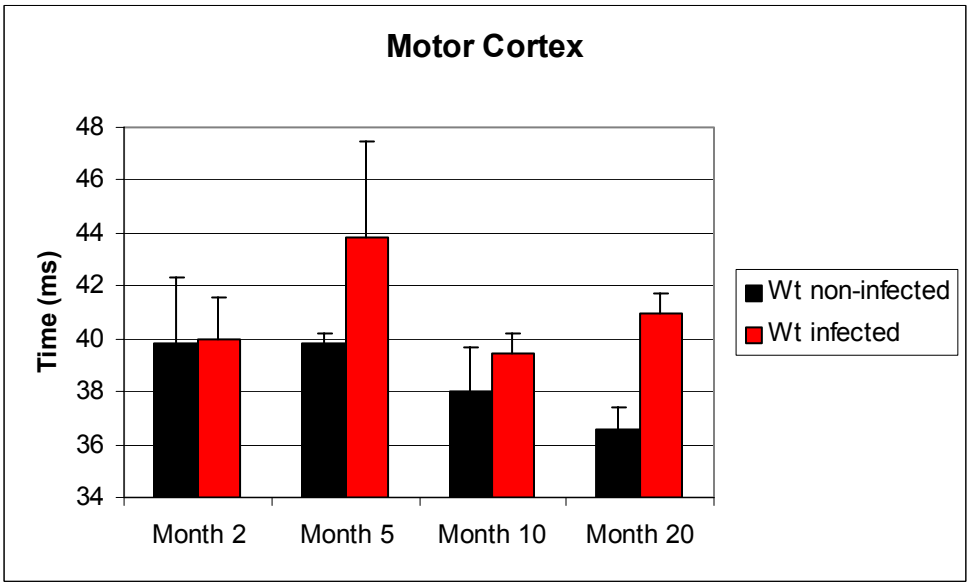

Figure 29: A T_2 comparison of right (A) and left (B) retrosplenial cortex regions in Wt non-infected and Wt infected mouse groups.

A)

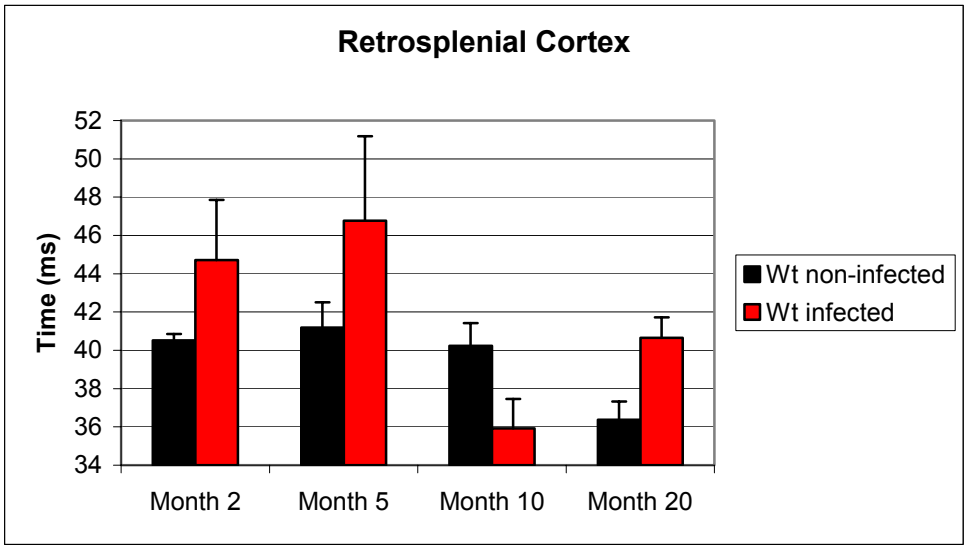

B)

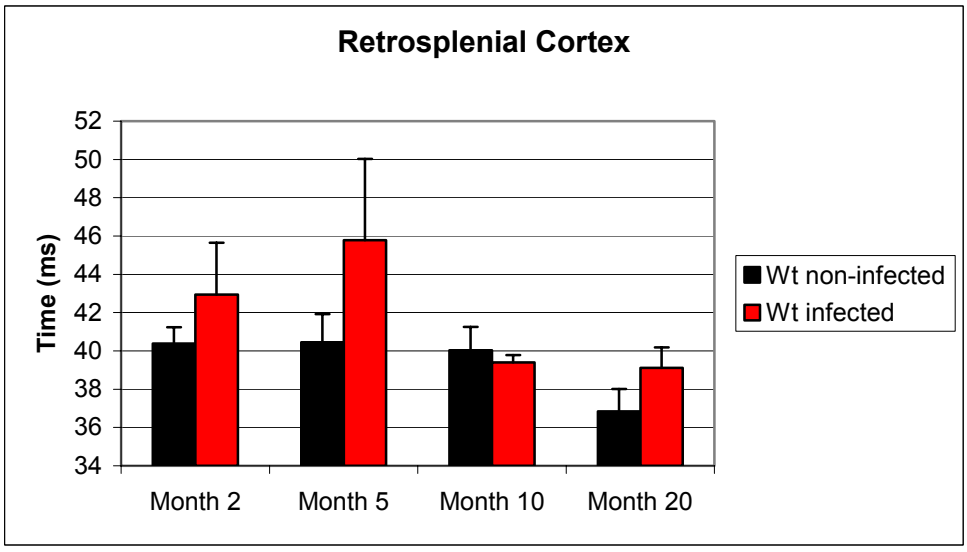

Figure 30: A T_2 comparison of right (A) and left (B) hippocampus regions in Wt non-infected and Wt infected mouse groups.

A)

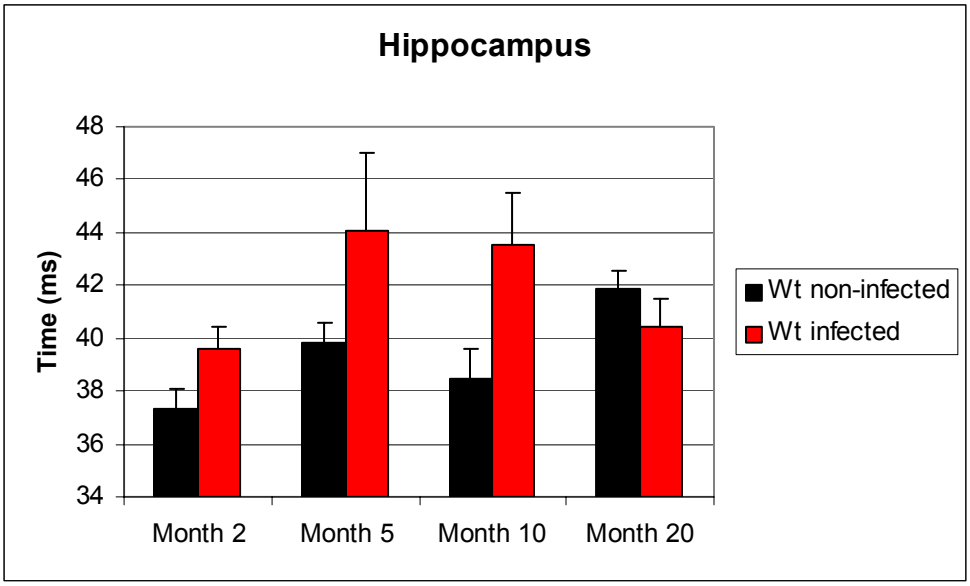

B)

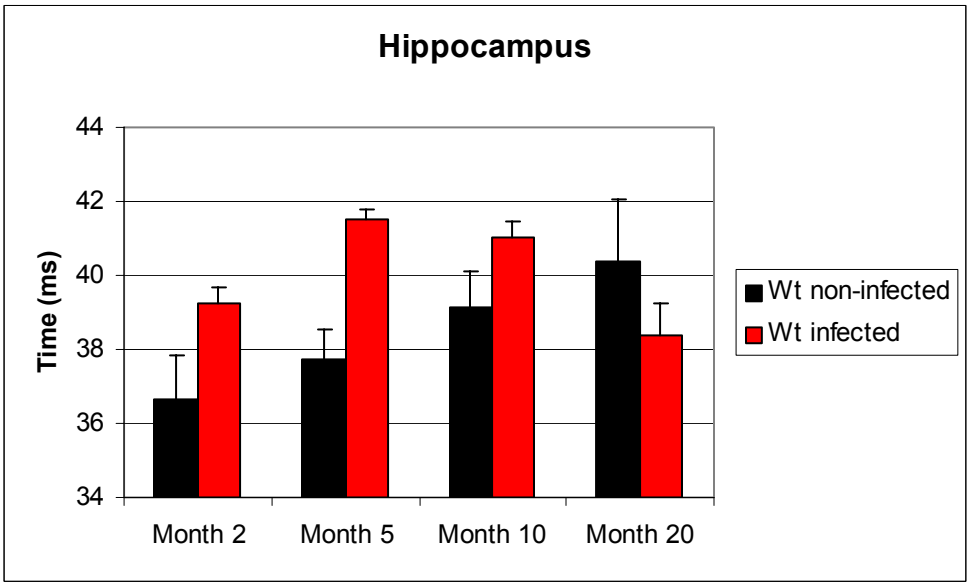

There were no statistically significant changes in T_2 values observed in the Wt non-infected group between month 2 and month 5 measurements (Figures 22-24, for a detailed comparison see Figures 28-30). Average T_2 values were similar between month 2 and month 5 in the cortex regions and a slight elevation in month 5 was seen in the hippocampus in the Wt non-infected group (Figures 28-30).

3.3.4 APP/PS non-infected and infected groups:

The APP/PS infected group showed a marked increase in T_2 compared to the APP/PS non-infected group in all ROIs measured at month 20 (Figures 22-24). The APP/PS infected group had very similar T_2 time measurements at month 2 and month 20 in the cortex regions (Figures 22 and 23). An increase in T_2 was observed in the hippocampus at month 20 in the APP/PS infected group compared to month 2 (Figure 24). An increase in T_2 from month 2 to month 5, as seen in the Wt infected group, was observed in all regions of the APP/PS infected group (Figures 22-24). The APP/PS non-infected group showed no apparent increase in T_2 in month 5 compared to month 2 in the hippocampus (Figure 24). A decrease in T_2 was seen in all regions of the cortex of the APP/PS non-infected group between month 2 and month 5 (Figures 22 and 23).

To investigate differences in the month 20 T_2 values, a parametric Student t-test or a non-parametric Mann-Whitney U-test was used to compare the APP/PS infected group to the APP/PS non-infected group (Figure 31-33). A significant difference in T_2 was apparent in 5 out of the 6 regions tested between infected and non-infected APP/PS groups; including a significant increase in the motor cortex on the left ($p=0.002$ using a Student t-test) and right side ($p=0.007$ using a Student t-test), the retrosplenial cortex on

Figure 31: A T_2 comparison of right (A) and left (B) motor cortex in APP/PS non-infected and APP/PS infected mouse groups.

A)

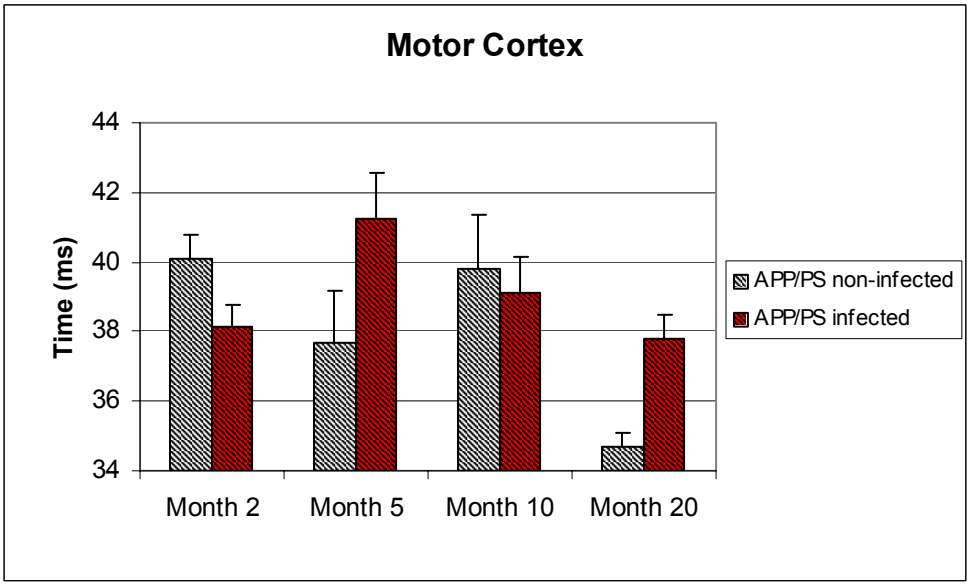

B)

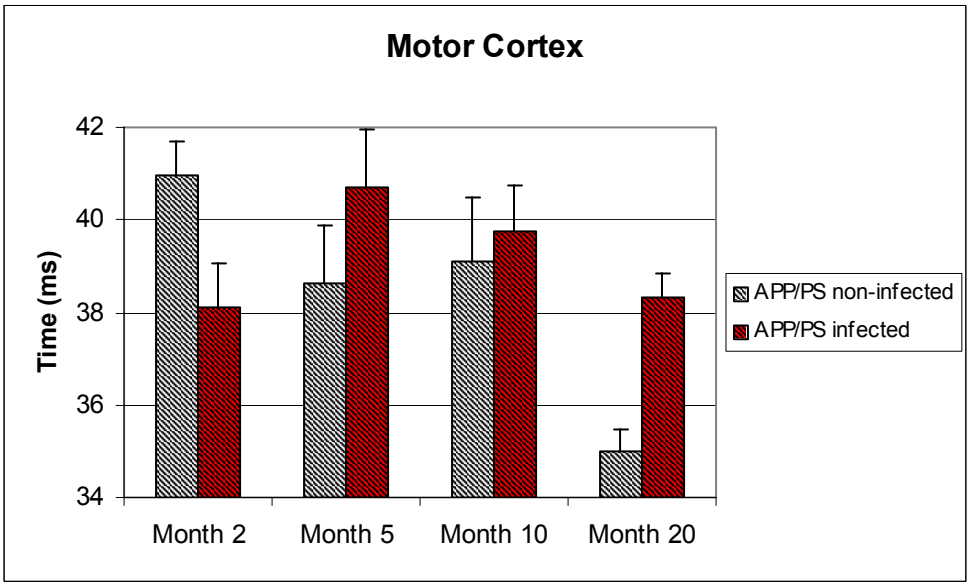

Figure 32: A T_2 comparison of right (A) and left (B) retrosplenial cortex in APP/PS non-infected and APP/PS infected mouse groups.

A)

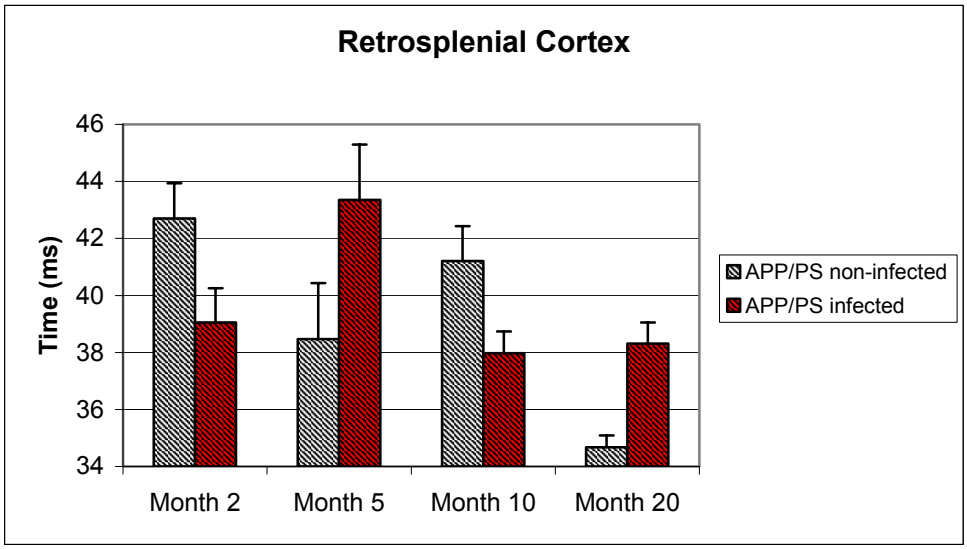

B)

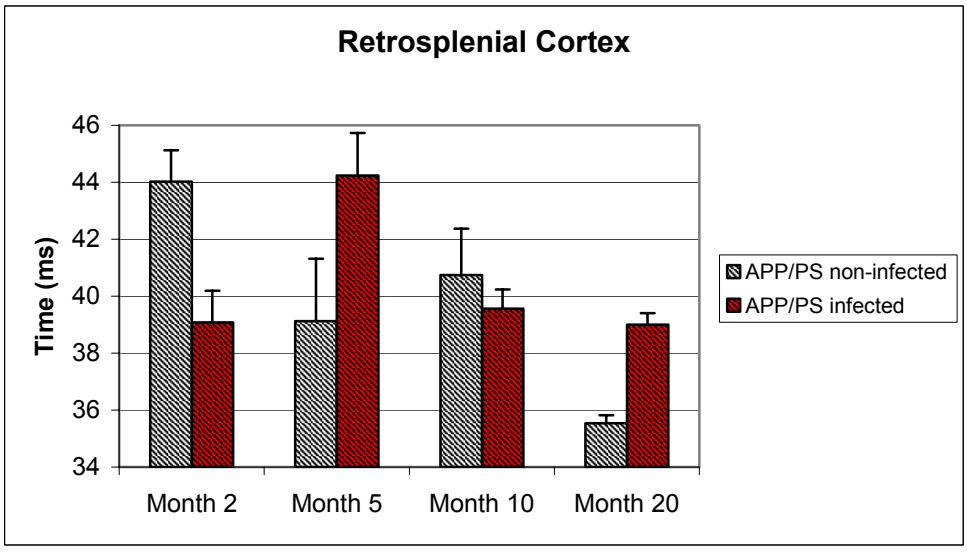

Figure 33: A T_2 comparison of right (A) and left (B) hippocampus in APP/PS non-infected and APP/PS infected mouse groups.

A)

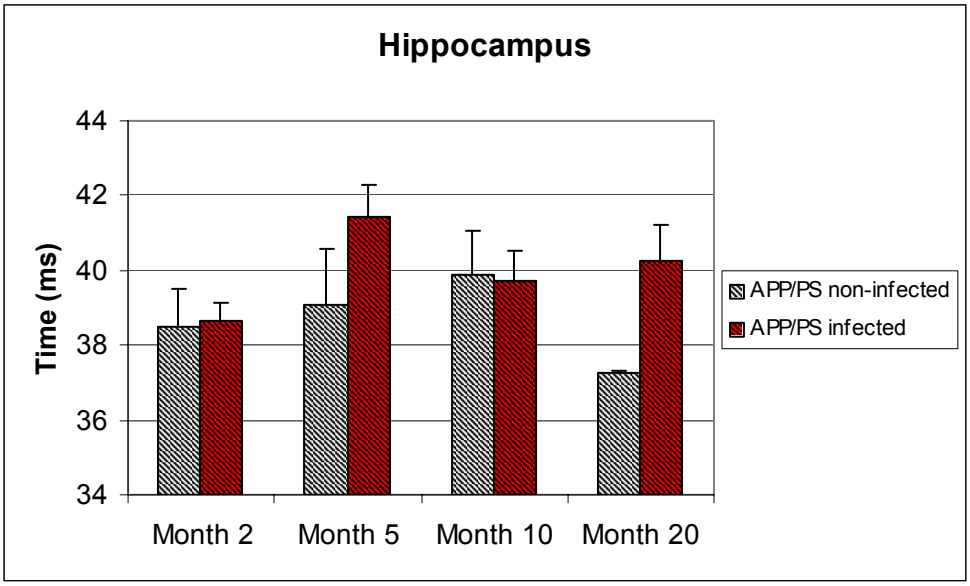

B)

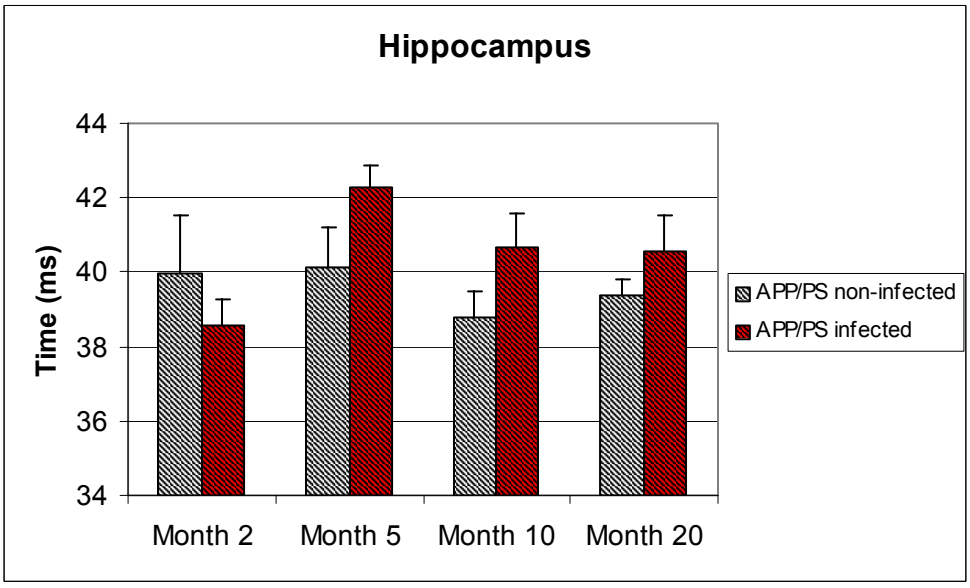

the left (p=0.0003 using a Student t-test) and right side (p=0.016 using a Mann-Whitney U- test), and the right side of the hippocampus (p= 0.016 using the Mann-Whitney U-test) (Figures 31-33). Although the mean T_2 time in the left side of the hippocampus was longer in the infected compared to the non-infected APP/PS group, this change was not significant (Figure 33).

A Duncan's multiple range test was used to compare changes in T_2 within the APP/PS non-infected group at different time points. A significant decrease in T_2 was shown between month 2 and month 5 in the left (p= 0.033) and right (p=0.048) retrosplenial cortex (Figures 31 and 32). A comparison of T_2 changes within the APP/PS infected group was also analyzed using Duncan's multiple range test. A significant increase in T_2 was observed from month 2 to month 5 in all 6 areas tested in the APP/PS infected group (Figure 31-33). p-Values included p= 0.009 for right and p= 0.0276 left hippocampus regions, p= 0.012 for right, and p= 0.049 for the left motor cortex and p= 0.0336 for the right and p= 0.008 for the left retrosplenial cortex. A decrease in T_2 was observed in all regions following month 5 in the APP/PS infected group. A significant decrease in T_2 was observed between month 5 and month 10 in the right (p=0.016) and left (p=0.012) retrosplenial cortex, right hippocampus (p=0.049) and the right motor cortex (p=0.041) in the APP/PS infected group (Figure 31-33).

3.3.5 APP/PS and Wt infected comparison:

A Duncan's multiple range test was used to compare differences in T_2 values between months 5 and month 10 in the APP/PS and Wt infected groups. A significant decrease in T_2 was observed between month 5 and month 10 in the Wt infected group in

the right motor cortex (p=0.042) and the right retrosplenial cortex (p=0.013) (Figures 22-24). A significant decrease in T_2 was observed in the left hippocampus of Wt infected mice between months 5 and month 20 (p=0.003) (Figures 22-24).

The same comparisons between month 5 and later time points were made in the APP/PS infected group using a Duncan's multiple range test. A significant decrease in T_2 was observed from month 5 to month 10 in the right hippocampus (p=0.049), right motor cortex (p=0.041), right retrosplenial cortex (p=0.016) and left retrosplenial cortex (p=0.012) (Figures 22-24). A decrease in T_2 was observed between month 5 and month 20 in the left motor cortex in the APP/PS infected group, however this observation was not significant.

4. Discussion

4.1 General comments:

The relationship between infectious agents and chronic disease is not fully understood, however, the presence of infectious agents in the brain have been proposed as a possible mechanism for AD pathology (63). Conflicting reports have shown a relationship between *C. pneumoniae* and plaque pathology associated with AD (4, 44, 48, 56) while others indicate findings were not reproducible in subsequent experiments under slightly different conditions (20, 54, 62). Conflicting evidence for or against a role of *Chlamydia* in AD plaque progression is the primary motive for this study.

Epidemiological evidence suggests that the rate of *C. pneumoniae* infection is as high as 70% in populations in the Western world and re-infections are common (4). If a *Chlamydia* infection has an impact on chronic disease it is a major public health concern. It has been suggested that to follow up on these findings, researchers need to investigate whether *Chlamydia* changes or enhances the development of different aspects of the disease such as plaque progression *in vivo* (63). This study addresses the impact *C. muridarum* infection, representative of a natural infection in the mouse, on AD associated plaque progression in a well-developed transgenic animal model of AD.

4.2 Changes in body weight:

The APP/PS transgenic mice and Wt controls in this study were derived from F2 hybrids of C57BL/6 and C3H/HeJ mice (36). Previous studies have shown C57BL/6 mice lose approximately 15% of body weight following an intranasal inoculation of 4000 IFU of *C. muridarum* at 10 DPI (85). In another study a test was performed to determine

susceptibility to a *C. muridarum* infection in both C57BL/6 and C3H/HeJ strains of mice by intranasal infection with 1500 IFU *C. muridarum* (58). C57BL/6 mice were more resilient to the infection, shown by a minimal amount of body weight loss and exhibiting a 100% survival rate, while C3H/HeJ mice lost approximately 25% of their body weight by 14 DPI and had a much lower survival rate (58). All mice infected with 1000 IFU in this study lost weight. Mice showed a body weight loss that ranged from 8%-20% (Figure 15 and Appendix 3). Body weight loss observed in infected mice presented here was similar to the values reported in the literature (from 15-25%) (58, 85).

The differences in the range (8%-20%) of body weight loss observed here compared to literature values may be attributed to a number of factors. Variation in the inoculum can be excluded because *C. muridarum* was obtained from the same stock as used by Yang and Brunham (85). The smaller inoculum size of 1000 IFU of *C. muridarum* for intranasal infection in this study may have had an effect on some mice to lose less weight then in previous reports. The mice in this study were from a different genetic background than in the previous reports. In this study, mice were from a crossed C57BL/6 and C3H/HeJ background (C3B6). These mice may be more susceptible to infection than the single background C57BL/6 mice and less susceptible to infection than C3H/HeJ mice (58). Body weight loss may be directly related to the transgene manipulations, which are known to make APP mice more susceptible to premature death then non-transgenic mice (32) (personal communication with Dr. Borchelt, University of Florida). Variations in susceptibility of APP/PS transgenic mice to infection may account for different patterns of weight loss exhibited by the APP/PS infected group (Appendix 3).

An inoculum size of 1000 IFU was chosen to cause infection with a minimal mortality (personal communications with Dr. Xi Yang). The range of weight loss observed here was similar to that seen in other studies indicating the mice were infected. Ensuring a maximum survival was important as cost restrictions prevented the availability of extra mice.

C. muridarum infected mice exhibited symptoms indicative of an acute infection, including piloerection and walking with an abnormal posture. These visual signs, taken with body weight loss data, were further evidence of the establishment of an acute *C. muridarum* infection in the lungs of mice infected with 1000 IFU (85). By approximately 20 DPI these symptoms no longer were exhibited in infected mice. The body weight gain observed in infected mice at approximately 15 DPI in Wt mice and 28 DPI in APP/PS mice indicate that the animals recovered from the infection.

4.3 Serology:

At the end of the experiments (20 months), after euthanasia, an ELISA was conducted to determine if levels of *C. muridarum* specific Ab in sera of infected mice were elevated compared to uninfected mice. *Chlamydia* species elicit a host immune response that has important implications for the design of this study. The humoral immune response in the mouse, in response to the *C. muridarum* infection, resulted in Ab production for clearance of the initial infection as well as providing long-term immunity to a subsequent infection (85). *C. muridarum* elicits a Th-2 response, which activates plasma B cells, resulting in Ab production. IgG2a and IgA specific Ab's to *C. muridarum* were selected to test mouse serum for a previous exposure to the infection.

The differences between infected and non-infected mice could only be compared qualitatively due to the very low (almost non-existent) titre in non-infected mice (Figure 16 – elution profile and Appendix 4 - titre). A comparison of average Ab titres for IgG2a and IgA is presented in the appendix section from the sera of all infected mice in the study, however, determination of exact levels was not the purpose of this experiment. The presence of Ab titers specific to *C. muridarum* are an indicator of past infection with the bacteria. This validated the model of an infection established in the lungs following a 1000 IFU intranasal inoculation with *C. muridarum* as previously shown by Yang and Brunham (85). The absence of IgG2a and IgA titres in mice administered a sham intranasal inoculation with SPG buffer confirmed the absence of infection in non-infected groups. Small OD values observed in the non-infected mice were likely due to non-specific binding of the secondary Ab to the primary *C. muridarum* specific Ab in the ELISA (Appendix 1, personal communication with Dr. Xi Yang).

4.4 Plaque pathology in the mouse model:

4.4.1 Plaque pathology within groups:

To investigate the effect of a *Chlamydia* infection on AD plaque pathology, APP/PS and Wt mice were infected with *C. muridarum* at approximately 10 weeks of age and then euthanized at 18 months post infection. At that time brains were harvested to determine if an infection at 2 months with *C. muridarum* would cause plaque like pathologies in the brains of Wt mice. The plaque burden and plaque distribution in APP/PS transgenic mice was tested to observe if there were alterations in existing plaque pathology resulting from infection.

Plaque pathology was completely absent in the anterior and posterior tissue sections in both Wt infected and Wt uninfected mice stained with Congo red dye (Figure 17). The Wt uninfected group showed no traces of βA deposits as expected since AD is not a natural disease in mice. This group was a negative control for Congo red staining, due to the absence of βA in mouse brain sections (Figure 17 and 18). The absence of plaque pathology in the Wt infected group showed that plaque pathology is not caused by 1000 IFU of *C. muridarum* inoculated intranasally at age 2 months. The negative result was not surprising as mice naturally do not develop plaque pathology associated with AD, however it was crucial to answer the following question: can plaque pathology be induced with a natural *C. muridarum* infection *in vivo*? The negative results show conclusively that infection with *C. muridarum* via intranasal inoculation alone does not induce plaque pathology associated with AD if the required genes for AD are not present. At 20 months post infection a significant plaque burden was observed in age matched non-infected APP/PS mice. A statistical comparison could not be made as there were no plaques present in Wt non-infected and Wt infected mice.

4.4.2 The effect of infection on overall plaque burden:

The APP/PS non-infected and APP/PS infected groups both exhibited plaque pathology at 20 months of age. A trend of a higher overall plaque burden was found in the APP/PS group infected with *C. muridarum* when compared to the APP/PS non-infected group (Figure 20). The result is not considered statistically significant at 95% confidence levels, likely due to the low statistical power from the limited number of 4 animals per group ($p=0.157$). This is a good p-value based on the sample size and

suggests a trend of higher plaque counts in the APP/PS infected group compared to the APP/PS non-infected group.

The question is: why would there be a trend of a higher overall plaque burden in the APP/PS infected group compared with the APP/PS non-infected group? APP is a precursor to the βA protein, which accumulates in extracellular deposits and is identified as one of the hallmarks of AD (27). As described earlier, there is evidence of an inflammatory reaction in the brain in response to the plaque deposits. The immune response is directed by stimulation of microglia and monocytes (33). In a previous study of the APP/PS transgenic model it was shown that microglial cells were attracted to the site of plaque formation and are activated but do not participate in clearance of the plaques, although they might restrict growth (53). Neuritic dystrophy, or abnormal changes in immature neurons, was shown in neurons near βA plaques in APP mice (53). Alterations in dendritic spines and axonal dystrophies are precursor events in neurodegeneration. Recent evidence confirms apoptotic changes including DNA fragmentation and caspase-3 activation resulting in apoptosis of pyknotic neurons in mice 21-26 months of age (83). Another study revealed a loss of approximately 50% of monoaminergic neurons in the forebrain in aged APP/PS mice (45). Results from these studies suggest that βA associated plaque accumulation in the APP/PS mouse model induces an inflammatory response that results in precursor events to neurodegeneration, resulting in neuronal cell death in aged APP/PS mice.

If *C. muridarum* is able to enter the brain it is plausible that it may have an impact on inflammatory events near or at the site of plaque pathology. If the inflammation cascade is altered there may be an impact on the overall plaque burden, especially if

progression of plaque formation is in some way regulated by an inflammatory response in the brain. A correlation was shown between LPS and induced neuroinflammation in the brain in the hippocampus of rats resulting in an increase in accumulation of βA protein (28). LPS has also been shown to have an effect on APP progression through immunoreactive neurons in cortex and hippocampus in APP/PS mice (71). Interestingly there were elevated plaque numbers observed in this study in the hippocampus regions in the APP/PS infected group, however these differences proved not to be significant ($p=0.121$). The mechanism for the increase in plaque burden due to LPS is not well understood, however, it was speculated that it may trigger CNS inflammation by activating microglia and astrocytes, releasing TNFα and interleukin-1β (14, 28, 38). This indicates that immune system regulators can alter APP processing. This notion may be applied here because, if *C. muridarum* was able to enter the brain, it may induce an immune response and influence plaque pathology in the infected APP/PS transgenic mice.

4.4.3 The effect of infection on plaque distribution:

ROIs (motor cortex, retrosplenial cortex, hippocampus, striatum, anterior and posterior somatosensory cortex) used to determine overall plaque burden were examined individually to determine plaque distribution. The regions were chosen based on previous findings of plaque pathology in APP/PS transgenic mice (29, 36, 87). Plaque distribution was investigated in detail to observe if any specific areas of the brain were affected by the *C. muridarum* infection. The APP/PS infected group areas were compared to the APP/PS non-infected group areas to determine the impact of infection on

plaque distribution in the chosen ROIs. Plaque counts were higher in the APP/PS infected group in all areas except for the posterior somatosensory region (Figure 21). Plaque counts were low in the striatum in both the APP/PS infected and APP/PS non-infected groups. Plaque counts were close in both anterior and posterior somatosensory regions in the APP/PS infected and non-infected groups (Figure 21). The plaque counts were not statistically significant in the hippocampus ($p=0.12$) and striatum ($p=0.13$). The reason for the trend in higher plaque burden in the hippocampus in the APP/PS infected group compared to the APP/PS non-infected is unclear, however, the hippocampus is an area of the brain commonly affected by AD (36).

4.5 MR discussion:

4.5.1. MR overview:

The striatum had very few plaques in both the APP/PS infected and the APP/PS non-infected groups therefore the region was not examined in MR experiments. The striatum is also a larger area and is located further from the surface coil than the cortex or hippocampus regions. As a result, MR signal to noise was relatively poor in areas of the striatum. The hippocampus and cortex regions are areas typically investigated in the literature for the APP/PS mouse model (36). In histological studies there was very little difference in plaque counts in the somatosensory cortex between the APP/PS infected and non-infected groups, therefore the somatosensory regions were not included in the MR study.

4.5.2 AD modeled in the transgenic mouse:

The changes in T_2 values observed in the Wt non-infected group were a direct result of the animal aging and therefore act as a negative control to the non-infected APP/PS group. A trend of steady decrease in T_2 values was found in the cortex regions of the Wt non-infected group from month 2 to month 20 (Figures 22-24). Interestingly there was an increase in T_2 values in the hippocampus of non-infected Wt mice (Figures 22-24). The steady decrease in T_2 in the cortex and increase in T_2 in the hippocampus are the patterns that are associated with the normal aging process in the mouse brain, since Wt non-infected mice are not carriers of the APP/PS transgenes associated with AD.

The pattern of decreasing T_2 time from month 2 to month 20 was consistent in both non-infected Wt and non-infected APP/PS groups in cortex regions (Figure 25 and 26), but not in hippocampus regions (Figure 27). Furthermore, within the APP/PS non-infected group a decrease in T_2 occurred in all areas, including significant decreases in all 4 areas of the cortex and in the right hippocampus (Figures 25 and 26). The significant decreases observed in the cortex of the non-infected APP/PS group are related to events leading up to and including plaque pathology. The shorter T_2 values observed in the cortex region of non-infected APP/PS mice are consistent with the literature findings (29, 35, 76).

βA plaques are known to cause hypointensities in T_2 values in APP/PS mice (10, 29, 76, 81). The trend of shorter T_2 times is consistent with observations made in this study and may be associated with the presence βA plaques accumulating in the brain in the APP/PS transgenic group. These subtle differences observed in this study may result from a number of different possibilities including the physiological changes associated

with the nature of the plaques deposition. These physiological changes are not always associated with a lack of water in the tissue but rather change in tissue composition or cell death. Plaques are hydrophobic in nature and the presence of a hydrophobic plaque in the brain would reduce fluidity in the tissue (29). The amyloid protein is in β sheet conformation therefore the plaque composition is more of a solid mass, compared to surrounding tissue (27, 50). A plaque composed of βA would appear stiffer and exhibit less fluidity than surrounding healthy brain tissue (lipid etc.) (35, 76). Another important factor is the iron accumulation associated with the plaque accumulation (35). Iron is a natural MR contrast agent for plaques because of its magnetic properties and its effect of reducing T_2. Poor blood perfusion of damaged areas in the brain is associated with less fluidity (water) in the tissue (23, 41). In summary, there are a number of possibilities that may contribute to hypointensities in T_2 such as the hydrophobic nature of the plaque, conformation of the plaque, iron accumulation and changes in perfusion of the brain over the course of disease (29, 35, 76). It is possible that any one of these factors or a combination of two or more of these characteristics or events may contribute to hypointensities in T_2 observed in the APP/PS non-infected mouse group compared with the Wt non-infected group.

Although shorter T_2 times were observed in the APP/PS non-infected group compared to the Wt non-infected group in all regions tested at month 20, a significant difference was only found in the right hippocampus (Figures 25-27). Although changes were not as apparent between the APP/PS and Wt non-infected groups by comparing the final time point at month 20, a decrease in T_2 was observed in the right hippocampus between month 10 and month 20 in the non-infected APP/PS (Figure 27). This decrease

may be further evidence of physiological changes in the hippocampus occurring in the later stages of disease relating to APP/PS transgene expression.

In summary all regions tested in the non-infected APP/PS group showed decreases in T_2 over the course of the experiment, including 5 out of 6 areas with significant decreases in T_2 from month 2 to month 20 (Figure 22-24). The Wt non-infected mice showed a similar pattern of decrease in T_2 in the cortex regions, but the decreases were not significant. Both areas of the hippocampus in the non-infected Wt group had an increase in T_2 from month 2 to month 20. These observations indicate that there is a factor contributing to a significant decrease in T_2 within the APP/PS non-infected group that is not apparent in the Wt non-infected group. Interestingly, Congo red staining of tissue sections in APP/PS non-infected mice and Wt non-infected mice revealed plaque pathology in the APP/PS non-infected group and a complete absence in the Wt non-infected group (Figure 18). It can be concluded that the plaque pathology observed in the tissue sections from the non-infected APP/PS group directly influenced the changes in T_2 observed in MR studies.

4.5.3 Modeling infection with MR:

To assess the impact of infection on the brain in the mouse model the Wt infected group was compared to the Wt non-infected group. T_2 values observed at month 5 were higher than T_2 values observed at month 2 in all regions tested within the Wt infected group (Figures 28-30). This pattern of hyperintensity was not observed in the Wt non-infected group. As previously described, the Wt non-infected group displayed a steady increase in T_2 values in the hippocampus and values remained virtually unchanged from

month 2 to month 5 in the cortex (Figures 28-30). A hyperintensity in T_2 at the time point following intranasal inoculation (month 5) is an important observation as there could be a number of reasons for this change. The longer T_2 times at month 5 are likely related to the events resulting from an acute *C. muridarum* infection at month 2 or residual persistence of intracellular *Chlamydia* that may not have been completely cleared (6).

The initial *Chlamydia* infection could have an impact on the brain by entering following systemic dissemination, often associated with the persistence state in the bacterial lifecycle (6, 17). Entry to the brain may be accomplished through the interaction of the entire organism or bacterial components with the BBB (66). All gram-negative bacteria, including *C. muridarum*, have LPS toxin on the surface of the bacterial cell wall. LPS was shown to have a negative impact on the integrity of the BBB (66). The increased permeability of the BBB in the presence of LPS may allow *Chlamydia* to cross the barrier and damage the brain. Usually when the BBB is compromised the brain undergoes a stress phase often resulting in water accumulation due to the effect of pathogens or unwanted compounds on cell homeostasis. These events may lead to the longer T_2 times observed at month 5 in all regions tested in the Wt infected group (Figure 22-24).

A greater variation at month 5 with regards to the SEM of the average T_2 times is apparent in the Wt infected group in most regions tested. This observation can be viewed in the summaries of results (Figures 22-24). The SEM appeared much greater in month 5 than other time points measured within the group. This variation may be associated with changes linked to *Chlamydia* infection at month 2. *C. muridarum* may affect individual

mice to different degrees, perhaps based on the host immune response or BBB permeability. These may result in a *C. muridarum* infection that is more severe in certain mice, thus contributing to the large variation at month 5.

C. muridarum infection was shown to cause changes in T_2 in Wt mice. When comparing the Wt infected group to the Wt non-infected group a longer T_2 value was observed in the final time point (20 months) in cortex regions of the Wt infected group (Figure 22 and 23). A significant hyperintensity in T_2 was observed in both sides of the motor cortex as well as the right side of the retrosplenial cortex (Figure 28 and 29). The hyperintensities observed in the cortex of the infected Wt mice may be associated with changes in the brain that are initiated earlier from infection.

In summary, the only difference between these groups was that the Wt infected mice were infected with *C. muridarum* and Wt non-infected mice were administered a sham SPG buffer inoculum at month 2. It can thus be concluded that the increase in T_2 observed from month 2 to month 5 are related to the effects of the infection. From body weight data in can be concluded that infected mice were stabilized by approximately 15 DPI in Wt mice and 28 DPI in APP/PS mice after which regular weight gain occurred (Figure 15). Interestingly, the effects of the infection can still be found months after the initial acute infection is cleared. It can be concluded that the effects of the infection are still detected in the brain long after mice have appeared to recover from infection.

4.5.4 Role of infection on plaque progression:

The purpose of this study was to assess the impact of an infection on the plaque progression associated with AD. Infecting one APP/PS transgenic group with *C.*

muridarum and administering a sham inoculation to another APP/PS transgenic group addressed this challenge. An increase in T_2 values was observed between month 2 and month 5 within the APP/PS infected group. This result was contrary to observations in the APP/PS non-infected group, where a decrease in T_2 occurred in all cortex regions and areas of the hippocampus remained relatively unchanged (Figures 31-33). The increase at month 5 in the APP/PS infected group was similar to the increase in T_2 found in the Wt infected group. The main distinction between the two groups was the increase at month 5 was significant in APP/PS infected group in all regions tested, while the increase in T_2 was only significant in the left hippocampus of the Wt infected group (Figure 31-33). Mice were infected with *C. muridarum* at month 2 following the initial MR imaging session. This manipulation was the only distinguishing feature between the APP/PS infected and non-infected groups. From these observations it can be concluded that the effect of the infection combined with the events leading up to and including initial plaque formation in the APP/PS infected group caused physiological changes in the brain tissue, resulting in a significant elevation in T_2 at month 5 that wasn't apparent in the Wt infected group.

A decrease in T_2 was observed in all regions tested following the increase in T_2 at month 5 in the APP/PS infected group (Figures 31-33). As previously described, decreases in T_2 values occurred from month 2 to month 20 in the APP/PS and Wt non-infected groups, with significant decreases occurring within the APP/PS non-infected group. The significant decreases in T_2 values in subsequent measurements following month 5 in the APP/PS infected group are thought to be associated with the effect of plaque pathology and are therefore related to the APP/PS transgenes (Figures 22-24).

This decrease in T_2 after month 5 in the APP/PS infected group mirrored the pattern exhibited by both the APP/PS and Wt non-infected groups from month 2 to month 20. This strongly suggests that the effect of infection caused changes in the tissue fluidity in the brain in the months immediately following infection, but the effects dissipated and mice showed a similar pattern of a decrease in T_2 similar to both APP/PS and Wt non-infected mice. The pattern of decrease in T_2 after month 5 occurs in both Wt and APP/PS infected groups. This provides further evidence that the physiological changes from infection disappear in the T_2 measurements following month 5.

To investigate the impact of infection on AD, T_2 values were compared at month 20 in APP/PS infected and APP/PS non-infected groups. Longer T_2 times were observed in the APP/PS infected group compared to the APP/PS non-infected group in all regions tested (Figures 22-24). Longer T_2 values were significant in 5 of the 6 regions examined (Figure 31-33). A significant decrease in T_2 from month 2 to month 20 in all cortex regions was observed in the APP/PS non-infected group (Figures 25-26). Interestingly, this trend was not found in the APP/PS infected group between the time periods of month 2 to month 20 (Figures 31-33). Areas of the cortex had very similar T_2 values at months 2 and 20, while an increase in T_2 was seen in the hippocampus in the APP/PS infected group (Figures 31-33). The underlying biochemical or physiological changes reflected in the longer T_2 times observed at month 5 in APP/PS infected mice appear to have had an impact on changes in the brain at month 20, where longer T_2 values were observed compared to the APP/PS non-infected group. The increase was similar in the Wt group, however the increase in T_2 was not significant from month 2 to month 5.

It can be concluded that the effect of infection has a stronger influence on T_2 values compared to the effect of events leading to and including plaque accumulation at month 5. This is an important distinction because the proteins derived from APP/PS transgenes have been shown to have a shortening effect on T_2 in previous studies where plaque progression was examined without the influence of infection (29, 76, 79). The net effect of both the APP/PS transgenes and *C. muridarum* infection observed at month 5 is a masking of the hypointensities associated with AD plaque progression (observed in the non-infected APP/PS group), which eventually becomes apparent at the later time points (Figures 31-33).

5. Conclusions and Future Directions

5.1 Conclusions:

This is the first study of its kind to infect a C3H and C57BL/6 crossbreed of APP/PS transgenic mouse with a non-lethal inoculum of *C. muridarum* for the purposes of examining the long-term effects of infection on plaque pathology associated with AD in a longitudinal study.

Mice infected with *C. muridarum* displayed the typical characteristics expected of an illness, including visual observations such as piloerection and abnormal posture as well as a marked body weight loss. Body weight loss was stabilized at approximately 15 DPI in Wt infected mice and 28 DPI in APP/PS infected mice. All infected mice gained weight in co-linear pattern with non-infected mice after the effects of infection were cleared (Figure 15). Serology experiments of samples obtained at euthanasia at 18 months post infection provided concrete evidence of a prior exposure to *C. muridarum* in all mice infected with the bacteria at 2 months.

Brain tissue was harvested after euthanasia, sectioned and stained with Congo red. Both infected and non-infected Wt mice showed a negative result in the histology for AD plaques. This indicated that infecting B6C3 mice intranasally with a 1000 IFU of *C. muridarum* at 2 months of age was not sufficient to induce brain plaque pathology in Wt mice. The infection had an impact on final plaque burden in APP/PS mice at 18 months post infection, where a trend of higher plaque counts was observed. Histology showed an inhomogeneous distribution of plaques in the brains of APP/PS mice. Plaque distribution also varied with respect to infection, notably in the hippocampus region, where higher plaque counts were observed in infected mice.

MR imaging is a powerful tool for monitoring (non-invasively) the subtle changes in fluidity associated with both water content and structural changes in brain tissue. In this work MR was able to detect changes in tissue composition in the brain resulting from both the APP/PS transgenes and the effect of infection. Significant decreases in T_2 were observed within the APP/PS non-infected group in most areas tested compared to the Wt non-infected group. This observation is important for modeling plaque progression associated with AD in the APP/PS transgenic mouse model. An increase in T_2 value was observed in all mice infected with *C. muridarum* in month 5 compared to month 2. This is an important distinction, because there is a hyperintensity in T_2 in both APP/PS and Wt groups, thus it can be concluded that this increase is directly related to infection rather then the impact of the APP/PS transgene. In fact, the APP/PS infected group showed a significant increase in T_2 in month 5 compared to month 2 in all regions tested. This is conclusive evidence that the effect of both the APP/PS transgenes and *C. muridarum* infection is reflected in the early increase in T_2 from month 2 to month 5. The effect was also observed at the end point of month 20 where T_2 times were significantly longer in all areas tested in APP/PS infected mice compared to the APP/PS non-infected control group. The change in T_2 resulting from infection has important implications in looking at the effect of infection on the AD model. It appears that the changes in the brain resulting from infection at 5 months are able to mask the effect of the plaque pathology resulting from the APP/PS transgenes. After month 5 T_2 changes reflect a pattern that is similar to the APP/PS non-infected group, which displays a gradual decrease in T_2 over time. MR was actually able to detect changes in the body long after the acute infection was cleared based on change in body weight data. According to the changes in body weight, the

effect of infection virtually cleared at approximately 15 DPI in Wt mice and 28 DPI in APP/PS mice (Figure 15 and Appendix 3). According to body weight change, the infected mice appear to gain weight in a co-linear fashion with uninfected mice after recovery. However, MRI provides valuable additional information since it is apparent that the infection continues to have an effect on the brain long after body weights have recovered.

When MRI was used to evaluate the effects of infection *in vivo*, hyperintensities in T_2 times were observed in APP/PS infected mice compared to APP/PS control mice both at month 5 and month 20. Together these results suggest that infection with *Chlamydia* may indeed have an impact on the development of AD. The differences in T_2 values reported here were significant and therefore can be used as biomarkers to model the effect of a *Chlamydia* infection on AD plaque progression *in vivo*.

5.2 Future directions:

The conclusions reached in this study are important for considerations of future studies to investigate the nature of the relationship between *Chlamydia* and AD.

AD is characterized by both βA plaque formation and neurofibrillary tangles composed of abnormal tau protein. It would be interesting to look for biomarkers in MR data related to tau protein accumulation and to investigate if the progression of tangles is impacted by a *Chlamydia* infection. The triple transgenic model of AD would be a suitable choice for this type of experiment as these mice express APP, PS and tau in one animal (55). A combination of two or more risk factors may be required to initiate βA associated plaque development in a Wt mouse. The allele for ApoE4, a protein involved

in cholesterol metabolism, is a known risk factor in sporadic AD (19, 74). Since the cause of sporadic AD is unknown it would be interesting to investigate whether infecting an Apoe4 transgenic mouse may initiate plaque progression.

A notable area of improvement is in the field of engineering better transgenic mouse models for studying AD plaque progression. The congenic lines are from a single background rather then a hybrid and the main feature making this an attractive model for a longitudinal study is a decrease in experimental variability by promoting phenotypic uniformity due to the single background (67).

This work showed that infection had a clear impact on plaque progression in the APP/PS model. To determine the exact nature of the relationship between plaque progression and infection, a stroke model could be used to increase BBB permeability, thus determining whether or not *Chlamydia* is an opportunistic infection. The exact nature of the relationship could be further investigated by attempting to culture viable *Chlamydia* from the brain.

Histological techniques indicated a trend of higher plaque counts in the infected APP/PS group compared to the non-infected APP/PS group. A power analysis indicated that 15 animals would be the appropriate sample size to find statistically significant differences in overall plaque burden with a statistical power of 80% (and a type I error < 0.05) based on the results presented in this study. A power analysis determined that 9 animals would be the required sample size to attain a statistically significant difference between groups, at a power of 80% (with a type I error <0.05) in the hippocampus.

Testing for evidence of viable *C. muridarum* or trace components from a past infection would serve as a good follow up study to this work, confirming that active

bacteria was present in the brain of infected mice at some point (4). If *C. muridarum* was able to be cultured from brain tissue samples this would confirm an active infection. This would also validate experiments conducted in Dr. Xi Yang's laboratory where *C. muridarum* mRNA was isolated from brain tissues of infected mice. The presence of *Chlamydia* mRNA in the brain is evidence that the bacteria were viable at one time, indicating changes (inflammatory, cell death) may have occurred as a result of pathology.

An investigation into changes in tissue composition could be investigated by infrared microscopy analysis (13). These studies would give insight into biomarkers associated with infection in the brain. Brain tissue samples could be tested for activated microglial cells by conducting an immunohistochemistry assay of tissue sections with primary antibodies specific to Iba-1, a known marker for activated microglial cells (72). This would determine if there was a variation in the immune response in the brain. This would make it possible to determine whether immune response in the brain, as measured by microglial activation, varied according to the number of plaques in a given brain region.

A combination of these different approaches should provide a better insight to the impact of a *Chlamydia* infection on chronic AD.

Reference List

1. **Airenne, S., H. Surcel, H. Alakarppa, K. Laitinen, J. Paavonen, P. Saikku, and, A. Laurila.** 1999. *Chlamydia pneumoniae* infection in human monocytes. Infect. Immun. **67:**1445-1449.

2. **Appelt, D. M., M. R. Roupas, D. S. Way, M. G. Bell, E. V. Albert, C. J. Hammond, and B. J. Balin.** 2008. Inhibition of apoptosis in neuronal cells infected with *Chlamyophila* (*Chlamydia*) *pneumoniae*. BMC Neurosci. **9:**1-13.

3. **Bachmaier, K., N. Neu, L. M. Maza, S. Pal, A. Hessel, and J. M. Penninger.** 1999. *Chlamydia* infections and heart disease linked through antigenic mimicry. Science. **283:**1335-1339.

4. **Balin, B. J., H. C. Gerard, E. J. Arking, D. M. Appelt, P. J. Branigan, J. T. Abrams, J. A. Whittum-Hudson, and A. P. Hudson.** 1998. Identification and localization of *Chlamydia pneumoniae* in the Alzheimer's brain. Med. Microbiol. Immunol. **187:**23-42.

5. **Ballabh, P., A. Braun, and M. Nedergaard.** 2004. The blood-brain barrier: an overview structure, regulation, and clinical implications. Neurobiol. Dis. **16:**1-13.

6. **Beatty, W. L., R. P. Morrison, and G. I. Byrne.** 1994. Persistent *Chlamydiae*: from cell culture to a paradigm for *Chlamydia* pathogenesis. Microbiol. Rev. **58:**686-699.

7. **Benveniste, H. G., Einstein, K. R. Kim, C. Hulette, and G. A. Johnson.** 1999. Detection of neuritic plaques in Alzheimer's disease by magnetic resonance microscopy. PNAS. **96:**14079-14084.

8. **Binder, L. I., A. L. Guillozet-Bongaarts, F. Garcia-Sierra, and R. W. Berry.** 2005. Tau, tangles, and Alzheimer's disease. Biochimica et Biophysica Acta. **1739:**216-223.

9. **Boelen, E., F. R. M. Stassen, A. J. A. M. van der Ven, M. A. M. Lemmens, H. P. J. Steinbusch, C. A. Bruggeman, C. Schmitz, and H. W. M. Steinbusch.** 2007. Detection of amyloid beta aggregates in the brain of BALB/c mice after *Chlamydia pneumoniae* infection. Acta. Neuropathol. **114:**255-261.

10. **Braakman, N., J. Matysik, S. G. Van Duinen, F. Verbeek, R. Schliebs, H. J. De Groot, and A. Alia.** 2006. Longitudinal assessment of Alzheimer's β amyloid plaque development in transgenic mice monitored by in vivo magnetic resonance microimaging. J. Magn. Reson. Imaging. **24:**530-536.

11. **Butel, J. S**. 2000. Viral carcinogenesis: revelation of molecular mechanisms and etiology of human disease. Carcinogenesis. **21**:405-426.

12. **Chakeres, D. W., and P. Schmlabrock.** 1992. Fundamentals of magnetic resonance imaging.Williams and Wilkins, Baltimore.

13. **Choo, L., D. L. Wetzel, W. C. Halliday, M. Jackson, S. M. LeVine, and H. H. Mantsch.** 1996. In situ characterization of β-amyloid in Alzheimer's diseased tissue by synchrotron Fourier transform infrared microspectroscopy. Biophys. J. **71:**1672-1679.

14. **Combs, C. K., J. C. Karlo, S. Kao, and G. E. Landreth.** 2001. β amyloid stimulation of microglia and monocytes results in TNFα dependent expression of inducible nitric oxide synthase and neuronal apoptosis. J. Neurosci. **21:**1179-1188.

15. **Elster, A. D.** Questions and answers in magnetic resonance imaging. 1994. 1-156, Mosby, St. Louis.

16. **Falangola, M. F., V. V. Dyakin, S. P. Lee, A. Bogart, J. S. Babb, K. Duff, R. Nixon, and J. A. Helpern.** 2007. Quantitative MRI reveals aging associated T_2 changes in mouse models of Alzheimer's disease. NMR Biomed. **20:**343-351.

17. **Fan, Y., S. Wang, and X. Yang.** *Chlamydia trachomatis* (Mouse Pneumonitits Strain) induces cardiovascular pathology following respiratory tract infection. 1999. Infect. Immun. **67:**6145-6151.

18. **Franklin, K. B. J., and G. Paxinos.** 2008. The mouse brain in stereotaxic coordinates third edition. Elsevier, New York.

19. **Gerard, H. C., K. L. Wildt, J. A. Whittum-Hudson, Z. Lai, J. Ager, and A. P. Hudson.** 2005. The load of *Chlamydia pneumoniae* in the Alzheimer's brain varies with APOE genotype. Microb. Pathogenesis. **39:**19-26.

20. **Gieffers, J., E. Reusche, W. Solbach, and M. Maass**. 2000. Failure to detect *Chlamydia pneumoniae* in brain sections of Alzheimer's disease patients. J. Clin. Microbiol. **38(2):**881-882.

21. **Glenner, G. G., and C. W. Wong.** 1984. Alzheimer's disease: initial report of the purification and characterization of a novel cerebrovascular amyloid protein. Biochem. Bioph. Res. Co. **120:**885-890.

22. **Goate, A., M. C. Chartier-Harlin, M. Mullan, J. Brown, F. Crawford, L. Fidani, L. Giuffra, A. Haynes, N. Irving, L. James, R. Mant, P. Newton, K. Rooke, P. Roques, C. Talbot, M. Pericak-Vance, A. Roses, R. Williamson, M. Rossor, M. Owen, and J. Hardy**. 1991. Segregation of a missense mutation in the amyloid precursor protein gene with familial Alzheimer's disease. Nature. **349:**704-706.

23. **Grohn, O. H., M. I. Kettunen, M. Penttonen, J. M. Oja, P. C. Van Zijl, and R. A. Kauppinen**. 2000. Graded reduction in cerebral blood flow in rats as detected by the nuclear magnetic resonance relaxation time T_2: a theoretical and experimental approach. J. Cereb. Blood Flow Metab. **20:**316-326.

24. **Guo, Q., L. Sebastian, B. L. Sopher, M. W. Miller, C. B. Ware, G. M. Martin, and M. P. Mattson.** 1999. Increased vulnerability of hippocampal neurons from presenilin-1 mutant knock-in mice to amyloid β-peptide toxicity: central roles of superoxide production and caspase activation. J. Neurochem. **72:**1019-1029.

25. **Halme, S., J. Latvala, R. Karttunen, I. Palatsi, P. Saikku, and H. M. Surcel.** 2000. Cell mediated immune response during primary *Chlamydia pneumoniae* infection. Infect. Immun. **68:**7156-7158.

26. **Hammerschlag, M. R.** 2002. The intracellular life of *Chlamydiae*. Seminars in Pediatric Infectous. Diseases. **13:**239-248.

27. **Hardy, J., and D. J. Selkoe. 2002.** The amyloid hypothesis of Alzheimer's Disease: progress and problems on the road to therapeutics. Science. **297:**353-356.

28. **Hauss-Wegrzyniak, B., P. Dobrzanski, J. D. Stoehr, G. L. Wenk.** 1998. Chronic neuroinflammation in rats reproduces components of neurobiology of Alzheimer's disease. Brain Res. **780:**294-303.

29. **Helpern, J. A., S. Lee, M. F. Falangola, V. V. Dyakin, A. Bogart, B. Ardekani, K. Duff, C. Branch, T. Wisniewski, M. J. de Leon, O. Wolf, J. O'Shea, and R. A. Nixon**. 2004. MRI assessment of neuropathology in a transgenic mouse model of Alzheimer's Disease. Magn. Reson. Med. **51:**794-798.

30. **Hogan, R. J., S. A. Mathews, S. Mukhopadhyay, J. T. Summersgill, and P. Timms**. 2004. *Chlamydia* persistence: beyond the biphasic paradigm. Infect. Immun. **72:**1843-1855.

31. **Hudson, A.P.** 2001. What is the evidence for a relationship between *Chlamydia pneumoniae* and late-onset Alzheimer's disease? Lab. Med. **32:**680-695.

32. **Hsiao, K. K., D. R. Borchelt**, **K. Olson**, **R. Johannsdottir**, **C. Kitt**, **W. Yunis**, **S. Xu,C. Eckman**, **S. Younkin**, **D. Price**, **C. Iadecola**, **H. B. Clark, and G. Carlson**. 1995. Age-related CNS disorder and early death in transgenic FVB/N mice overexpressing Alzheimer amyloid precursor proteins. Neuron. **15:**1203-1218.

33. **Itagaki, S., P. L. McGeer, H. Akiyama, S. Zhu and D. Selkoe.** 1989. Relationship of microglia and astrocytes to amyloid deposits of Alzheimer disease. J. Neuroimmunol. **24:**173-182.

34. **Itzhaki, R. F., M. A. Wozniak, D. M. Appelt, and B. J. Balin.** 2004. Infiltration of the brain by pathogens causes Alzheimer's disease. Neurobiol. Aging. **25:**619-627.

35. **Jack, C. R., T. M. Wengenack, D. A. Reyes, M. Garwood, G. L. Curran, B. J. Borowski, J. Lin, G. M. Preboske, S. S. Holasek, G, Adriany, and J. F. Poduslo.** 2005. In vivo magnetic resonance microimaging of individual amyloid plaques in Alzheimer's transgenic mice. J. Neurosci. **25:**10041-10048.

36. **Jankowsky, J. L., D. J. Fadale, J. Anderson, G. M. Xu, V. Gonzales, N. A. Jenkins, N. G. Copeland, M. K. Lee, L. H. Younkin, S. L. Wagner, S. G. Younkin, and D. R. Borchelt.** 2004. Mutant presenilins specifically elevate the level of 42 residue β amyloid peptide *in vivo*: evidence for augmentation of a 42-specific γ secretase. Hum. Mol. Genet. **13:**159-170.

37. **Jankowsky, J. L., H. H. Slunt, T. Ratovitski, N. A. Jenkins, N. G. Copeland, and D. R. Borchelt.** 2001**.** Co-expression of multiple transgenes in mouse CNS: a comparison of strategies. Biomol. Eng. **17:**157-165.

38. **Kalehua, A. N., D. D. Taub, P. V. Baskar, J. Hengenihle, J. Munoz, M. Trambadia, D. L. Speer, M. G. De Simoni, and D. K. Ingram.** 2000. Aged mice exhibit greater mortality concomitant to increased brain and plasma TNF-α levels following intracerebroventricular injection of lipopolysaccharide. Gerontology. **46:**115-128.

39. **Kim, W. J., H. Y. Lee, M. E. Lee, and S. J. Lee.** 2006. Serology of *Chlamydia pneumoniae* in patients with chronic cough. Respirology. **11:**805-808.

40. **Kosik, K. S., C. L. Joachim, and D. J. Selkoe.** 1986. Microtubule-associated protein tau is a major antigenic component of paired helical filaments in Alzheimer disease. Proc. Natl. Acad. Sci. **83:**4044-4048.

41. **Kurt, M. A., D. C. Davies, M. Kidd, K. Duff, S. C. Rolph, and K. H. Jennings**. 2001. Neurodegenerative changes associated with beta-amyloid deposition in the brains of mice carrying mutant amyloid precursor protein and mutant presenilin-1 transgenes. Exp. Neurol. **171:**59-71.

42. **Lendon C. L., F. Ashall, and A. M. Goate.** 1997. Exploring the etiology of Alzheimer's disease using molecular genetics. J. Am. Med. Assoc. **277:**825-831.

43. **Levinson, W., and E. Jawetz.** 2002. Medical microbiology and immunology. 221-225, McGraw-Hill, New York.

44. **Little, C. S., C. J. Hammond, A. MacIntyre, B. J. Balin, and D. M. Appelt.** 2004. *Chlamydia pneumoniae* induces Alzheimer-like amyloid plaques in brains of BALB/c mice. Neurobiol. Aging. **25:**419-429.

45. **Liu, Y., M. Yoo, A. Savonenko, W. Stirling, D. L. Price, D. R. Borchelt, L. Mamounas, W. E. Lyons, M. E. Blue, and M. K. Lee.** 2008. Amyloid pathology is associated with progressive monoaminergic neurodegeneration in a transgenic mouse model of Alzheimer's disease. J. Neurosci. **28:**13805-13814.

46. **Luna, L. G.** 1992. Histopathalogical methods and color atlas of special stains and tissue artifacts. American Histo. Labs Inc. 366-367.

47. **MacIntyre, A., R. Abramov, C. J. Hammond, A. P. Hudson, E. J. Arking, C. S. Little, D. M. Appelt, and B. J. Balin.** 2003. *Chlamydia pneumoniae* infection promotes the transmigration of monocytes through human brain endothelial cells. J. Neurosci, Res. **71:**740-750.

48. **Mahony, J.B., J. Woulfe, D. Munoz, D. Browning, S. Chong, and M. Smieja.** 2000. Identification of *Chlamydia pneumoniae* in the Alzheimer's brain. 7th International Conference on Alzheimer's Disease and Related Disorders. **1120:** World Alzheimer Congress.

49. **Mahony, J., J. Woulfe, D. Munoz, S. Chong, D. Browning, and M. Smieja.** 2000. *Chlamydia pneumoniae* in the Alzheimer's brain—is detection hampered by low copy number? Proceedings of 4th meeting of the European society for *Chlamydia* Research, Helsinki, Finland; 299-300.

50. **Masters, C. L., G. Simms, N. A. Weinman, G. Multhaup, B. L. McDonald, and, K. Beyreuther.** Amyloid plaque core protein in Alzheimer's disease and Down syndrome. 1985. Proc. Natl. Acad. Sci. **82:**4245-4249.

51. **Mattson, M. P.** 2003. Infectious agents and age-related neurodegenerative disorders. Aging Research Reviews. **6:**1-12.

52. **McClarty, G., H. D. Caldwell, and D. E. Nelson.** 2007. *Chlamydial* interferon gamma immune evasion influences infection tropism. Curr. Opin. Microbiol. **10:**47-51

53. **Meyer-Lehmann, M., T. L. Spires-Jones, C. Prada, M. Garcia-Alloza, A. de Calignon, A. Rozkalne, J. Koenigsknecht-Talboo, D. M. Holtzman, B. J. Bacskai and, B. T. Hyman.** 2008. Rapid appearance and local toxicity of amyloid-β plaques in a mouse model of Alzheimer's disease. Nature. **451:**720-725.

54. **Nochlin, D., C. M. Shaw, L. A. Campbell, and C. C. Kuo.** 1999. Failure to detect *Chlamydia pneumoniae* in brain tissues of Alzheimer's disease. Neurology. **53(8):** 1888.

55. **Oddo, S., A. Caccamo, M. Kitazawa, B. P. Tseng, and F. M. LaFerla.** 2003. Amyloid deposition precedes tangle formation in a triple transgenic model of Alzheimer's disease. Neurobiol. Aging. **24:**1063-1070.

56. **Ossewaarde, J. M., S. K. Gielis-Proper, A. Meijer, and P. J. M. Roholl**. 2000. *Chlamydia pneumoniae* antigens are present in the brains of Alzheimer patients, but not in the brains of patients with other dementias. Proceedings of 4th meeting of the European Society for *Chlamydia* Research, Helsinki, Finland: 301-302.

57. **Poduslo, J. F., T. M. Wengenack, G. L. Curran, T. Wisniewski, E. M., Sigurdsson, S. I. Macura, B. J. Borowski, and C. R. Jack Jr.** 2002. Molecular targeting of Alzheimer's amyloid plaques for contrast-enhanced magnetic resonance imaging. Neurobiol. Dis. **11:**315-329.

58. **Qiu, H., J. Yang, H. Bai, Y. Fan, S. Wang, X. Han, L. Chen, and X. Yang.** 2004. Less inhibition of interferon-γ to organism growth in host cells may contribute to the high susceptibility of C3H mice to *Chlamydia trachomatis* lung infection. Immunology. **111:** 453-461.

59. **Read, T. D., R. C. Brunham, C. Shen, S. R. Gill, J. F. Heidelberg, O. White, E. K. Hickey, J. Peterson, T. Utterback, K. Berry, S. Bass, K. Linher, J. Weidman, H. Khouri, B. Craven, C. Bowman, R. Dodson, M. Gwinn, W. Nelson, R. DeBoy, J. Kolonay, G. McClarty, S. L. Salzberg, J. Eisen, and C. M. Fraser.** 2000. Genome sequences of *Chlamydia trachomatis* MoPn and *Chlamydia pneumoniae* AR39. Nucleic Acids Res. **28:**1397-1406.

60. **Rey-Ladino, J., X. Jiang, B. R. Gabel, C. Shen, and R. C. Brunham**. 2007. Survival of *Chlamydia muridarum* within dendritic cells. Infect. Immun. **75:**3707-3714.

61. **Rice, D. P., H. M. Fillit, W. Max, D. S. Knopman, J. R. Lloyd, and S. Duttagupta.** 2001. Prevalence, costs, and treatment of Alzheimer's disease and related dementia: a managed care perspective. Am. J. Manag. Care. **7:**809-818.

62. **Ring, R. H., and J. M. Lyons**. 2000. Failure to detect *Chlamydia pneumoniae* in the late-onset Alzheimer's brain. J. Clin. Microbiol. **38(7):**2591-2594.

63. **Robinson, S. R., C. Dobson, and J. Lyons.** 2004. Challenges and directions for the pathogen hypothesis of Alzheimer's disease. Neuro. Bio. Aging. **25:**629-237.

64. **Rosano, C., and A. B. Newman**. Cardiovascular disease and risk of Alzheimer's disease. 2006. Neurol. Res. **28:**612-620.

65. **Rosen G. D., A. G. Williams, J. A. Capra, M. T. Connolly, B. Cruz, L. Lu, D. C. Airey, K. Kulkarni, and R. W. Williams.** 2000. The Mouse Brain Library @ www.mbl.org. Int Mouse Genome Conference **14:** 166. www.mbl.org.

66. **Salkeni, M. A., J. L. Lynch, T. Ostamis-Price, and W. A. Banks.** 2009. Lipopolysaccharide impairs blood-brain barrier P-glycoprotein function in mice through prostaglandin and nitric oxide-independent pathways. J. Neuroimmune. Pharmacol. **4:**276-282.

67. **Savonenko, A. V., G. M. Xu, D. L. Price, D. R. Borchelt, and A. L. Markowska.** 2003. Normal cognitive behavior in two distinct congenic lines of transgenic mice hyperexpressing mutant APPswe. Neurobiol. Dis. **12:**194-211.

68. **Schellenberg, G. D.** 1995. Genetic dissection of Alzheimer's disease, a heterogeneous disorder. Proc. Natl. Acad. Sci. **92:**8552-8559.

69. **Scheuner, D., C. Eckman, M. Jensen, X. Song, M. Citron, N. Suzuki, T. D. Bird, J. Hardy, M. Hutton, W. Kukull, E. Larson, E. Levy-Lahad, M. Viitanen, E. Peskind, P. Poorkaj, G. Schellenberg, R. Tanzi, W. Wasco, L. Lannfelt, D. Selkoe, and S. Younkin.** 1996. Secreted amyloid β-protein similar to that in the senile plaques of Alzheimer's disease is increased *in vivo* by the presenilin 1 and 2 and APP mutations linked to familial Alzheimer's disease. Nat. Med. **2:**864-870.

70. **Schild, H. H.** 1990. MRI made easy. H. Heenemann GmbH & Co, Berlin.

71. **Sheng, J. G., S. H. Bora, G. Xu, D. Borchelt, D. L. Price, and V. E. Koliatsos**. 2003. Lipopolysaccharide-induced-neuroinflammation increases intracellular accumulation of amyloid precursor protein and amyloid β peptide in APPswe transgenic mice. Neurobiol. Dis. **14:**133-145.

72. **Solomon, S. S., S. Kyrkanides, J. A. Olschowka, J. H. Miller, R. E. Johnson, and M. K. O'Banion.** 2007. Sustained hippocampal IL-1β overexpression mediates chronic neuroinflammation and ameliorates Alzheimer plaque pathology. J. Clin. Invest. **117:**1595-1604.

73. **Stooper, B. D., P. Saftig, K. Craessaerts, H. Vanderstichele, G. Guhde, W. Annaert, K. Von Figura, and F. Van Leuven.** 1998. Deficiency of presenilin-1 inhibits the normal cleavage of amyloid precursor protein. Nature. **391:**387-390.

74. **Strittmatter, W. J., and A. D. Roses.** 1996. Apolipoprotein E and Alzheimer's disease. Annu. Rev. Neurosci. **19:**53-77.

75. **Swanborg, R. H., D. L. Boros, J. A. Whittum-Hudson, and A. P. Hudson.** 2002. Molecular mimicry and horror autotoxicus*:* do C*hlamydial* infections elicit autoimmunity? FEMS Micobio. Lett. **217:**167-172.

76. **Tayara, N. T., A. Volk, M. Dhenain, and B. Delatour**. 2007. Transverse relaxation time reflects brain amyloidosis in young APP/PS1 transgenic mice. Magn. Reson. Med. **58:**179-184.

77. **Verhoeff, N. P., A. A. Wilson, S. Takeshita, L. Trop, D. Hussey, K. Singh, H. F. Kung, M. P. Kung, and S. Houle.** 2004. *In-vivo* imaging of Alzheimer disease beta-amyloid with [11C]SB-13 PET. AM. J. Geriatr. **12:**584-595.

78. **Wada, H., K. Nakajoh, T. Satoh-Nakagawa, T. Suzuki, T. Ohrui, H. Arai, and, H. Sasaki.** 2001. Risk factors of aspiration pneumonia in Alzheimer's disease patients. Gerontology. **47:**271-276.

79. **Wadghiri, Y. Z., E. M. Sigurdsson, M. Sadowski, J. I. Elliott, L. Yongsheng, H. Scholtzova, Y. T. Cheuk, G. Aguinaldo, M. Pappolla, K. Duff, T. Wisniewski, and D. H. Turnbull.** 2003. Detection of Alzheimer's amyloid in transgenic mice using magnetic resonance microimaging. Magn. Reson. Med. **50:**293-302.

80. **Wengenack, T. M., G. L. Curran, and J. F. Poduslo.** 2000. Targeting Alzheimer amyloid plaques *in vivo*. Nat. Biotechnol. **18:**868-872.

81. **Wengenack, T. M., C. R. Jack, M. Garwood, and J. F. Poduslo.** 2008. MR microimaging of amyloid plaques in Alzheimer's disease in transgenic mice. Eur. J. Nucl. Med. Mol. Imaging. **35:**S82-S88.

82. **Willatt, J. M., H. K. Hussain, S. Adusumilli, and J. A. Marrero.** 2008. MR imaging of hepatocellular carcinoma in the cirrhotic Liver: challenges and controversies. Radiology. **247:**311-330.

83. **Yang, D., A. Kumar, P. Stavrides, J. Peterson, C. M. Peterhoff, M. Pawlik, E. Levy, A. M. Catalado, and R. A. Nixon.** 2008. Neuronal apoptosis and autophagy cross talk in aging PS/APP mice, a model of Alzheimer's disease. Am. J. Pathol. **173:**665-681.

84. **Yang, X., K. T. HayGlass, and R. C. Brunham**. 1996. Genetically determined differences in IL-10 and IFN-γ responses correlate with clearance of *Chlamydia trachomatis* mouse pnuemonitis. J. Immunology. **156**:4338-4344.

85. **Yang, X., and R. C. Brunham.** 1998. Gene knockout B cell-deficient mice demonstrate that B cells play an important role in the initiation of T cell response to *Chlamydia trachomatis* (mouse pneumonitits). J. Immunology. **161:**1439-1446.

86. **Zar, J. H. 1996.** Biostatistical Analysis third edition. Prentice Hall. Upper Saddle River, New Jersey.

87. **Zhang, J., P. Yarowslky, M. N. Gordon, G. Di Carlo, S. Munireddy, and P. C. M. Van Zijl.** 2004. Detection of amyloid plaques in mouse models of Alzheimer's disease by magnetic resonance imaging. Magn. Reson. Med. **51:**452-457.

Appendices

Appendix 1: An example of UV ELISA plate.
Depicted are optical density readings obtained with a microplate reader representing *C. muridarum* specific IgA titres in uninfected mouse serum (1-7) and infected mice (8-15).

Dilution	OPTICAL DENSITY RAW VALUES OBSERVED FOR IgA						
	1	2	3	4	5	6	7
1x	0.417	0.411	0.517	0.158	0.169	0.289	0.342
2x	0.302	0.307	0.366	0.109	0.109	0.187	0.230
4x	0.237	0.205	0.253	0.076	0.086	0.133	0.210
8x	0.067	0.131	0.189	0.051	0.053	0.081	0.113
16x	0.148	0.091	0.142	0.036	0.039	0.066	0.079
32x	0.106	0.066	0.098	0.027	0.032	0.049	0.100
64x	0.084	0.039	0.063	0.025	0.030	0.042	0.054
128x		0.031	0.048	0.027	0.045	0.042	0.044

Dilution	OPTICAL DENSITY RAW VALUES OBSERVED FOR IgA							
	8	9	10	11	12	13	14	15
1x	2.112	2.360	1.091	1.585	1.979	1.233	1.644	2.168
2x	2.603	2.113	1.053	1.405	1.709	1.429	1.458	2.013
4x	2.182	2.014	1.008	1.621	1.575	1.209	1.276	1.866
8x	1.997	2.121	0.887	1.296	1.476	1.159	1.231	1.730
16x	1.767	1.648	0.713	1.259	1.709	0.822	1.077	1.636
32x	1.731	1.444	0.499	1.107	1.354	0.689	0.924	1.545
64x	1.607	1.354	0.332	0.939	1.100	0.545	0.753	1.522
128x		1.069	0.215	0.679	0.882	0.349	0.527	1.404

Appendix 2: A detailed method for Congo red staining.

1. Fixate the left side of mouse brain in 10% buffered neutral formalin (Sigma-Aldrich, Oakville, ON, Canada).
2. Fixed tissue remained in formalin for a minimum of one month before being dehydrated through a series of ethanol changes (70%, 85%, 90%, three changes at 100%), two changes of xylene (100%) before being embedded in hot paraffin, preserving the tissue in paraffin blocks for histological analysis.
3. Cut paraffin sections at 12 μM with microtome.
4. Deparaffinize in 2 changes of xylene for 2 minutes each.
5. Hydrate to distilled water with 2 changes of absolute alcohol, 95% alcohol, 2 minutes each.
6. Dissolve alum in water without heat; add and dissolve Hematoxylin. Add the sodium iodate, citric acid and the glycerin. Shake to dissolve.
7. Immerse sections in Congo red solution for 1 hour.
8. Rinse off excess stain in 2-3 changes of water.
9. Differentiate in alkaline alcohol solution for 3-5 seconds. Agitate constantly until the background appears clear and the amyloid deposits stand out in a pink to red colour.
10. Wash in running water for 5 minutes.
11. Stain in Mayers Hematoxylin for 5 minutes.
12. Wash in running water for 10 minutes.
13. Dehydrate in 95% and absolute alcohol, 2 changes each.

14. Clear in xylene, 3 changes for 2 minutes each.
15. Mount cover glass with mounting media using manual method or automatic coverslipper.
16. Final stain is reddish violet – stain tissue keeps for months (Luna LG).

Appendix 3: Individual changes in body weight (grams) for APP/PS infected mice.

DPI	Mouse 11	Mouse 12	Mouse 13	Mouse 14	Mouse 15
2	22	21	21	20	18
5	23	22	19	21	19
8	24	22	20	21	20
12	25	23	20	21	19
13	25	23	20	21	20
14	25	23	21	22	20
15	26	23	22	22	21
17	23	23	22	24	23
20	24	23	21	22	23
22	22	24	21	24	24
24	24	26	24	23	21
26	25	24	24	22	21
27	26	25	25	24	22
28	26	25	25	25	22

Appendix 4: Individual mouse serum IgG2a and IgA titres (log_{10}).
Serum samples were obtained 20 months after an intranasal inoculation with *C. muridarum* in Wt and APP/PS transgenic mice. Serum Ab titres were derived using the $OD_{0.5}$ reading as a cut-off value.

Mouse		**Ab Titres**	
Mouse ID #	Infected/non-infected	IgG2a	IgA
1 – WT	Non-infected	0.000	0.008
2 – WT	Non-infected	0.000	0.090
3 – WT	Non-infected	0.000	0.166
4 – APP/PS	Non-infected	0.000	0.000
5 – APP/PS	Non-infected	0.000	0.000
6 – APP/PS	Non-infected	0.000	0.063
7 – APP/PS	Non-infected	0.279	0.000
8 – WT	Infected	3.003	3.607
9 – WT	Infected	2.813	2.827
10 – WT	Infected	2.083	1.504
11 – APP/PS	Infected	3.592	2.598
12 – APP/PS	Infected	2.636	2.493
13 – APP/PS	Infected	2.919	1.951
14 – APP/PS	Infected	4.787	2.161
15 – APP/PS	Infected	2.877	5.715

Appendix 5: The mill is used to create a mouse probe.
There are many steps in creating an MR probe; one step includes cutting sections of the plastic on the mill shown here. Engineers at The Institute for Biodiagnostics designed and created MR probes for this study.